Exergy Loss Minimization for Chemical Processes

Y Kansha*, M Ishizuka, Y Kotani, and A Tsutsumi

Institute of Industrial Science, The University of Tokyo

*e-mail: kansha@iis.u-tokyo.ac.jp

Abstract

In this paper, a current trend of the process design method for chemical processes is described and a new energy saving technology, self-heat recuperation based on exergy loss minimization is introduced. In this technology, whole process heat is recirculated into the process without any heat addition, leading to considerable energy saving of the processes.

INTRODUCTION

The reduction of carbon dioxide (CO2) emission has become a major target in efforts to suppress global warming. The combustion of fossil fuels for heating produces a large amount of CO2, which is the main contributor to global greenhouse gas effects. Hence, the reduction of energy consumption for heating is a very important issue nowadays. Recently, energy saving technology has attracted increased interest in many countries for suppressing global warming and reducing the use of fossil fuels. However, many conventional energy saving technologies represented by heat recovery such as pinch technology [1, 2], which exchanges heat between the hot and cold streams in a process, has been applied to thermal processes [3-9], are based only on the 1st law of thermodynamics, energy conservation.

A simple example of this pinch technology is the application of a feed-effluent heat exchanger in thermal processes, wherein heat is exchanged between feed (cold) and effluent (hot) streams to recirculate the self heat of the stream. To exchange the heat, an additional heat source must be required, due to the temperature difference between two streams for heat exchange. These conventional heat recovery technologies are distinguished by cascading heat utilization. In these technologies, the required additional heat is provided by the exhausted heat from the other process or by the combustion of fuels. Although net energy input seems to be reduced by using exhausted heat as the additional heat, the top of heat cascade, the heat is also provided by the combustion of fossil fuels, leading to exergy destruction during energy conversion from chemical energy to heat.

In contrast, many researchers have paid attention to the analysis of process exergy and irreversibility through consideration of the second law of thermodynamics. However, many of these investigations show only the calculation results of exergy analysis and the possibility for energy savings of some processes [10, 11], but few of them clearly describe methods for reducing the energy consumption of processes [12, 13]. Based on these analyses, a heat pump has been applied to thermal processes, in which the ambient heat or the process waste heat is generally pumped to heat the process stream by using working fluid compression. Although it is well-known that a heat pump can reduce energy consumption and exergy destruction in a process, the heat load and capacity of the process stream are often different from those of the pumped heat. Thus, a normal heat pump still possibly causes large exergy destruction during heating. In heat recovery technologies, vapor recompression has been applied to evaporation, distillation, and drying, in which the vapor evaporated from the process is compressed to a higher pressure and then condensed, providing a heating effect. The condensation heat of the stream is recirculated as the vaporization heat in the process by using vapor recompression. However, many investigators have only focused on latent heat and few have paid attention to sensible heat. As a result, the total process heat cannot be recovered, indicating the potential for further energy savings in many cases. Recently, Kuchonthara et al. proposed an energy-recuperative, integrated gasification power generation system through exergy analysis and developed design methods for the system [14-16].

Based on exergy recuperation, Kansha et al. developed self-heat recuperation technology [17], applied it to several chemical processes, and showed the potential energy savings compared with conventional counterparts [18-21]. Kansha et al. present a simple calculation technique for the minimum energy required for thermal processes that was derived numerically from the point of view of irreversibility and compares between self-heat recuperative thermal processes and conventional processes using simulation to examine the energy saving potential of their processes [22].

In this paper, self-heat recuperation technology is summarized and then the possibility of the new process design method by the exergy minimization is illustrated.

SELF-HEAT RECUPERATION

Self-heat recuperation technology [17] facilitates recirculation of not only latent heat but also sensible heat in a process, and helps to reduce the energy consumption of the process by using compressors

and self-heat exchangers based on exergy recuperation. In this technology, i) a process unit is divided on the basis of functions to balance the heating and cooling loads by performing enthalpy and exergy analysis and ii) the cooling load is recuperated by compressors and exchanged with the heating load. As a result, the heat of the process stream is perfectly circulated without heat addition, and thus the energy consumption for the process can be greatly reduced.

The exergy (EX) of stream during heat transfer is generally described by the following equation;

$$EX = (H - H_0) - T_0(S - S_0) \quad (1)$$

while H is an enthalpy, S is an entropy and T is a temperature. Subscript 0 denotes the standard condition.

The differential heat (dQ) is transferred from the hot stream to cold stream without temperature change of both streams during heat transfer. Then, the exergy changes of both streams by heat transfer can be calculated by the following equations with the law of energy conservation.

$$\begin{aligned} dEX_{hot} &= dH_{hot} - T_0 dS_{hot} \\ &= -dQ - T_0 dS_{hot} \quad (2) \\ dEX_{cold} &= dH_{cold} - T_0 dS_{cold} \\ &= -dQ - T_0 dS_{cold} \quad (3) \end{aligned}$$

Here, dH is the enthalpy change and dS is the entropy change of both streams. Thus, exergy loss (dEX_{loss}) associated with this differential heat (dQ) can be derived as Eq. (4).

$$\begin{aligned} dEX_{loss} &= -(dEX_{hot} + dEX_{cold}) \\ &= T_0 (dS_{hot} + dS_{cold}) \quad (4) \end{aligned}$$

To make sure the chemical process, a process stream is heated in a thermal process to satisfy the condition of the following process (X), as shown in Fig. 1(a). In this figure, a combustor was divided into two parts; reactor and heat exchanger, to make clear their functions. T_i and T_o are the input and output temperatures of the process stream to the heater, and in particular, T_o is the required temperature for the subsequent process (X). Exergy loss in conventional thermal processes such as a fired heater normally occurs during heat transfer between the reaction heat of fuel combustion and the heat of the process stream. This exergy loss mainly is caused by irreversibility during heat transfer. Meanwhile, when no heat loss is assumed in this operation, the total reaction heat from fuel combustion transfers to the process stream heat because of the law of energy conservation. The fuel combustion reaction is assumed to occur at constant temperature (T_r) and pressure. Therefore, the exergy loss ($EX_{h.t.1}$) can be derived from the following equation when the process stream is assumed to be a gas and the heat capacity (C_P) of the stream is assumed to keep constant during heat transfer in the heater:

$$EX_{h.t.1} = T_0 (\Delta S_R + \Delta S) \quad (5)$$

Here, ΔS_R is the entropy change of the fuel combustion reaction and ΔS is the entropy change of the process stream during heat transfer. Fig. 1 (b) shows a temperature-entropy diagram for this heat transfer. In this figure, the exergy loss represented by the gray colored area and the area lower than the composite curve of the process stream represents the amount of heat provided in the heater, if the stream temperature is close to standard temperature during heat transfer and temperature difference is much smaller than the temperature. In other words, the greater the gray colored area, the larger the exergy loss during heat transfer. Thus, to reduce the exergy loss during heat transfer, clearly the gray colored area must be reduced.

In contrast, a thermal process based on self-heat recuperation technology has been developed as shown in Fig. 2(a), in which the total heat of the process stream is recirculated by using heat exchangers and compressors. In this process, energy for compression is required to drive the internal heat circulation according to the irreversibility. Thus, it can be said that this process is inherently designed by accounting for this minimum exergy loss for heat transfer.

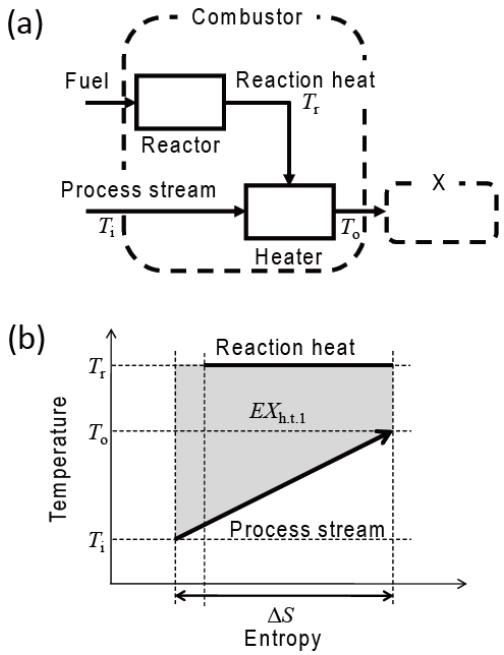

Fig. 1. A conventional thermal process: a) flow diagram b) temperature-entropy diagram

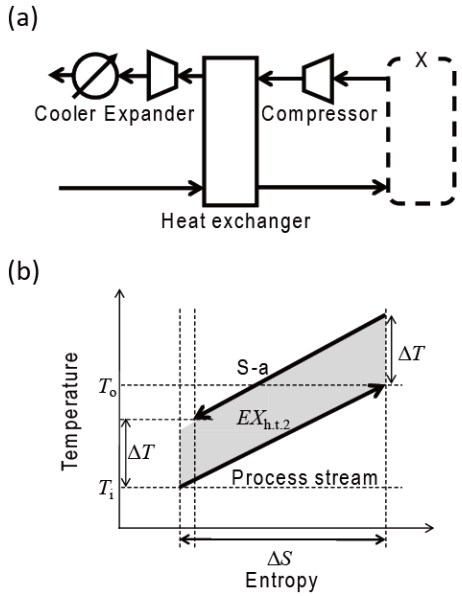

Fig. 2. A self-heat recuperative thermal process: a) flow diagram b) temperature-entropy diagram

As well as Fig. 1, the exergy loss represented by the gray colored area and the area lower than the composite curve of the process stream represents the amount of heat provided in the heater, if the stream temperature is close to standard temperature during heat transfer and temperature difference is much smaller than the temperature [22].

In fact, Kansha et al. reported comparisons between the energy required for self-heat recuperative processes and the conventional counterparts by by PRO/II Ver. 8.1 [17], and simultaneously Kansha et al. compared the theoretical energy required for heat circulation of the thermal process calculated from exergy loss of heat transfer with these values (c.f. Tables 1 and Table 2) [22].

As real fluids, butane was used for the gas stream, and benzene (boiling point 353.2 K) was used for the vapor/liquid stream. In the calculations for all cases, the streams were heated from 300 K to a set temperature T_o, and the flow rate of the stream, F, was 100 kmol/h. The Soave-Redlich-Kwong equation of state was used as considering the real gas stream. The minimum temperature difference for heat exchange was assumed to be 10 K. The pressure ratio in the compressor was set to maintain a constant temperature increase of 10 K owing to compression. The efficiency of the heat exchanger was 100% (i.e., no heat loss), and the adiabatic efficiencies of the compressor and expander were 100%.

From these analyses and results, it can be seen that the self-heat recuperation technology is not only an energy saving technology, but also a technology categorized into exergy loss minimization. Thus, processes designed by following self-heat recuperation drastically reduce the energy consumption as compared with conventional counter parts.

This technology has been applied to several chemical processes [17-21]. From these case studies, this technology works effectively, leading to drastic energy saving. Moreover, authors applied this technology to the actual distillation section for bioethanol purification. As a result, the distillation process designed based on self-heat recuperation consumes only 15% energy of the conventional distillation process for bioethanol production [23].

FURTHER ENERGY SAVING DESIGN METHOD BY EXERGY LOSS MINIMIZATION

Although self-heat recuperation technology is a useful technology for chemical process energy saving, it still has a potential for development a further energy saving process design method from exergy loss minimization point of view. This is simply because this technology mainly concern process heat energy circulation, but it does not concern the pressure drop during heat transfer, mixing and other exergy losses. In fact, Eq. (1) does not include the pressure related term to make this equation simple, because the exergy ratio of heat is considerably small as compared with other works in many cases, leading to large exergy loss. Energy caused by pressure drop changes to heat by friction between heat exchanger surface and process fluid, and this friction causes the exergy loss.

In industry, there are many types of heat exchangers. One of the most commonly used heat exchanger type is a shell and tube. In this type pressure drop of the process stream as liquid is not so large. However, this pressure drop, especially gas stream, directly affects to exergy loss that depends on heat exchanger types. Thus, we need to add the PV term to Eq. (1) where P is pressure and V is volume of the process stream. At the same time, it is necessary to consider about the other exergy losses such as above mentioned mixing and chemical reactions.

Table 1. Comparison of energy requirements (butane)

	Self-heat recuperation				Heat recovery		theoretical energy required
T_1 [K]	W_C [kW]	W_E [kW]	W_{net} [kW]*	Q_{HX} [kW]	Q_{FH} [kW]	Q_{HX} [kW]	W_{theory} [kW]
350	30.0	25.6	4.4	147.7	31.0	116.7	3.7
400	34.0	25.4	8.6	313.7	34.6	279.1	7.3
450	37.5	25.0	12.5	497.0	38.0	459.0	10.6

* $W_{net} = W_C - W_E$ Fluid: Butane 100 kmol/h

Table 2. Comparison of energy requirements (benzene)

	Self-heat recuperation		Heat recovery		theoretical energy required
T_1 [K]	W_{net} [kW]*	Q_{HX} [kW]	Q_{FH} [kW]	Q_{HX} [kW]	W_{theory} [kW]
400	34.93	1195.4	897.3	298.1	33.6

* $W_{net} = W_C$ Fluid: Benzene 100 kmol/h

CONCLUSION

In this paper, self-heat recuperation technology which categorized into process exergy minimization is summarized by analytical and practical points. In this technology, all of the process heat is recirculated into the process by using heat exchangers and compressors without any heat addition, leading to perfect internal heat circulation. As a result, most of the chemical processes which designed based on this technology drastically reduce the energy consumption. After that, the possibility of the modification of self-heat recuperation technology by the exergy minimization is discussed.

ACKNOWLEDGMENT

The authors appreciate financial support provided by the JSPS Grant-in Aid for Young Scientists (B) (grant number: 24760727).

REFERENCES

[1] T.D. Eastop, and D. R. Cro ; Energy Efficiency for Engineers and Technologists, Longman Scientific & Technical, London, U.K. 1990 pp. 203–246.

[2] I. C. Kemp; Pinch Analysis and Process Integration: A User Guide on Process Integration for the Efficient Use of Energy, 2nd ed., Butterworth-Heinemann, Elsevier, Burlington, U.S.A. 2007 pp. 15–40

[3] B. Linnhoff, D. R. Mason, and I. Wardle "Understanding Heat Exchanger Networks," Comput. Chem. Eng., vol. 3, pp. 295–302, 1979

[4] J. Cerda, A. W. Westerberg, D. Mason, and B. Linnhoff "Minimum Utility Usage in Heat Exchanger Network Synthesis," Chem. Eng. Sci., vol. 38, pp. 371–387,1983

[5] B. Linnhoff., D. R. Mason, and I. Wardle "Understanding Heat Exchanger Networks," Comput. Chem. Eng.,vol. 3, pp. 295–302, 1979

[6] B. Linnhoff, and E. Hindmarsh "The Pinch Design Method for Heat Exchanger Networks," Chem. Eng. Sci., vol. 38, pp. 745–763, 1983

[7] B. Linnhoff "Pinch Analysis—A State-of-the-Art Overview," Chem. Eng. Res. Des., vol. 71, pp. 503–522, 1993

[8] B. Linnhoff, and A. R. Eastwood "Overall Site Optimization by Pinch Technology," Chem. Eng. Res. Des., vol. 75, pp. S138–S144, 1997

[9] M. Ebrahim, and A. Kawari "Pinch Technology: An efficient Tool for Chemical-Plant and Capital-Cost Saving," Appl. Energy, vol. 65, pp. 45–49, 2000

[10] M. J. Lampinen, and M. A. Heillinen "Exergy Analysis for Stationary Flow Systems with Several Heat Exchange Temperatures," Int. J. Energy Res., vol. 19, pp. 407–418, 1995

[11] R. W. Grubbström "An Attempt to Introduce Dynamics into Generalized Exergy Consideration," Appl. Energy, vol. 84, pp. 701–718, 2007

[12] R. Chengqin, L. Nianping and T. Guangfa; "Principle of Exergy Analysis in HVAC and Evaluation of Evaporative Cooling Schemes," Build. Environ., 37, 1045–1055 (2002)

[13] S. K. Som, and A. Datta "Thermodynamic Irreversibilities and Exergy Balance in Combustion Processes," Prog. Energy Combust. Sci., vol. 34, pp. 351–376 , 2008

[14] P. Kuchonthara, and A. Tsutsumi "Energy-Recuperative Biomass Integrated Gasification Power Generation System," J. Chem. Eng. Japan, vol. 36, pp 846–851, 2003

[15] P. Kuchonthara, S. Bhattacharya and A. Tsutsumi "Combination of Thermochemical Recuperative Coal Gasification Cycle and Fuel Cell for Power Generation," Fuel, vol. 84, pp. 1019–1021, 2005

[16] P. Kuchonthara, and A. Tsutsumi "Energy-Recuperative Coal-Integrated Gasification/Gas Turbine Power Generation System," J. Chem. Eng. Japan, vol. 39, pp. 545–552 , 2006

[17] Y. Kansha, N. Tsuru, K. Sato, C. Fushimi and A. Tsutsumi "Self-Heat Recuperation Technology for Energy Saving in Chemical Processes," Ind. Eng. Chem. Res., vol. 48, pp. 7682–7686 , 2009

[18] Y. Kansha, N. Tsuru, C. Fushimi, K. Shimogawara and A. Tsutsumi "An Innovative Modularity of Heat Circulation for Fractional Distillation," Chem. Eng. Sci., vol. 65, pp. 330–334 , 2010

[19] Y. Kansha, N. Tsuru, C. Fushimi and A. Tsutsumi "Integrated Process Module for Distillation Processes Based on Self-Heat Recuperation Technology," J. Chem. Eng. Japan, vol. 43, pp. 502–507, 2010

[20] Y. Kansha, A. Kishimoto, T. Nakagawa and A. Tsutsumi "A Novel Cryogenic Air Separation Process based on Self-Heat Recuperation," Sep. Purif. Technol., vol. 77, pp. 389–396 , 2011

[21] K. Matsuda, K. Kawazuishi, Y. Hirochi, R. Sato, Y. Kansha, C. Fushimi, Y. Shikatani, H. Kunikiyo and A. Tsutsumi "Advanced Energy Saving in the Reaction Section of Hydro-Desulfurization Process with Self-Heat Recuperation Technology," Appl. Therm. Eng., vol. 30, pp. 2300–2306 2010

[22] Y. Kansha, Y. Kotani, M. Aziz, A. Kishimoto, and A. Tsutsumi "Evaluation of a Self-Heat Recuperative Thermal Process Based on Thermodynamic Irreversibility and Exergy," J. Chem. Eng. Japan, vol. 46, pp. 87–91, 2013

[23] Webpage, Institute of Industrial Scienc, The University of Tokyo http://www/publication/press.html # 2012/02/02

Modeling of triple bed circulating fluidized bed flow behavior based on equivalent circuit model

Masanori Ishizuka, Yuping Liu, Yasuki Kansha and Atsushi Tsutsumi

Institute of Industrial Science, The University of Tokyo, Japan
*e-mail: a-tsu2mi@iis.u-tokyo.ac.jp

Abstract

It has been proposed triple bed circulating fluidized bed coal gasifier to achieve high-efficiency coal gasification combined cycle power generation. The proposed triple bed circulating fluidized bed coal gasifier has a bubble fluidized bed as a steam gasifier, riser as a char combustor and downer as a pyrolyser. We proposed a novel method for analyzing the fluidized bed. We applied an analogy between flow behavior of fluidized bed and electric circuit with correlations of pressure to voltage, solid mass flux to electric current. Equivalent circuit model was used to calculate step response flow behavior of fluidized bed.

INTRODUCTION

Triple bed circulating fluidized bed coal gasifier has been proposed to achieve high-efficiency coal gasification combined cycle power generation [1-3]. The proposed triple bed circulating fluidized bed coal gasifier has a bubble fluidized bed as a steam gasifier, riser as a char combustor and downer as a pyrolyser. It consists of a downer, bubbling fluidized bed, riser, moving bed, gas solid separator and distributor. Thus, it is a very complex system. For stable operation and controlling of the system, model for the fluid state of the circulating fluidized bed is necessary. In addition, by modeling the useful information for scale-up and design can be obtained.

Fluid integrated circuits and fluid devices are modeled by an equivalent circuit of an electric circuit in the research field of microfluidic devices. These models have been carried out aiming to integrate and raise the functionality of the fluid device [4-7]. By equivalent circuit model fluidic devices, design and analysis can be performed using a similar procedure to an electric circuit design techniques, such as semiconductor integrated circuits and printed circuit boards. So, designing can be performed by the circuit simulator. In addition, it is possible to design the entire fluidic device system as integrated electric circuit device and the fluid control system. In this study, we modeled a fluidized state of the fluidized bed using the equivalent circuit of an electric circuit applying the analogies between the electrical characteristics of an electrical circuit and the fluidized bed flow characteristics. The response characteristics of a triple bed circulating fluidized bed's downer modeled by an equivalent circuit was compared to the response characteristics of the pressure response of the downer. The possibility of an equivalent circuit model has been evaluated.

EQUIVALENT CIRCUIT MODELING

A. Equivalent Circuit Model

The modeling was carried out assuming the electric circuit based on the similarity of the microfluidic circuit about the similarity between the electrical circuit and the electrical characteristics of the flow properties of the fluidized bed. We assumed the relationship between pressure difference and the potential difference as a driving force, electrons and particles as a carrier and solid mass flux and current. Based on this assumption, we can obtain the following relation with the flow characteristics due to the similarity of the electrical circuit. A flow resistance was defined (2) using analogy with Ohm's law (1). Definition of the inertance of the fluidized bed (4) was defined from analogy of the inductance definition of the electrical circuit (3). Definition of compliance (6) was obtained from the definition of capacitance (5).

$$V = IR \tag{1}$$

$$P = FsRa \tag{2}$$

$$V = L\frac{dI}{dt} \tag{3}$$

$$P = Ma\frac{dFs}{dt} \tag{4}$$

$$I = C\frac{dV}{dt} \tag{5}$$

$$Fs = Ca\frac{dP}{dt} \tag{6}$$

The obtained similarity between the electrical characteristics of the electrical circuit and the flow characteristics of fluidized bed are shown in Table 1. In the case of forming an electrical circuit, it is necessary to satisfy the law of Kirchhoff's current

law and voltage law respectively. This is to balance the material and energy balance exactly. Storing kinetic energy of the particles in the fluidized bed is simulated as energy storage of coil in the electrical circuit. The accumulation of energy due to changes in particle concentration is simulated as energy storage of capacitor in the electrical circuit. It should be noted that in this study we are not expecting a change in the volume of the fluidized bed.

Assuming a downer shown in Fig. 1(a), the circuit resistance R, reactance L, capacitance C is connected can be modeled as an equivalent circuit in Fig. 1(b). This circuit has been described expressed in each one element of R, L, and C as the lumped parameter system. Further, each element has become the voltage across the voltage applied to each is added to the series. Thus, it is satisfied the Kirchhoff's voltage law. Also considered in the downer of the fluidized bed, which is the driving force and pressure are applied to the entire. Therefore, if you do the equivalent circuit model in the intensive system, you can be described by the series connection of each element. And also satisfy the Kirchhoff's current law because of the series connection.

Table 1. Analogy between flow behavior of fluidized bed and electric circuit

Fluidizations	Electronics
Particles	Electrons
Solid mass flux Fs (kgs^{-1})	Current I (A)
Pressure drop P (Pa)	Voltage drop V (V)
Resistance Ra ($Paskg^{-1}$)	Resistance R ($\Omega = VA^{-1}$)
Capacitance Ca ($kgPa^{-1}$)	Capacitance C ($F = AsV^{-1}$)
Inertia Ma (Pas^2kg^{-1})	Inductance L ($H = VsA^{-1}$)

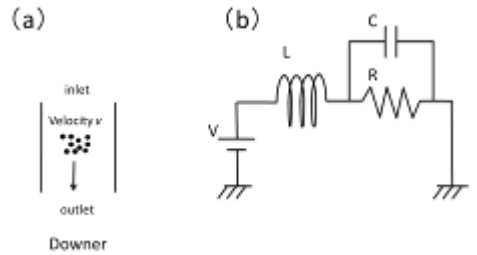

Fig. 1. Equivalent circuit model of the downer flow (a) schematic image of downer (b) equivalent circuit model of downer flow with lumped element model

B. *Measurement and analysis*

We evaluated the output voltage when the input voltage is changed in step to the equivalent circuit of downer as shown in Fig. 2. We calculated the voltage change in capacitance using the "SPICE" program. We gave a constant voltage E to the equivalent circuit as shown in Figure 1b. At this steady state is reached the constant current flow I in the circuit (Fig. 3). The capacitance of the equivalent circuit serves to the constant voltage when a constant current is flowing. Also, there is no voltage change in reactance due to the constant current. Voltage drop proportional to the current is generated in the resistor R according to Ohm's law (1). When the voltage E = 0 at t = 0, the current flow in the circuit I(t) varies as a function of time. Change in voltage V(t) at the capacitance is also a function of time. When the input voltage changes, voltage drop proportional to the current is generated in the resistor R. The reactance delay is decreased in current functions to prevent the current change. In addition, the capacitance slows the voltage drop functions to prevent the voltage change. Step response of the equivalent circuit downer was calculated as a change in capacitance voltage generated. Energy storage in downer particle retention is expressed as the amount of charge stored in the capacitance C of the equivalent circuit. This allows us to achieve a result equivalent to a step change in particle concentration at the entrance of the downer, and the variation in results for the pressure difference in the downer.

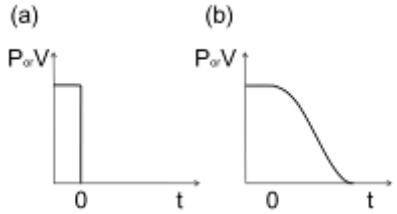

Fig. 2. Step response of pressure/voltage profile in downer (a) input (b) output

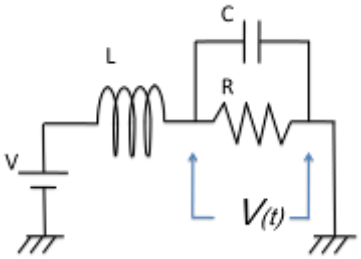

Fig. 3. Equivalent circuit of the downer flow

C. *Experiment*

A step response experiment of the downer was carried out using a circulating fluidized bed cold model consisting of bubbling fluidized bed, downer and riser. Downer is 1.3 m height and 0.05 m inner diameter (Fig. 4). Pressure measurement taps were placed in the inlet and outlet part of downer. The distance between the two taps is 1.2m. Distributor to the top of the downer inlet is installed and is given the air from the air supply port of the distributor to supply downward flow in the downer. Supply control to downer particles was performed using a butterfly

valve at the top of the distributor. Gas-solid separator was installed for the purpose of separation of gas and particles at downer exit. Bubbling fluidized has rectangular cross-section, with a dispersion plate 0.37 m width and 0.08 m depth. No. 8 sand (80μm average diameter) was used as a fluidized particle and bed height was 1.06 m.

The operation condition of riser gas superficial velocity (Ugr) was 6 m/s and downer gas superficial velocity (Ugd) were changed from 0 to 3 m/s. We formed a stable particle circulation. As a step input, we have to stop the supply of particles to close the butterfly valve. The pressure fluctuations were measured in the downer when the valve is closed at t = 0. The pressure measurement was recorded to PC at a sampling rate of 50Hz using the data logger (CONTEC, AIO-163202FX-USB), controller (Keyence, AP-V41A) and pressure sensor (Keyence, VP-48).

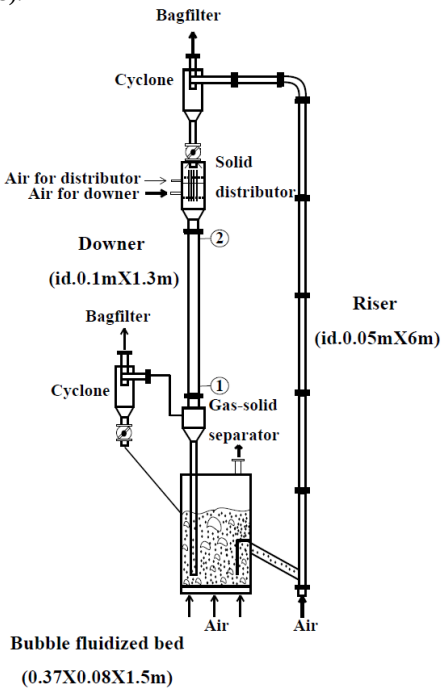

Fig. 4. Experimental setup of downer step response

RESULTS AND DISCUSSION

Fig. 5 shows the results of the measured pressure difference when particle circulation was performed by changing Ugd for 0 - 3 m/s. The particle feed to downer was stopped when t = 0 s. There was a dead time after the outage. And then, the downer pressure was reduced gradually. Assuming spherical particles and free-fall in downer, the terminal velocity was estimated from bulk density 2600 kg/m3 and particle size 80 μm. The average time of the particles passing through the distance between the pressure taps in downer was 2.4 s. which is a reasonable amount of time considering that the pressure difference variation is obtained by the particles stay in the system including a distributor. Because the solid mass flux of this circulating fluidized system depends on the Ugr, this experimental condition of solid mass flux was constant. The particle holdup in the downer was reduced by increasing the Ugd. Hence the initial pressure difference decreased as Ugd was increased. The initial pressure also attenuated in shorter time with increasing Ugd.

We performed step response of the equivalent circuit model expressed in a series circuit RLC by SPICE processing system. Circuit equation for the voltage shown in equation (7) is able to have three different solution overdamping, critical damping and underdamping. However, in case of experimental downer systems, the underdamping solution is not suitable compared to the fluctuations of the pressure difference as shown in Figure 5. The results calculated by the SPICE processing system is depicted on figure 5. The value of element in this case was R = 2000 Ω, L = 1.0 mH, C = 500 μF, and E = 40 V.

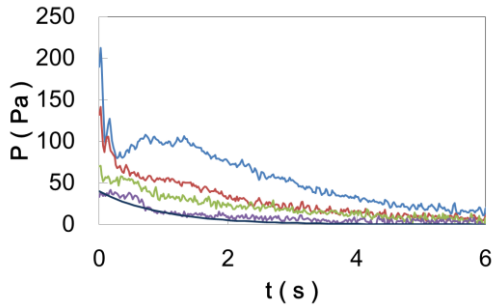

Fig. 5. Representative result of pressure profile in downer Ugr=6m/s, Ugd -0m/s , -1m/s, -2m/s, -3m/s, -equivalent circuit model

In Fig. 5, step response differential pressure fluctuations and transient characteristics calculated from the equivalent circuit model of downer shows a similar trend can be seen. In this experiment, delay in response to the step input was provided by the retention of the particles in a distributor and downer. In the equivalent circuit model, each component R, L and C was set to determine the time constant of the voltage change. Pressure difference during steady state operation in different Ugd was due to the difference of the particle hold-up in the downer. It can be represented by changing the initial voltage E in the equivalent circuit model. The equivalent

CONCLUSION

We made a model of flow behavior in the fluidized bed by an equivalent circuit model of an electrical circuit using of similarity between electronics and fluidics. The flow behavior of the fluidized bed has some analogies with electric analog circuits such as pressure to voltage, solid mass flux to electric current.

By assuming correspondence of voltage to pressure, solid mass flux to current respectively, we have modeled a flow property of the downer by equivalent circuit in the lumped parameter system including capacitor, resistor and coil. The step response of the equivalent circuit model was calculated using SPICE processing system, which is the electric circuit simulation software. Comparing the resulting from a step change in the supply of fluidized particle and step response of the equivalent circuit model of fluidized bed's downer, a good agreement has been obtained. The potential of modeling the flow conditions of a fluidized bed by an equivalent electric circuit is shown.

ACKNOWLEDGMENT

This study is supported by the New Energy and Industrial Technology Development Organization (NEDO).

REFERENCES

[1] Marek Turowski, Zhijian Chen and Andrzej Przekwas. Automated Generation of Compact Models for Fluidic Microsystems. Analog Integrated Circuits and Signal Processing, 29:27-36 (2011)

[2] Aveek N. Chatterjee and N. R. Aluru. Combined Circuit/Device Modeling and Simulation of Integrated Microfluidic Systems. Journal of Microelectromecanical Systems, 14(1): 81-95 (2005)

[3] Kwang W. Oh, Kangsun Lee, Byungwook Ahn and Edward P. Furlani. Design of pressure-driven microfluidic networks using electric circuit analogy. Lab on a Chip, 12:515-545 (2012)

[4] Todd Thorsen, Sebastian J. Maerkl and Stephen R. Quake. Microfluidic Large-Scale Integration. Science 298:580-584 (2002)

[5] Eric W. Lam and Gregory A. Cooksey. Microfluidic Circuits with tunable flow resistances. Applied Physics Letters 89:164105 (2006)

[6] H. Takao, M. Sugiura, M. Ishida, K. Terao, T. Suzuki, F. Shimokawa, F. Oohira. Micro fluidic circuit design with "spice" simulation. Proc. IEEE MEMS 2011:1154-1157, Jan. 23-27, Cancun, Mexico (2011)

[7] Guoqin Guan, Chihiro Fushimi, Atsushi Tsutsumi. Prediction of flow behavior of the riser in a novel high solids flux circulating fluidized bed for steam gasification of coal or biomass. Chemical Engineering Journal 164: 221-229 (2010).

Bioelectricity from Plant Microbial Fuel Cell

M. A. Moqsud* and J. Yoshitake

Department of Civil and Environmental Engineering, Yamaguchi University, Japan
*e-mail: azizul@yamaguchi-u.ac.jp

Abstract

In this study, a novel investigation has been carried out to produce green energy (mainly bioelectricity) by using paddy plant microbial fuel cell and soil mixed with compost in Japan. Six buckets full of same soil were used with carbon fiber as the electrodes for the test. In five buckets, the rice plants were planted and another bucket was kept without rice plant, however, the external resistance of 100 ohm was used for all cases. It was observed that the cell with rice plant and compost mixed showed the higher value of voltage with time. The peak value of voltage showed around 700 mV with rice plant with 3% compost however it was around 90% lower in the case of without rice plant.

INTRODUCTION

Microbial fuel cells (MFCs) are bio-electrochemical transducers that convert microbial reducing power (generated by the metabolism of microorganisms), into electrical energy [1-4]. They use the available substrates from renewable sources and convert them into harmless by-products with simultaneous production of electricity [4-5]. Attempts have been made to apply MFC systems to recover electric power from marine and river beds (termed sediment MFC or benthic MFC) [6-7]. These systems utilize the natural potential gradient between the sediment and upper oxic water, and electrons released by the microbial oxidation of organic matter flow from the anode to cathode through an external circuit. Although the power output from SMFCs is moderate, such levels of output are considered to be sufficient to serve as remote power source in aquatic environments. Plant MFCs with living plants are also a way to get green energy [8]. In PMFCs, plant roots directly fuel the electrochemically active bacteria at the anode by excreting rhizodeposits [6, 8-10]. A paddy field is a flooded parcel of arable land used for growing rice and other semiaquatic crops. In Japan, rice paddy fields cover 2.5 million ha and occupy more than 50% of the total arable land areas in this country (Ministry of Agriculture, Forestry and Fisheries 2006). When a paddy field is flooded, the soil immediately below the surface becomes anaerobic [11] and a community of anaerobic microbiota (comprised mainly sulfate-reducing bacteria, iron-reducing bacteria, fermenting bacteria and methanogenic archaea) is established [12-13]. Since a potential gradient is known to be formed between the soil and the flooded water, it was anticipated that an SMFC system could operate in a paddy field. Rice MFC is an ecological solar cell in which plant photosysthesis is coupled to the microbial conversion of organics into electricity. Resource recovery as bio-electricity from waste material is a burning question now-a-days both in the developed countries as well as developing countries. Again, the annual organic waste generated from the food industry and kitchen garbage in Japan is about 20 million tons per year [5]. Most of this waste is directly incinerated with other combustible waste, and the residual ash is disposed of in landfills. However, incineration of this water-containing waste is energy-consuming and results in the production of dioxins. Instead of considering the organic waste as waste, it should be considered as valuable biomass for resource recovery. The scarce of electricity is one of the major hinders for development of many countries. Depletion of energy reserves, global warming and the concern of environmental pollution are inspiring the search for new environment-friendly and sustainable energy production methods all over the world. Moreover, the recent Fukushima nuclear power plant accident in Japan after the east Japan earth quake and tsunami has become a great concern to find the alternate source of electricity rather than the traditional one. Both in developing countries and the industrialized countries people are trying to find a way how to collect the maximum recovery of resource from the unwanted or discarded materials. On the other hand, according to united nation's statistics, around 1.6 billion people are living without electricity in the current world. In some developing countries, they can provide half of the demand of the electricity. The scarce of electricity is one of the major hinders for development for many nations. Again, from the characteristics analysis of the solid waste of most of the developing countries, it is found that the major portion (more than 80%) of the total solid waste is comprising of organic waste which is not usually get much attention for recycling or resource recovery. This unmanaged organic waste causes environmental pollution and consequently affects the public health. So the objective of this study is to evaluate or compare of bio-electricity generation by reusing the compost with soil so that this organic waste can be recycled as well as give some sorts of solution to the electricity scarce population in paddy microbial fuel cell.

MATERIALS AND METHODS

A. *Laboratory tests*

Fig. 1 shows the set up for the laboratory tests. A 10 liter capacity plastic bucket was used for the rice MFC in the laboratory for electricity generation experiments during the rice cropping season (from June to September) in 2012 in Yamaguchi University campus, Japan. The soil of the experiment was collected from Yamaguchi prefecture, Japan and classified as Onoda soil (Density of soil particle 2.712, pH 7.81, and Organic matter content 7.5 %). The rice plants were planted on that soil. The rice plants which were used in the experiment are same rice plants which are famous brand rice for Yamaguchi Prefecture in Honshu Island, Japan. Carbon fiber (Toray Industries, Inc. Tokyo**)** was used for both anode and cathode. The anode was set approximately 5cm below the surface of the soil, while the cathode was placed immediately above the soil surface but under the water. These electrodes were connected via epoxy-encapsulated wires, and the circuit was completed using an external resister of 100 ohm. The voltage across the resister was monitored by the voltmeter everyday at 11 am. A bucket (No. 6 in Fig.1) of same capacity was also prepared for the same setup except the rice plant for comparing the electricity generation with rice plant or without rice plants. Buckets 1, 2 and 5 are prepared with the same soil without mixing any compost/ organic fertilizer. Bucket 3 and bucket 4 are prepared with compost of 1% and 3% of the total soil. Fig. 1 illustrates the test set up for MFC for all the cases.

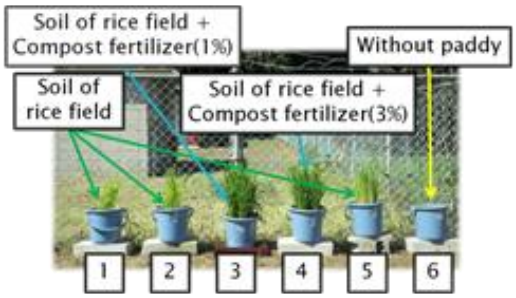

Fig. 1 Paddy Microbial Fuel Cells set up

Polarisation curves and power density-current curves were made by using different resisters and internal resistances and power densities were calculated as described elsewhere (Logan 2006). In brief, electrode output was measured in volts (*V*) against time. The current I in Amperes (*A*) was calculated using Ohm's law, $I = V/R$, where *V* is the measured voltage in volts (*V*) and R is the known value of the external load resistor in Ohms. From this it is possible to calculate the power output *P* in watts (*W*) of the MFCs by taking the product of the voltage and current i.e. $P = I \times V$. Current density was calculated using $I = V/aR$, where *a* is the electrode surface area. Figure 1 shows the test set up for the rice plant microbial fuel cell experiment.

Electrode output was measured in volts (*V*) against time. The current I in Amperes (*A*) was calculated using Ohm's law, $I = V/R$, where *V* is the measured voltage in volts (*V*) and R is the known value of the external load resistor in Ohms. From this it is possible to calculate the power output *P* in watts (*W*) of the MFCs by taking the product of the voltage and current i.e. $P = I \times V$. Current density was calculated using $I = V/aR$, where *a* is the electrode surface area.

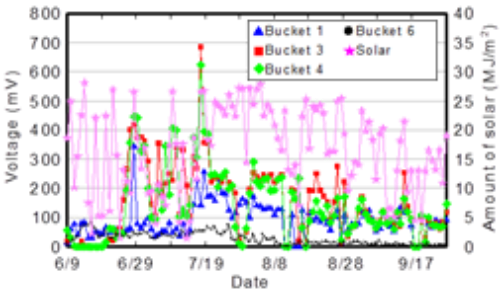

Fig. 2: Variation of voltage with duration and amount of solar radiation

RESULTS AND DISCUSSION

Fig. 2 illustrates the amount of voltage in rice PMFC in the soil. It is observed that the voltage value showed higher with paddy than without paddy. Plants continuously provide an input of organic matter to the soil throughout their plant life [4]. During growing season, organic carbon enters the soil as rhizodeposits. In rice paddies, rhizodeposition counts for 200kg organic C/ha crop cycle. In a flooded rice system, this substantial input of organic material is transformed into methane to the extent that rice agriculture worldwide contributes 7-20% of the total methane emission [9]. Rhizodepositton was shown to be the main origin of methane evolution in rice paddies, with a share of 25% from excudates and 75% from decomposing root residues. Next to being a source of greenhouse gases, these rhizospheric processes also represent a significant loss of energy from the rice system: rice plants lose substantial amount of trapped solar energy as rhizodeposition, while the gaseous end product of the anaerobic composition thereof, methane, has a high energetic value. It would most certainly be interesting to recuperate this flow of energy from living plants, as it represents a true source of green energy. The maximun voltage generated in our study was around 700 mV in PMFC with rice plant. The voltage increased gradually and then it became constant and finally it started to decrease when the rice plants ready to harvest. The voltage generation for the case of without paddy was almost constant. The small amount of voltage was generated due to the potential

difference between anode and cathod and also probably the organic matter decomposition phenomenon in the soil.

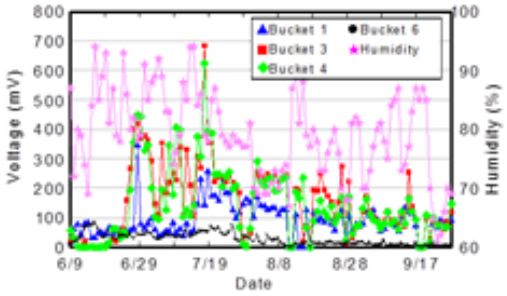

Fig. 3: Variation of voltage with duration and humidity of the Air

Fig. 3 illustrates the variation of voltage with duration and humidity. It is observed that there is no such relation of humidity and voltage generation for all the cases; however, a small variation was observed during the initial stage of the experiment. Bucket 3 and 5 (with compost) shows higher value of voltage with the higher amount of humidity. However, after the crops began to bloom the similarity did not so prominent.

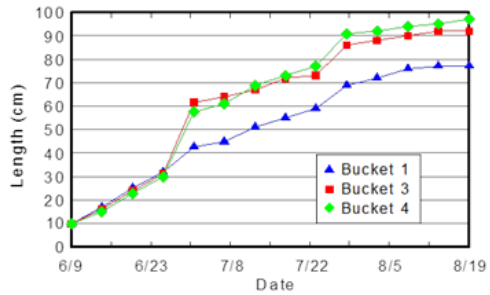

Fig. 4: Variation of length of the paddy plant with time

Fig. 4 illustrates the growth of the rice plant in different weeks. It is observed that the growth of the rice plant was quite satisfactory. The size of rice plant when it was planting was around 10 cm but within 4 weeks it grows around 60 cm. The final size of the rice was quite similar with the final size of the rice plant in the real paddy field in Yamaguchi area. So it is proved that the additional electricity generation did not have any effects to the growth of the rice plants. So, we do not need to destroy any food product (like corn and soybean for bio-fuels) to get bio-electricity from plant MFC. On the otherhand, when the compost was mixed with soil, the growth of the rice plants was very fast and also became bigger than the paddy plant without compost fertilizer.

Fig. 5 shows the polarization curve of the MFC by using PMFC. A polarization curve is used to characterize current as a function of voltage. The polarization curve shows how well the MFC maintains a voltage as a function of the current production. This polarization curve in Fig. 5 was created on August, 23rd from bucket no. 4. The trend of the polarization curve was very much similar with the polarization curve which was stated in other literature of MFC [14-16].

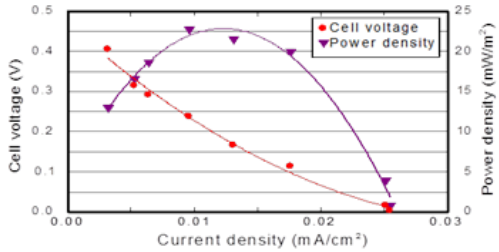

Fig. 5 Polarization curve in PMFC test

CONCLUSION

In this study, MFC method was used for the bio-electricity generation by using the rice plant in the soil and compost fertilizer. The voltage generation in this PMFC is around 700 mV with the rice plant. This amount of voltage is satisfactory and almost 5 times higher than previous reported result. The growth of the rice was also reasonable and maximum length was around 90-100 cm. So the additional bio-electricity harvesting did not give any bad influence to the growth of the plant life. The paddy MFC can be used for the bio-electricity generation both in the developed country as well as electricity inadequate developing countries.

The organic waste can be recycled as compost generation and can be used for enhancing the voltage generation in paddy MFC. The PMFCs by using compost is proved to be a good way to green electricity generation as well as the recycle of organic waste to maintain the healthy and pollution free environment. Though the amount of electricity is smaller in PMFC by using compost, however, it is very much needed for the future green energy era as we should not needlessly damage any food products for bio-energy as we used to do bio-ethanol or biodiesel from corn and soybean in the background of millions of people in the world cannot get food every day.

ACKNOWLEDGMENT

The authors acknowledge the helps of Mrs. Yamada for the soil and the paddy collection. The authors also wish to acknowledge the financial support by Grant-in-Aid for Scientific Research (21360227, 23656299) from Japan Society for the Promotion of Science and JST revitalization promotion program (A-step) (241FT0057).

REFERENCES

[1] Allen RM, Bennetto HP. Microbial Fuel cells. Electricity production from carbohydrates. *Journal of Applied Biochemistry and Biotechnology*. 1993, Vol. 39-40, pp. 27-40.

[2] Bennetto HP. Microbial fuel cells. In: Life chemistry reports. London: Harwood Academic; 1984. pp. 365-453.
[3] Logan, BE and Regan, JM. Electricity producing bacterial communities in microbial fuel cells. Trend Microbiology. 2006, Vol. 14, pp. 512-518.
[4] Moqsud, MA, Omine, KN Yasufuku. A Comparison Study of Bio-electricity Generation by Using Kitchen Garbage and Bamboo Waste in Microbial Fuel Cell. *Proceedings of the 27th International Conference on Solid Waste Technology and Management,* 11-14th March, 2012, Philadelphia, USA, 1052-1061.
[5] Moqsud, M.A., Omine, K. and Yasufuku, N. Bio-electricity Generation by Using Rice Plant Microbial Fuel Cell in Ariake clay. The 47th Japanese geotechnical society annual conference. 14-16 July, 2012, Hachinohe, Japan, pp. 440-445.
[6] De Schamphelaire et al. Microbial fuel cells generating electricity from rhizodeposits of rice plants. Environmental science and Technology. 2008. Vol. 42.pp. 3053-3058.
[7] Moqsud, M. A. and Omine, K. Green energy from bamboo by Microbial fuel cell. Proceedings of the 2nd International conference on environmental aspects of Bangladesh, 10-11th September, 2011, Kitakyushu, Japan, 145-149.
[8] Strik,D. et al. Green electricity production with living plants and bacteria in a fuel cell. International Journal of energy research. 2008, Vol. 32,pp. 870-876.
[9] Kaku, N,Yonezawa, N, Kodama, Y and Watanabe, K Plant/microbe cooperation for electricity generation in a rice paddy field. Applied Microbiology and Biotechnology, 2008, Vol. 10, pp. 1007-1014.
[10] Helder M et al. Concurrent bio-electricity and biomass production in three plant-microbial fuel cells using Spartina anglica, Arundinella anomala and Arundo donax. Bioresource Technology. 2010. Vol. 101,pp. 3541-3547.
[11] Takai Y . The mechanism of reduction in paddy soil. Japan Agriculture Research. 1969, Vol. 4, pp. 20-23.
[12] Chin KJ, Hahn D, Hengstmann U, Liesack W, Janssen PH . Characterization and identification of numerically abundant culturable bacteria from the anoxic bulk soil of rice paddy microcosm. Applied Environmental Microbiology. 1999. Vol. 65, pp. 5042-5049.
[13] Grosskopf R, Janssen PH, Leisack W. Diversity and structure of the methanogenic community in anoxic rice paddy soil microbes as examined by cultivation and direct 16S rRNA gene sequence retrieval. Applied Environmental Microbiology. 1998, Vol.64, pp. 960-969.
[14] Ishii S, Hotta Y, Watanabe K (2008). Methanogenesis versus electrogenesis: morphological and phylogenetic comparisons of microbial communities. Biosci Biotechnology Biochemistry. Vol. 72, pp. 286-294.
[15] Satoh A, Watanabe M, Ueki A and Ueki K. Physiological properties and phylogenetic affiliations of anaerobic bacteria isolated from roots of rice plants cultivated on a paddy field. Anaerobe. 2002, Vol. 8,pp. 233-246.
[16] Strik,D., Timmers, R.,Helder, M.,Steinbusch,J.J.K., Hameters, H. and Buisman, J.N. .Microbial solar cells: applying photosysthetic and electrochemically active organisms. Trends in Biotechnology, 2011, Vol.29, No.1, pp. 41-49.
[17] Timmers, R.A et al. Long term performance of a plant microbial fuel cell with Spartina anglica. Applied Microbiology and Biotechnology. 2010.Vol.86, pp 973-981.

Study on Adsorption Cooling System - Fundamental to System Evaluation

T Miyazaki*, Il EL-Sharkawy, BB Saha, and S Koyama

Faculty of Engineering Sciences, Kyushu University, Japan
International Institute for Carbon-Neutral Energy Research, Kyushu University, Japan
*e-mail: tmiyazak@kyudai.jp

Abstract

The main feature of adsorption cooling technology is its ability to deliver cooling energy utilizing low-temperature levels thermal energy. Generally, hot water produced by solar thermal collector, heat output from cogeneration system, or low temperature waste heat from industrial processes is converted to chilled water of around 10 °C. The system is energy conservative because it recovers low-grade thermal energy to produce a useful output. On the other hand, the system tends to be bulky mainly because of low energy intensity of the low grade thermal energy. The goal of our study is to develop an innovative adsorption cooling system achieving improvement in adsorption uptake and kinetics, and optimum system design. In this paper, outline of our research activities is briefly summarized.

INTRODUCTION

Adsorption cooling is a technology that converts the low-grade thermal energy to a useful cooling. Generally, hot water produced by solar thermal collector, heat output from cogeneration system, or low temperature waste heat from industrial processes is converted to chilled water of around 10 °C. The system is energy-saving because it recovers low-grade thermal energy to produce a useful output.

In addition, these systems have the advantages of their simplicity in construction and operation and almost no electricity usage. It is also possible to use environmentally benign refrigerants such as water, ethanol and methanol. On the other hand, the system tends to be bulky mainly because of low energy intensity of the low grade thermal energy. When low temperature heat source is used as a driving energy input, heat sink temperature should be as low as possible to increase its performance theoretically. Under a present status, the systems of 10 kW refrigeration capacity to more than 100 kW refrigeration capacity are commercialized, and these systems use cooling water as lower temperature heat sink, and it causes large footprint of the system also. To apply the adsorption cooling system to room air-conditioning or automobile air conditioning, the air-cooling technology is necessary.

The main goal of our studies is to develop innovative adsorption cooling systems to expand application field of adsorption cooling technology. Our research activities aim to improve the fundamentals of adsorption characteristics of adsorbent-refrigerant pairs in terms of adsorption capacity and kinetics. Design and development of compact heat exchangers is also another topic of our ongoing research activities. In this paper, our research topics, which spans from theoretical analysis to system evaluation, are outlined.

ADSORPTION COOLING SYSTEMS

A general structure of adsorption cooling systems is depicted in Fig.1. It consists of two pairs of adsorber-phase change heat exchanger. During one of the pairs is working under evaporation-adsorption process, another pair is working under desorption-condensation process. After a certain time, the processes are switched and next evaporation-adsorption and desorption-condensation processes starts. By this alternating operation, chilled water is generated continuously at the evaporator.

A typical adsorbent-refrigerant pair was silica gel-water [1], but recently, a low temperature regeneration type zeolite become more popular as adsorbent of adsorption cooling system combined with water refrigerant. For heat pump application, carbon-ammonia pair is also mainly studied [2]. For ice making application, ethanol [3-4] or methanol is generally used as refrigerant [5]. As a combination with activated carbon, CO_2, HCFC, HFC and HFO refrigerants are also investigated [6-9].

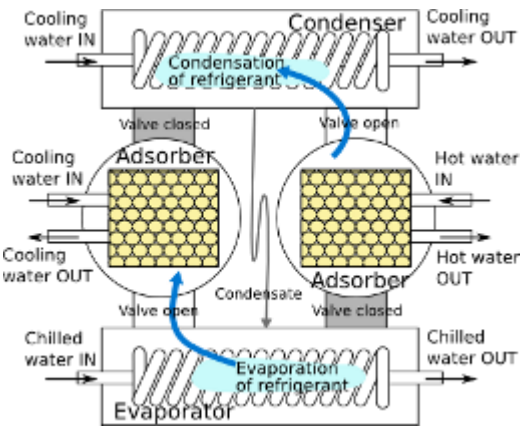

Fig. 1. A general structure of adsorption cooling system.

ADSORPTION EQUILIBRIUM AND KINETICS

The performance of the adsorption cooling system is dominated by adsorption equilibrium and kinetics. One of our main studies is to characterize the adsorbent-refrigerant pair from the viewpoint of effective adsorption, which is the difference of adsorption uptake between adsorption and desorption under equilibrium basis, and adsorption speed. Figs. 2, 3 and 4 show adsorption isotherms of three different refrigerants, ethanol, R32, and R1234ze(E), respectively, onto activated carbon powder (Maxsorb III). R32 and R1234ze are a group of HFC refrigerants but global warming potential is small enough compared with conventional HFCs. Especially, R1234ze has an extremely small global warming potential, which is 6.

It is shown that activated carbon has a large adsorption capacity against ethanol and HFC refrigerant. The performance of the adsorption cooling system using these refrigerants will have a large difference between ethanol and HFCs because of the thermophysical properties of refrigerants as well as operating conditions of adsorption cycles.

Ethanol has larger evaporation heat compared with HFCs, which results in better coefficient of performance (COP). On the other hand, adsorption speed of HFC refrigerants will be much faster than ethanol under temperature conditions of cooling application. It means that switching time of adsorption and desorption can be shortened and cooling power can be increased. Another advantage of HFC refrigerants is volume capacity of refrigerant. They have much larger vapor density compared with ethanol, and therefore, compact design of heat exchanger and pipelines is feasible.

Detailed performance of these adsorbent-refrigerant pair will be provided by thermodynamic analysis and dynamic simulation of the system.

THERMODYNAMIC ANALYSIS

Thermodynamic diagrams are useful to analyze theoretical performances of any system based on thermodynamic cycles. Adsorption cycles can be analyzed using a so-called Dühring diagram, which is a P-T diagram with adsorption isochores. Fig. 5 shows an example of Dühring diagram for Maxsorb III-ethanol pair. The figure shows a conventional two-bed adsorption cycle and a two-stage evaporation type adsorption cycle, which is proposed by our group [10]. The two-stage evaporation cycle can be effectively realized by three adsorption bed configuration. The COP of the system can be improved because the effective adsorption is enhanced under the fixed temperature shift.

Another example of adsorption cycle analysis using a Dühring diagram is given in Fig.6. The figure shows the Dühring diagram on Maxsorb III-R32 pair. The adsorption cycle on the Dühring diagram showed a large difference between maximum and minimum adsorption with the regeneration temperature of 120ºC. Therefore, it is possible to use internal heat recovery for pre-heating of the adsorption bed. In this case, COP exceeds 0.3 and the improvement ratio was by more than 40%.

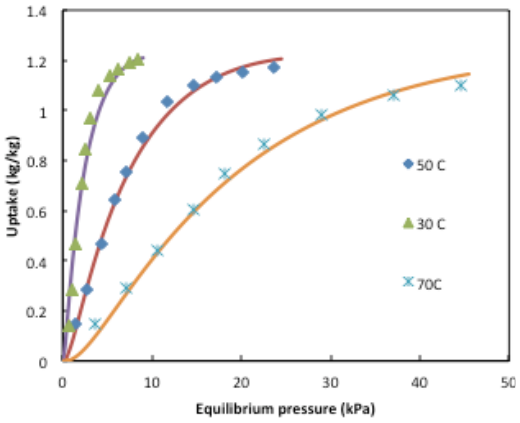

Fig. 2. Adsorption uptake of ethanol onto Maxsorb III.

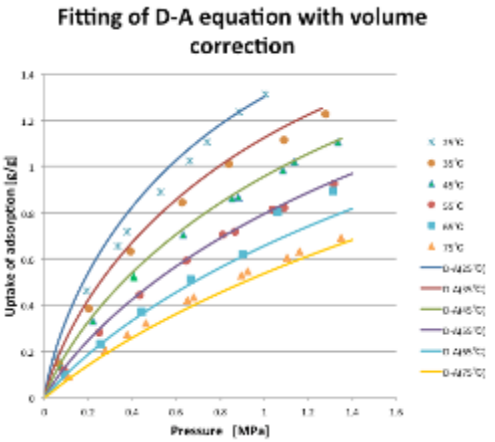

Fig. 3. Adsorption uptake of R32 onto Maxsorb III.

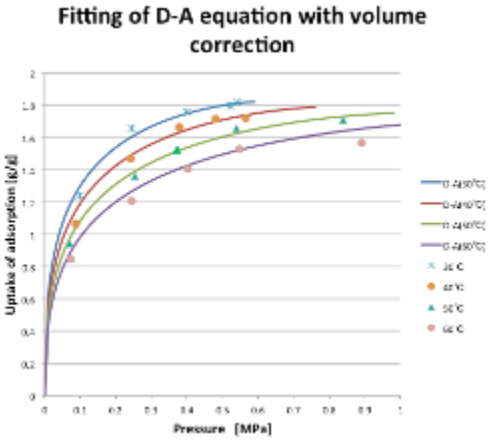

Fig. 4. Adsorption uptake of R1234ze onto Maxsorb III.

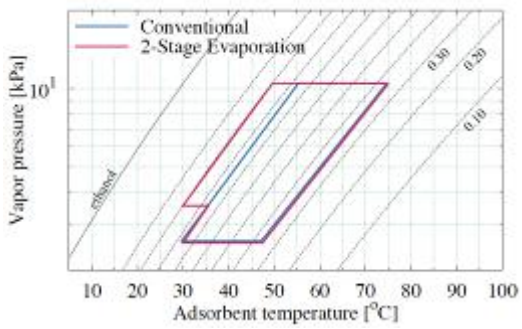

Fig. 5. Dühring diagram of Maxsorb III-ethanol pair and comparison of adsorption cycles.

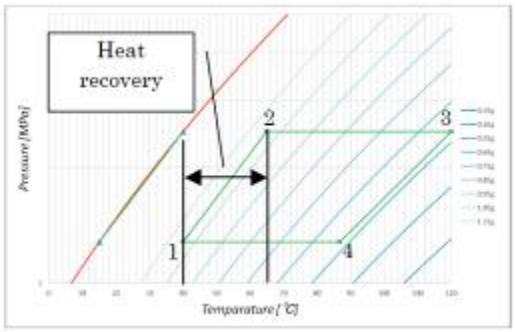

Fig. 6. Dühring diagram of Maxsorb III-R32 with single adsorption heat pump cycle at T_{vap}=15ºC T_{ads}=40ºC, T_{des}=120ºC.

DYNAMIC SIMULATION AND CYCLE OPTIMIZATION

Thermodynamic analysis reveals a theoretical performance of adsorption cooling cycle, while performance of actual machines can be predicted by dynamic simulation. Since transitional stage of adsorption/desorption switching causes large heat losses, the COP of actual machine is significantly affected by switching time of adsorption and desorption. Moreover, the switching process, usually it is called pre-heating/cooling process, requires a certain length of time, like 30-60s, to change the temperature and pressure levels of adsorbers, the length of the switching period also affects the performance of adsorption cooling systems. As a result, the optimization of cycle time, which consists of adsorption and desorption time and pre-heating and pre-cooling time, is essential to attain the best performance of adsorption cooling system. The optimization is more important and more difficult with advanced cycles, such as heat recovery cycles, because the number of parameters to optimize increase, and straightforward method is too time consuming.

A method to facilitate to find the global optimum of adsorption cooling system operation was proposed by our group using a meta-heuristics [11]. Particle swarm optimization (PSO) is an optimization method that mimics a flock of birds or school of fish [12]. A set of particles searches the optimal solution with interactive exchange of their experiences between neighbor particles. In our study, the PSO was successfully applied to the optimization of cycle time.

Fig. 7 shows the flow chart of the optimization. The PSO starts the calculation with random values for all particles. In each generation, the particles evaluate the objective function, and move to a better position by update equations. The PSO algorithm manipulates the values of the independent variables as input data to the cycle simulation program of the adsorption heat pump. The cycle simulation program performs the simulation using input values and boundary conditions, and outputs the performance indices such as SCP, COP and chilled water temperature. The PSO algorithm obtains these output values for the evaluation of the objective function and of the constraints. The PSO runs the simulation for all particles with different independent variable values. The process repeats for generations until the convergence criterion is satisfied.

By this optimization, the optimum cycle time settings for different heat source temperature, different heat capacity of the adsorbers were revealed. It was found that the effect of optimization was significant when lower driving temperature conditions because the adsorption rate is more critical under small driving force.

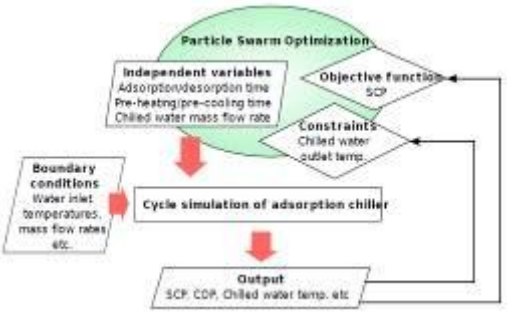

Fig. 7. Optimization of adsorption cooling system using a global optimization method (Particle Swarm Optimization).

EVALUATION OF SYSTEM PERFORMANCE

One of the main advantages of the adsorption cooling system is waste heat driven. Therefore, it is necessary to evaluate the total system such as a cogenerator and a waste heat driven chiller. We have evaluated a cogeneration system with adsorption chiller for office buildings. In office buildings, chillers will work at partial load conditions for most of the operating period because of the seasonal and hourly variation of cooling demand. Here, the optimization method was applied to improve the partial load condition of the adsorption chiller.

Fig.8 illustrates performance characteristics of adsorption chiller. The cooling capacity can be maximized at the optimum adsorption/desorption time. On the other hand, the COP will increase toward a theoretical COP with longer adsorption/desorption time. Therefore, by the control of adsorption/desorption time, the adsorption chiller can reduce the cooling output with improving COP.

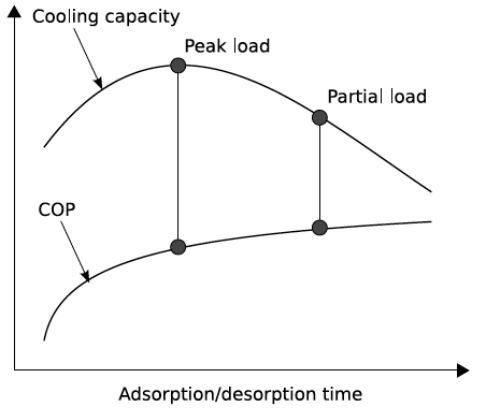

Fig. 8. Performance characteristics of adsorption chiller.

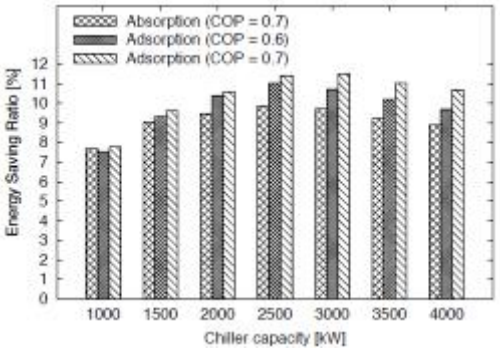

Fig. 9. Evaluation of energy saving ratio of a gas engine cogeneration system for office building. Energy saving ratio as a function of waste heat driven chiller capacity [13].

A gas engine cogeneration system for office building was evaluated and it was shown that by the optimized adsorption chiller with COP of 0.6 results in a larger energy saving ratio compared with absorption chiller with COP of 0.7 under a certain demand conditions (Fig. 9) This is because of the improved partial load COP.

SUMMARY

This paper presented an outline of our researches related with adsorption cooling systems, from fundamental adsorption characteristics to system optimization.

ACKNOWLEDGMENT

We would like to thank Japan Science and Technology Agency (JST), CREST for partially supporting our research activities on adsorption cooling systems.

REFERENCES

[1] K. Chihara and M. Suzuki, J. Chem. Eng. Jpn., 16 (1983), pp. 293-299.
[2] Tamainot-Telto et al., Int. J. Refrig. 32 (2009), pp. 1212-1229.
[3] B.B. Saha et al., Int. J. Refrig. 30 (2007), pp. 86-95.
[4] B.B. Saha et al., Int. J. Refrig. 30 (2007), pp. 96-102.
[5] I.I. El-Sharkawy et al., Int. J. Refrig. 32 (2009), pp. 1579-1586.
[6] B.B. Saha et al., Int. J. Refrig. 32 (2009), pp. 1563-1569.
[7] B. Choudhury et al., Applied Energy 104 (2013), pp. 554-567.
[8] S. Jribi et al., Appl. Therm. Eng. 50 (2012), pp. 1570-1575.
[9] B.B. Saha et al., J. Chem. Eng. Data 56 (2011), pp. 1974-1981.
[10] T. Miyazaki, A. Akisawa, B.B. Saha, Int. J. Refrig. 33 (2010), pp. 276-285.
[11] T. Miyazaki, A. Akisawa, Applied Thermal Engineering 29 (2009), pp. 2708-2717.
[12] J. Kennedy, R.C. Eberhart, Swarm Intelligence, Academic Press, 2001.
[13] T. Miyazaki et al., International Sorption Heat Pump Conference (ISHPC2008), 2008.

Fuel Efficient Strategies for Stopping a Car at the Signalized Intersections

Md. Abdus Samad Kamal*[1] and Md. Tawhidul Islam Khan[2]

[1*]Institute of Industrial Science, The University of Tokyo, Japan; *e*-mail: maskamal@ieee.org
[2]Graduate School of Science and Engineering, Saga University, Japan.

Abstract

Steady driving of a car is often interrupted by red traffic signal at intersections on urban roads. Avoiding aggressive braking to utilize kinetic energy of a car before stopping it at a red signal is one of the rules for eco-driving. This paper presents a simple method to determine the desired deceleration strategy of an individual car that minimizes the fuel consumption during stops. A simple experiment was conducted to determine the engine fuel cutoff period and the corresponding deceleration model of the car. Based on the deceleration model, the optimal stopping strategy in terms of speed-distance map is constructed. This map can be used to train the driver for eco-driving, or to develop an online eco-driving assistance system specific to that car. The proposed stopping strategy is numerically tested and estimated fuel consumption of the car is compared with traditional driving for an example case. Significant improvement in fuel consumption is confirmed from the test result.

INTRODUCTION

Driving style has a great influence on vehicle emissions and energy consumption. Eco-driving represents a driving culture to reduce extra fuel consumption of a car to travel the same distance by following some rules which suit to modern car engines and makes best use of advanced vehicle technologies [1, 2]. Most important rule for eco-driving is to drive a car steadily. However, in the traditional traffic control paradigm traffic flows at intersections are regulated by traffic lights or signs that restrict smooth drive of a car and increase inconveniences of frequent stops and idling. Frequent stops at the intersections are also a major cause of extra fuel consumption in a trip. In the United States, it is estimated that idling at intersections on urban roads alone costs about 2.8 billion Gallons of fuel each year [3], and about 7 percent of total trip fuel is wasted on signalized intersections due to slowing down and even stopping [4].

Extra fuel consumed at a red signal is often associated with slowing down to a stop, idling till the signal changes to green and the speeding up to the desired speed. When a car is braked at a high speed, its kinetic energy is wasted away as heat. However, if the car slows down smoothly without the brake pressed, its kinetic energy can be utilized. The modern engines have the feature of fuel cutoff mode, which may occur when the car is decelerating with no throttle input (accelerator pedal is not pressed) from a driver. During the fuel cutoff mode, the engine pumps air through the exhaust system rather than exhaust gas. Therefore, the engine also acts as a brake in addition to other resistance forces, e.g., aerodynamic drag, rolling friction. Depending on the engine characteristics of a car, the fuel cutoff period and corresponding braking rate differ. The optimal strategy for stopping a car is to move effortlessly and smoothly without further use of propelling power. Approaching slowly to the intersection ensures reuse of the kinetic energy during fuel cutoff that also reduces idling time and idling consumption.

This paper presents a very simple experimental method to determine the engine fuel cutoff period of a car with automatic transmission system and derives the optimal speed profile of the car approaching an intersection with red signal that maximizes fuel efficiency. More specifically, by analyzing the speed profile of a freely decelerating car, its deceleration model is approximated. Based on the decelerating model, the critical distance to release the throttle and brake at various speed are determined. An example of eco-driving strategy is illustrated for the case that the red signal appears when the car is closer than the critical distance. The proposed eco-driving strategy is compared with the traditional way of stopping a car at the red signal. The concept of determining the optimal speed profile of an individual car is simple but very useful. A driver can have the exact information about the critical distance to decelerate his car for eco-driving. The estimated speed-distance map can also be used in the online eco-driving assistance system.

FUEL CONSUMPTION IN A CAR

This section reviews fuel consumption characteristics of a car as given in [5] in order to understand the eco-driving principles. Normally, once an engine is started, it continues to rotate until its switch is turned off. Even when the accelerator is not pressed at idling, fuel is automatically injected to rotate the engine at a marginal speed. Fuel consumption of a car depends on torque, the twisting or rotating force that the engine exerts on the crankshaft, and rotational speed (given in round per minute or rpm) of the engine [6]. The typical engine torque-speed characteristic curves of a car are shown

in Fig. 1. The constant efficiency of the engine is shown by the elliptical curves. The constant power curves in the map are obtained by the torque and the rotational speed of the engine.

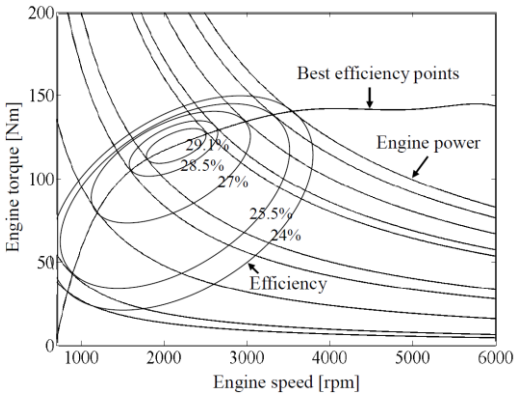

Fig. 1. Engine torque-speed characteristic map including constant power and efficiency curves. The best efficiency line shows the operating point of a continuous vector transmission system [5].

The mechanical power output of a car at any operating conditions can also be approximated from the car motion. The total resistance force I (N) acting on the car in terms of speed v (m/s) and acceleration a (m/s^2) is given by

$$F = \frac{1}{2}C_D\rho_a A_V v^2 + \mu Mg\cos(\theta(x)) + Mg\sin(\theta(x)) + Ma, \quad (1)$$

where C_D, A_V, μ, and θ are the drag coefficient, the air density, the frontal area of the vehicle, the rolling resistance coefficient, and the road slope angle as a function of location x, respectively. The energy consumption per second or the power required to overcome the resistance forces can be expressed as

$$P = Fv + P_c \quad (2)$$

where P_c is the power required to run the engine when the car is idling. This power, in terms of both speed and acceleration of the car, is related to the constant power curves in the engine characteristics map.

The rules for fuel efficient driving can be understood from the engine torque-speed curves and above equations. The shape of the torque curve and the range of the engine rpm at which driving power is obtained are also very important. If the car is manually driven, then excessive rpm of the engine should be avoided by quickly shifting the gears. As the rmp increases beyond some value the engine efficiency decreases. In automatic transmission (AT) systems, the gear is changed in steps to closely match with the best efficiency curves, and the driver has no choice over it. In the continuous vector transmission (CVT) system, the gear is changed continuously to keep the engine running on the best operating points.

It is desired that the engine should be operated in the high efficiency region, as shown in the map, which corresponds to some moderate driving power. In the case of steady speed, desired range is about 40-70 km/h depending on the engine. At very low or at very high steady speed the engine is not much efficient. If the car accelerates when its speed is high or run over the road with sharp up slope, the required driving power becomes very high that also drops the engine efficiency significantly. Therefore, moderate acceleration is recommended only when the car starts from standstill, and acceleration should be gradually decreased as the car approaches the steady desired speed.

The rule for fuel efficient braking due to a red signal at the intersection is different. The modern engines have the features of fuel cutoff mode which may occur when the car is decelerating with no throttle input from a driver. Some engine also system includes a fuel cutoff module and a cylinder deactivation module. The fuel cutoff module generates a fuel cutoff signal when a deceleration fuel cutoff condition occurs, wherein fueling to some cylinders of an engine is disabled based on the fuel cutoff signal. During the fuel cutoff mode, the engine pumps air through the exhaust system rather than exhaust gas. Therefore, the engine also acts as a brake in addition to other resistance forces, e.g, aerodynamic drag, rolling friction. Depending on the engine characteristics of a car and some other factors, the fuel cutoff period and corresponding braking rate differ. The optimal strategy for stopping a car is to move effortlessly and smoothly without further use of propelling power, i.e., without pressing the accelerator. Approaching slowly to the intersection ensure reuse of the kinetic energy during fuel cutoff that also reduces the idling time and idling consumption. The next section describes an experimental approach to determine the engine cutoff period and the corresponding deceleration model of a car.

EXPERIMENTAL OBSERVATION

The standard fuel consumption rate of a new car tested on a certain drive cycle is provided by the manufacturer. As a car gets older, the engine efficiency is deteriorated gradually. Although the exact consumption rate of a car cannot be estimated easily, the fuel cutoff period of a car can be estimated with little effort, which is described here. An about 9 years old Kei-Car, Subaru Pleo, was used in this experiment. A small video camera was mounted near the steering wheel in such a way that the speedometer of the car could be captured fully. The experiment was conducted by the author in a flat road without interfere of traffic signals or other vehicles, in Fukuoka City, Japan. When the car was run at a steady speed within the range 50-70 km/h,

the accelerator pedal was released and the driver's voice ``START'' was recorded to mark the start time of observation. The car gradually decelerated without pressing the brake to a speed of about 10 km/h, and the observation was closed with another voice of the driver ``END''. In a similar way, several tests were recorded on various road sections.

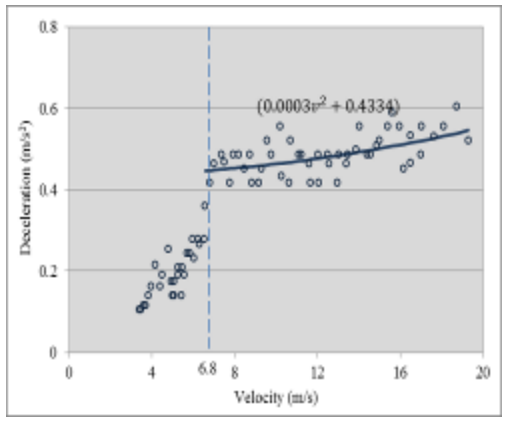

Fig. 2. The rates of deceleration plotted against the speed when the test car is freely running without throttle input or brake. The end of fuel cutoff speed is marked by the dotted vertical line below which the deceleration rate reduced significantly. The solid curve shows the approximated deceleration rate during fuel cutoff period.

Later these videos were played in slow motion and the speed of the car at each second was estimated manually. From these estimated data the rates of deceleration of the car at various speeds were computed. The needle deflection delay of the speedometer is ignored for simplicity. Fig. 2 shows the plot of deceleration rates of the car at various speeds without pressing the accelerator or brake by the driver. Due to manual estimation, acceleration data are a bit noisy. It is found that the rate of deceleration of the freely slowing car suddenly dropped at about 6.8 m/s (24.5 km/h) speed. This point is the approximate end of the engine cutoff point. Bellow this speed, the engine is automatically fueled to keep it rotating, although the driver does not press the accelerator.

Next, the deceleration rates at various speeds during the engine cutoff period, i.e., at speed above the 6.8 m/s, are estimated and plotted. Using the plotted data, a trend line of deceleration is obtained as shown in the figure. The engine cutoff deceleration rate b_{co} is approximated with the following relationship.

$$b_{co} = 0.0003v^2 + 0.4334. \quad (3)$$

This relationship is only valid for tested conditions on a flat and straight road with air-cooler off. If the air-cooler is on, the deceleration rate and cutoff point may be different, which needs to be experimented in the same way. Finally, including the effect of road gradient the acceleration rate (m/s^2) is approximated as follows.

$$a_{co} \approx -(0.0003v^2 + 0.4334 + g\sin\theta(x)), \quad (4)$$

where θ is the road gradient angle depending on the point x on the road, g is the Gravitational force.

FUEL EFFICIENT STOPPING STRATEGY

B. *Mapping of Critical Distance*

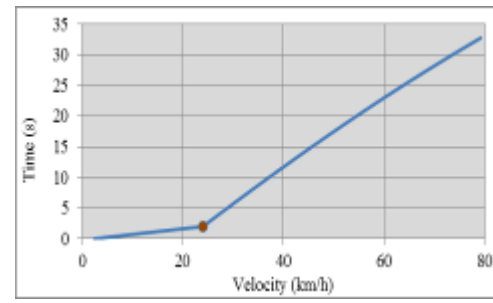

(a)

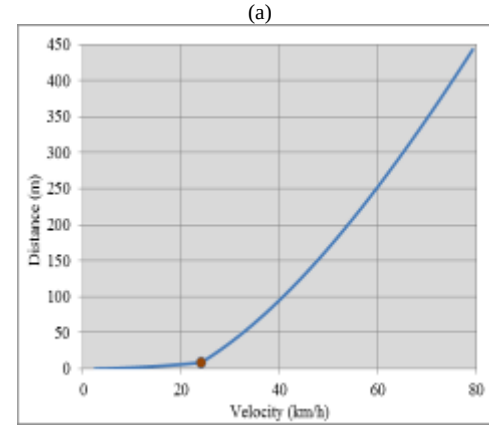

(b)

Fig. 3. The desired point of releasing the accelerator to activate engine cutoff during stopping phase at an intersection; (a) with respect to time, and (b) with respect to distance to the intersection.

The optimal strategy for stopping a car from its high speed state are to move effortlessly and smoothly without further use of propelling power, i.e. by releasing the accelerator and brake pedals during the fuel cutoff period, and finally apply the brake at the end of the cutoff period. This also minimizes the idling time of the car at the intersection, and reduces the idling consumption (if the engine is not stopped at idling). Therefore, the key point is to decide the critical distance to start the engine cutoff at the current speed of the car, i.e, timing of releasing the accelerator pedal that maximizes the running time without any fuel.

The ideal stopping pattern of the car is calculated using (4) and plotted in Fig. 3. The approximate time of releasing the accelerator pedal is given in Fig. 3 (a), and the approximate distance to the stopping point at the intersection is given in Fig. 3 (b). The

speed-distance relationship is more intuitive since the driver can see and estimate the distance. At any speed, the respective point on the curve states the critical distance from the stopping point at which the accelerator pedal should be released. For example, for maximizing the engine cutoff time the accelerator pedal of the car should be released at about 250 m and 100 m distance from the stopping point if its speed is 60 km/h and 40 km/h, respectively.

C. Eco-Driving Assistance

In the case a driver perceives a red signal from a distance longer than the critical one, the simplest way of eco-driving is to keep the current speed until the critical distance and then release the accelerator pedal. However, it is very likely that a red signal appears when a car is already closer to the intersection than the critical distance. In this case, the car should be braked moderately to a speed that matches the corresponding critical distance and then the accelerator pedal should be released.

Fig. 4 shows comparison of three stopping styles, Non-Eco (NEco), Eco, and Enhanced Eco (EEco) driving, for the same initial condition on a free road. At time t = 0 sec, the speed of the car is 60 km/h, distance from the intersection is 283 m, and the signal status is green. At t = 5 sec the signal turns into red and the remaining distance is only about 200 m, which is less than the critical distance at a speed of 60 km/h. At t = 35 the signal changes into green again, i.e., the red period has 30 sec duration. In the Non-Eco driving style, the car continues at the same speed and finally stops at about t = 13 sec at the intersection by applying the brake. The engine fuel cutoff is realized only for about 3.8 sec during braking from 60 to 24.5 km/h, and the car has to idle for about 15 sec at the intersection. In the case of Eco-driving, the car is braked moderately to catch up the desired speed-distance. Once its speed drops to 50km/h at a distance of 172 m, both the brake and accelerator pedals are released to maximize engine cutoff time, and finally stopped by braking.

Although, the actual signal changing time is unknown in advance, often it can be anticipated a few second early by the driver. More specifically, if the driver looks at the blinking signals for pedestrian, he can understand that the current green signal is going to turn soon. With such anticipative decision, the benefit of eco-driving can be enhanced further. EEco driving shows that the driver releases the accelerator 3 sec before the appearance of the red signals that increases the engine cutoff period of the vehicle. The fuel consumed by the car for the period of 35 sec is estimated as 11.37 ml 5.25 ml, and 3.19 ml for the case of NEco, Eco and EEco-driving, respectively. For this fuel estimation the fuel consumption formula and parameters of a typical car given in [5] is used.

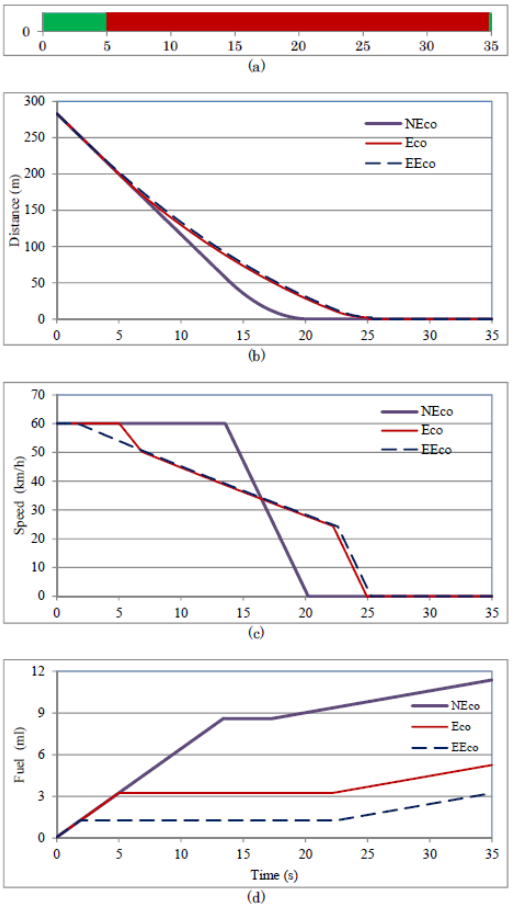

Fig. 4. Comparison of stopping styles at an intersection for the same situation by Non-Eco, Eco and Enhanced Eco-Driving of a car. (a) Status of traffic signal, green or red, (b) Distance from the intersection, (c) Speed of the car and (d) cumulative fuel consumption.

CONCLUSION

One of the eco-driving principles is to avoid aggressive braking and utilize kinetic energy of a car before stopping at an intersection due to a red signal. This paper has presented a simple experimental method to determine the optimal deceleration strategies of an individual car that minimizes the fuel consumption. By recording and analyzing the experimental driving data of a car, the engine fuel cutoff period and the corresponding rate of deceleration is approximated. Based on them, the desired stopping strategy in terms of speed versus critical distance is computed. Eco-driving based on this strategy is evaluated, and significant savings of fuel is observed compared with traditional driving in a simple stopping case of the car.

This speed-critical distance relationship is very simple to understand, and a driver can be trained for eco-driving of his own car. However, if the road has varying gradient, curvature or the car is loaded

differently, then the actual cutoff point needs to be computed. Such extension for an online assistance system will be studied in the future.

ACKNOWLEDGMENT

This research is partially supported by the Aihara Innovative Mathematical Modeling Project, the Japan Society for the Promotion of Science (JSPS) through the "Funding Program for World-Leading Innovative R&D on Science and Technology (FIRST Program)," initiated by the Council for Science and Technology Policy (CSTP).

REFERENCES

[1] Ecodriving – The Concept, Available online at http://www.ecodrive.org/en.

[2] M.A.S. Kamal, M. Mukai, J. Murata and T. Kawabe, "Ecological Driver Assistance System Using Model Based Anticipation of Vehicle-Road-Traffic Information," in IET Journal of Intelligent Transportation Systems, Vol. 4, Issue 4, pp. 244–251, Dec 2010.

(ア) Schrank, T. Lomax, and S. Turner, "Urban Mobility Report 2010," Mar. 2010.

[3] [4] S. C. Davis, S. W. Diegel, and R. G. Boundy, "Transportation Energy Data Book," Oak Ridge, TN, 2010.

[4] M.A.S. Kamal, M. Mukai, J. Murata and T. Kawabe, "Ecological Vehicle Control on Roads with Up-Down Slopes," in the IEEE Transactions on Intelligent Transportation Systems Vol12-1, May 2011.

[5] Handbook of Automobile Technology, Soc. Automotive Eng. Japan, Tokyo, Japan, 1990, vol. 1, ch. 1, pp. 13.16 (in Japanese).

Expanding Photovoltaic Systems in Japan by Feed-in Tariff: Progressing Photovoltaic Cluster "Solar Island Kyushu"

Yukihiko Nakata
Graduate School of Management, Ritsumeikan Asia Pacific University, Oita, Japan
e-mail: nakata@apu.ac.jp

Abstract

Renewable energy is strongly expected after Great East Japan Earthquake. Feed-in tariff (FiT) introduced in Japan from July 1st, 2012 to promote the renewable energy. PV systems rapidly increased and have a monopoly on renewable energy with 99.9% of the accredited system numbers. Thus, PV domestic shipments expand 2.7 times from the previous year. Many PV systems constructed in Japan including PV cluster "Solar Island Kyushu." The 2013 FiT price was reduced 10 % of solar energy, but others were deferred. Therefore, Japanese market of PV system is forecasted to become number one in 2013. It is clear that FiT is exploding PV systems and business in Japan. It was verified that the FiT Policy is very effective to promote the renewable energy in Japan.

INTRODUCTION

According to the accident of the Fukushima first nuclear power plant which followed the Great East Japan Earthquake, it is standing on the crisis of a radioactivity and an electric power supply. For this reason, the expectation for renewable energy is rapidly raising. Especially a solar cell not only can supply the electric power to the disaster area, but can contribute to the economic recovery of the disaster area.

Feed-in tariff (FiT) is a very effective policy mechanism designed to accelerate investment in renewable energy [1, 2]. The FiT obligate an electric power company to purchase the electric power which is generated by renewable energy at fixed price above market price during a fixed period at the installation time of the system. As the installation time becomes behind, this FiT price is reduced. Therefore, the FiT policy has the effect for investors to decrease the uncertainty and to encourage making an investment at an early stage. The electric power companies shift the additional cost above market price to all consumers and share the cost widely as the surcharge.

In fact, the FiT accelerated the investment in renewable energy and enhanced the instauration of renewable energy in Europe, such as Germany and Spain [3-6]. For example, photovoltaic (PV) system using solar cells rapidly installed in Germany and Spain. It caused finally increase of a consumer burden and economical confusion because of rising of electricity prices and suppressing the PV market in Europe [3-6].

In Japan, the FiT for surplus electricity, which is a kind of the FiT, was introduced from November 1, 2009. This system buys the surplus electric power excluding self-consumption from the electric power from the solar cell at the about twice market price, and the domestic market was expanded more than twice as the result of that introduction.

Furthermore, the general FiT, in which the all electric power from renewable energy is bought at above market price, was passed by Japan Diet on August 26, 2011. It became effective from July 1st, 2012. Chairman of the FiT assessment committee has presented the FiT in April 25, 2012 [7]. It almost accepted the industrial request. Thus, many companies welcome the FiT. This means FiT price is high as same as Germany price of 2 years ago.

Therefore, there is an awareness of the issues as follows. • Could the FiT expand the PV systems in Japan? • Could the FiT expand the PV business in Japan? Thus, the effect of FiT on PV installations and business in Japan are analyzed.

LITERATURE REVIEW OF FEED-IN TAFIFF

Klein investigated different FiT designs applied in Europe to promote electricity generation from renewable energy sources and discussed two basic FiT designs including fixed FiTs, which are paid the fixed price above market price to generator during a fixed period, and premium FiTs, which are paid the added price based on the market price [1]. Also, the distribution of the costs was assessed [1]. Mendonça investigated FiT based on the cases of Europe and USA and mentioned the implementation of FiT design in the future [2].

Oshima analyzed the framework and characteristics of FiT in Germany and the reason for Germany success to promote the renewable energy by FiT policy [3]. Frondel etc. researched the problem of FiT in Germany and recommended the reduction of FiT [4], and argued the renewable energy policy in Germany and need to ensure a viable and cost-effective introduction of renewable energies into the country's energy portfolio [5]. Álvarez et al. analyzed the effects of FiT policy on employment from the case of the bubble which happened in Spain by the solar cell [6]. Couture et al. categorized FiT models and examined the advantages and disadvantages of different FiT models [8]. Yamaguchi researched the result and problem of Spain and Germany [9, 10]. Schallenberg compared fixed feed-in tariff and premium feed-in tariff based on Spain and clarified the advantage and the disadvantage [11]. Del Rio built a theoretical framework for dynamic efficiency analysis and assessed the dynamic efficiency properties of the different design elements of feed-in tariffs [12].

In addition, there are some simulation approaches to calculate the optimum FiT. Zahedi developed an economical model to determine a feed-in tariff for grid-connected solar PV electricity in Australia [13]. Wand et al. examined potential effects of Germany's FiT policy for small roof-top solar PV systems installed between 2009 and 2030 using simulation model [14].

Takehama analyzed the case of Germany and simulated the cost and the effect introducing into Japan [15]. Ayob et al. explored Japanese energy policies and develop simulation model to calculate the tariff for Japanese case [16].

Also, recently, there are many researches of FiT regional effects, in Australia [17, 18], California of USA [19], Malaysia [20], Philippine [21], Taiwan [22] and Ontario of Canada [23].

However, there are not researches of the FiT in Japan after the FiT became effective.

METHODOLOGY

In this paper, the effect of FiT on PV installations and business in Japan are analyzed.

Data of International Energy Agency (IEA), Japan Photovoltaic Energy Association (JPEA), Agency for Natural Resources and Energy in Japan and PV News etc. were analyzed.

Also, field researches are conducted in Japan including Kyushu.

The author researched and developed the solar cell technologies at Sharp Corporation and researched USA solar cell industry at Stanford University from October 2009 to March 2010. On these experiences, the impact of FiT was researched in this paper.

PRESENT STUATIION OF SOLAR CELL INDUSTRY

A. *Solar cell production amount*

The world solar cell production amount is rapidly increasing as shown in Fig. 1 [24]. The total amount has increased rapidly to 32.9 GW in 2011. But, it was slightly deceased to 31.9GW in 2012, because European PV market has shrank by FiT price reduction. Solar cell module production is around 35.5GW in 2012 [24].

B. *National share of solar cell production*

Fig. 2 plots the changes in national share of solar cell production from 1997 to 2012 [24]. Japanese share reached a high point of about 50% in 2004. But, it fell to 6% in 2012 [24]. It may increase in 2013 [25].

Germany increased the share to 20 % in 2005 by introducing FiT. But, total European share reduced 3 % in 2012 [24], because of the bankrupt of Qcells in Germany. China rapidly increased the share to 62% in 2011. But, It kept almost same 62% in 2012 [24], because of the bankrupt of Suntech power. The U.S. share fell continuously from 40% in 1997 to 2% in 2012 [24]. Korea produced 770 MW in 2010 with 3% share [26].

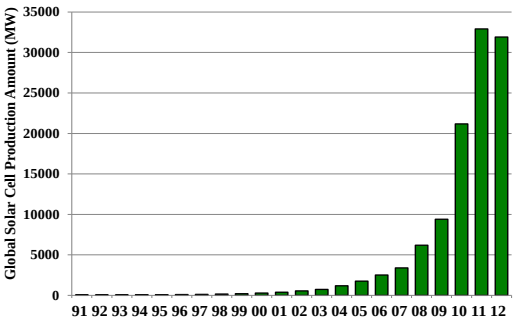

Fig.1. World solar cell production amount (author made from [24]).

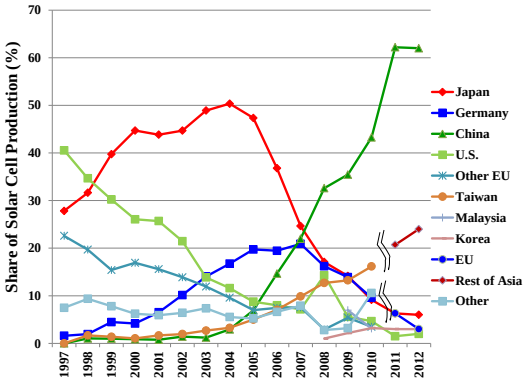

Fig. 2. National share of solar cell production (author made from [24])

Fig. 3 shows the installation of PV system per single fiscal year [27]. Germany extracts Japan in 2004 by introduction of the FiT and rapidly increases the installation. The installation in Germany is saturated and may reduce because of reduced FiT price. Spain installed 2.75GW in 2008 by the FiT. However the bubble burst and it was installed on almost single fiscal year. Same phenomenon may result in Italy. European PV market become to shrink by reduced FiT price. Instead of European Market, Japan, China and USA PV markets are rising up.

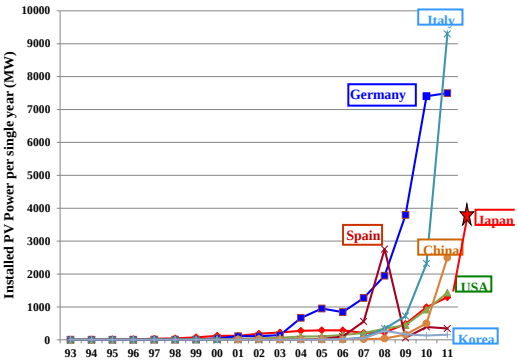

Fig. 3 Installation of PV system per single fiscal year (author made from [26])

EXPANDING PV SYSTEMS IN JAPAN BY FIT

A. Feed-in tariff in Japan

Japanese FiT of renewable energy was passed by Japan Diet in August 26, 2011 [28, 29]. This law obliges an electric power company to buy the electricity generated by the renewable energy sources (solar power, wind power, water power, geothermal power and biomass) at a fixed price during a fixed period. It became effective from July 1, 2012 [29].

All consumers pay the additional cost, which result from the purchase of the renewable energy at FiT by the electric power company, as the surcharge.

Although the FiT for surplus electricity applied only to the surplus electric power of PV system for household use, the new FiT was expanded to apply not only to solar power but to wind power, water power, geothermal power and the biomass by this law. However, the FiT for PV household use was kept the application to only surplus electric power as it was before.

The Minister of Economy, Trade and Industry (METI) gives the notify of the FiT price and period, based on the opinions of the neutral independent FiT assessment committee established newly, according to the classification of the source of renewable energy, an installation mode, a scale, etc. Moreover, to determine the FiT price, it includes considering the profits of the supplier of renewable energy electricity for three years after the enforcement, in order to promote the renewable energy.

The FiT assessment committee hears the requests from the renewable energy industries. Then, the chairman of the FiT assessment committee presented the FiT in April 25, 2012 [7]. The FiT is shown in Table 1. It almost accepted the industrial requests. Thus, many companies welcome the FiT. This means FiT price of PV is high as same as Germany price of 2 years ago. The FiT provides more incentives for investors as compared with the current FiT in Europe.

B. Accreditation of PV system

To obtain the FiT, the renewable energy system needs to be accredited. The data of the accredited renewable energy system are published by Agency for Natural Resources and Energy in Japan every month [30].

According to the data analysis of the accredited renewable energy system from July 2012 to February 2013 [30], PV system has a monopoly on renewable energy with 99.9% of the accredited system numbers.

In the case of output, the output ratio of the accredited renewable energy system from July 2012 to February 2013 is shown in Fig 4 [30]. Total PV output accounts for 93.8%. It break down by 49.3% of the mega solar system 1MW or more, 35.0% of 10-1000kW and 9.5% of 10kW or less. Wind power accounted for 4.8%.

Solar cell output is predictable accurately from the solar radiation data. The environment assessment is less stringent.

Table1. Feed-in trfif (Fit) Of 2012 in Japan [7]

Type of Energy	System Size	Feed-in Tariff (FiT)			Remark
		Committee Draft		Industry Request	
		Price (Yen/kwh)	Period (year)	Price (Yen/kwh)	
Solar	more than 10 kW	42	20	42	
	under 10 kW	42	10		Surplus
Wind	more than 20 kW	23.1	20	22～25	
	under 20 kW	57.75	20	50～55	
Geothermal	more than 1.5x 10^4 kW	27.3	15	25.8 (30MWclass)	
	under 1.5x 10^4 kW	42	15		
Hydro	1x 10^3 ～30x10^5 kW	25.2	20	24～34.06	
	200 ～1x10^3 kW	30.45	20		
	under 200 kW	35.7	20		
Biomass	various types	13.65～40.95	20	14.5～39	

In case of wind power, it is required the frequent data of wind speed. The environment assessment is harsh. Therefore, it takes two or three years to prepare.In case of geothermal and small hydro power, it takes a time for investigation and negotiations. For this reason, in the first year, PV system has monopoly. The other renewable energies are expected to grow in the following years.

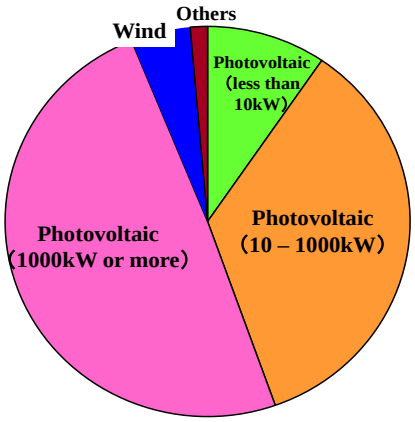

Fig 4. Ratio of accredited total power in Japan (author made from [30]).

The cumulative accredited PV power from July 2012 to February 2013 is categorized by regions as shown in Fig 5 [30]. It has become of the order Kyushu-Okinawa, Kanto, Hokkaido. South island of Kyushu has a large amount of solar radiation. PV systems are thriving. Kyushu is accounting for about 23% of the mega solar system. Thus, it is called PV cluster "Solar Island Kyushu." Kanto including Tokyo accounted for 22% of mega solar system, and has increased. North island of Hokkaido has a vast land, there are many application for mega solar system. But the transmission capacity of the electric power company is small; it exceeds the connection limit that can keep stable transmission. This situation put a crimp on the accreditation. After getting the accreditation, PV system is constructed buying the solar panels.

Fig. 6 shows the total shipment of solar cell by Japanese PV companies [31]. PV domestic shipments

expand from 1400GW in 2011 to 3800GW in 2012. It is 2.7 times increase from the previous year. This large increase of PV shipments comes of the effect of the FiT. PV export shipments are reduced from 1281GW in 2011 to 562GW in 2012 because European PV market has been shrunk [31].

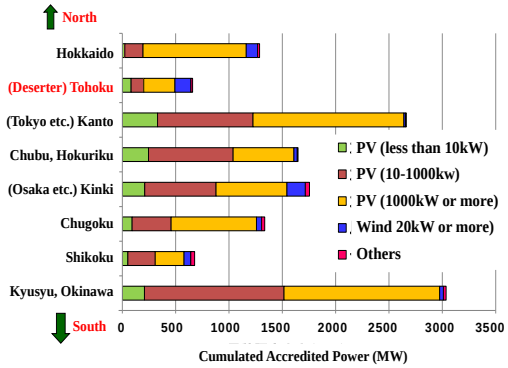

Fig. 5. Cumulative Accredited PV Power by Regions (author made from [30])

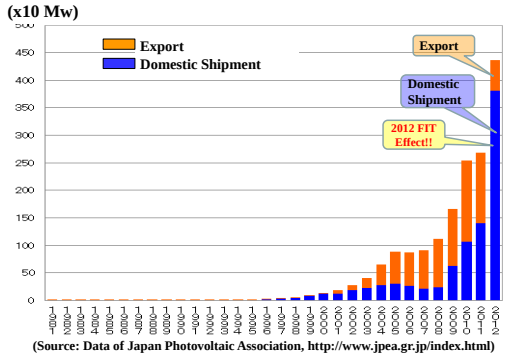

Fig. 6. Total Shipment of Solar Cell by Japanese PV Companies [31]

PROGRESSING "SOLAR ISLAND KYUSHU"

The PV cluster "Solar Island Kyushu" has four thin film solar cell companies and one module company as shown in Fig. 7.

Solar Frontier is the second-largest PV maker in Kyushu. It is a 100% subsidiary of Showa Shell Sekiyu, began research in solar energy in 1978 and commercial production of crystalline silicone modules began in 1983, and research on CIS (Copper Indium and Selenium) technology began in 1993. It is producing the compound thin film solar cell of CIS. The new plant in Miyazaki, Japan operated in 2011. Total production capability is 1000 MW/yea [32].

As shown in Fig. 5, "Solar Island Kyushu" has a large amount of solar radiation, PV systems are thriving with about 23% of the mega solar system.

One of the largest mega solar system with total 125MW are constructing at seaside industrial zone in Oita prefecture. The industrial zone developed in 1960s, and it lied idle. But, the industrial zone is utilizing for mega solar system because the FiT was introduced. JGC Corporation constructed and is operating the mega solar system with 26MW as part of the total system at the land of 350 thousand m^2 as shown in Fig. 8.

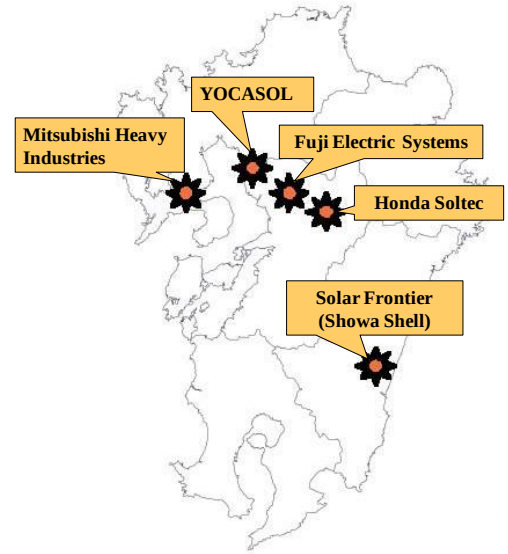

Fig. 7. PV Cluster "Solar Island Kyushu" (Author made)

Fig. 8. JGC Mega solar system with 26MW at Oita industrial zone (Author shot)

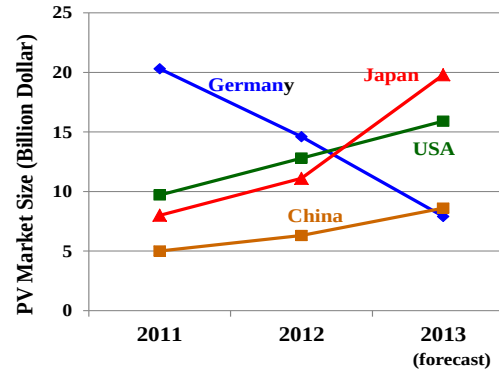

Fig. 9. Forecast of top four PV Markets in 2013 [25].

EXPECTING PV SYSTEM IN JAPAN

As described, PV systems in Japan are expanding by FiT. The 2013 FiT price was reduced 10% of solar energy, but it was deferred others [33].

Therefore, Japanese PV Market becomes number one getting ahead of Germany and USA in 2013 according to the forecast of IHS as shown in Fig. 9 [25].

CONCLUSIONS

FiT introduced in Japan from July 1st, 2012 to promote the renewable energy. The effect of the first year FiT on PV system was analyzed.

PV system has a monopoly on renewable energy with 99.9% of the accredited system numbers. Thus, PV domestic shipments expand 2.7 times from the previous year. Many PV systems constructed in Japan including PV cluster "Solar Island Kyushu."

The 2013 FiT price was reduced 10 % of solar energy, but others were deferred. Therefore, Japanese market of PV system is forecasted to become number one in 2013.

It is clear that FiT is exploding PV systems and business in Japan. It was verified that the FiT Policy is very effective to promote the renewable energy in Japan.

One of the issues is that PV system has a monopoly on renewable energy. It is necessary to expand to the other renewable energies. The other issue is that the surcharge will be increased for all users because the FiT price for PV system is high.

The FiT have to operate to overcome the issues to promote the renewable energies.

ACKNOWLEDGMENT

I express my appreciation for financial support from Tohoku University as "Regional Industry Reconstruction Research Program."

REFERENCES

[1] Arne Klein, "Feed-in Tariff Designs: Options to Support Electricity Generation from Renewable Energy Sources," VDM Verlag Dr. Müller, 2008.

[2] Miguel Mendonça, "Feed-in Tariffs: Accelerating the Development of Renewable Energy", Earthscan, 2007.

[3] Kenichi Oshima,; "German Expediencies to promote Renewable Energy – Framework and Fact of Feed-in tariff - (Japanese)," Ritsumeikan University human sciences research institute bulletin, No. 88, and p65-91, 2007.

[4] Manuel Frondel, Nolan Ritter, Christoph M. Schmidt, "Germany's solar cell promotion: Dark clouds on the horizon", Energy Policy, vol.36, pp. 4198-4204, 2008.

[5] Manuel Frondel, Nolan Ritter, Christoph M. Schmidt, Colin Vance, "Economic impacts from the promotion of renewable energy technologies: The German experience" Energy Policy, vol.38, pp. 4048-4056, 2010.

[6] Gabriel Calzada Álvarez, Raquel Merino Jara, Juan Ramón Rallo Julián , José Ignacio García Bielsa "Study of the effects on employment of public aid to renewable energy sources" PROCESOS DE MERCADO, Vol.VII, No.1, p1-14, 2010.

[7] Chairman's draft of Feed-in Tariff assessment committee of Ministry of Economy, Trade and Industry (Japanese), Available in http://www.meti.go.jp/committee/chotatsu_kakaku/006_haifu.html

[8] Couture, Toby, Yves Gagnon,; "An Analysis of Feed-in Tariff Remuneration Models: Implication for Renewable Energy Investment," Energy Policy, vol. 38, pp. 955-965, 2010.

[9] Mitsutsune Yamaguchi (Japanese) "Spain's Photovoltaic Experience –Light and Shadow", Nikkei Business Publications net ECO JAPAN, April 8, 2011, World Wide Web, http://eco.nikkeibp.co.jp/article/column/20110406/106293/?P = 1

[10] Mitsutsune Yamaguchi (Japanese) "German Photovoltaic advised Policy Change by IEA" Nikkei Business Publications net ECO JAPAN, April 25th, 2011, World Wide Web, http://eco.nikkeibp.co.jp/article/column/20110420/106392/

[11] Schallenberg-Rodriguez, Julieta; "Fixed feed-in tariff versus premium: A review of the current Spanish system," Renewable and Sustainable Energy Reviews, vol. 16, pp. 293-305, 2012.

[12] Pablo del Rio,; "The Dynamic Efficiency of Feed-in Tariffs: The Impact of Different Design Elements," Energy Policy, vol. 41, pp. 139-151,2012.

[13] Zahedi, Ahmad; "Development of an economical model to determine an appropriate feed-in tariff for grid-connected solar PV electricity in all states of Australia," Renewable and Sustainable Energy Reviews, vol. 13, pp. 871-878, 2009.

[14] Wand, Robert,; "Feed-in Tariff for photovoltaics: Learning by doing in Germany?" Vol. 88, pp. 4387-4399, 2011.

[15] Asami Takehama,; "the Feed-in Tariff introduction scenario to household photovoltaic towards low carbon social (Japanese)", Policy Science, vol. 17, special issue, pp. 93-123, 2010.

[16] Ayoub, Nasser, Yuji Naka,; "Governmental intervention approach to promote renewable energies-Special emphasis on Japanese feed-in tariff," Energy Policy, vol. 43, pp. 191-201, 2012.

[17] Zahedi, Ahmad; "A review feed-in tariff in Australia, what it is now and what it should be," " Renewable and Sustainable Energy Reviews, vol. 14, pp.3252-3255, 2010.

[18] Nelson, Tim, Paul Simshauser, Simon Kelley,; "Australian Residential Solar Feed-In Tariffs: Industry Stimulus or Regressive Form of Taxation?," Economic Analysis and Policy, vol. 41, pp. 113-129, 2011.

[19] Yaffe, David P,; "Are State Renewable Feed-in Tariff Initiative Truly Throttled by Federal Statutes after the FERC California Decision?," Electric Journal, vol. 23, pp. 9-16, 2010.

[20] Chua, Shing Chyi, Tick Hui Oh, Wei Wei Goh,; "Feed-in tariff outlook in Malaysia," Renewable and Sustainable Energy Reviews, vol. 15, pp.705-712, 2011.

[21] Varona, Philbert E.,; "Philippine regulator issues feed-in tariff rules," International Financial Law Review, vol. 30, pp. 59-59, 2011.

[22] Huang, Yun-Hsun, Jung-Hua Wu,; "Assessment of the Feed-in Tariff Mechanism for Renewable Energies in Taiwan," Energy Policy, vol. 39, pp. 8106-8115, 2011.

[23] Mabee, Warren E, Justine Mannion, Tom Carpenter,; "Comparing the Feed-in Tariff Incentives for Renewable Electricity in Ontario and Germany," Energy Policy, vol. 40, pp. 480-489, 2012.

[24] PV News, May and April 2008, May 2010, May 2011, May 2012 and Mat 2013.
[25] IHS, re-quote from The Nikkei (Newspaper) 30 July, 2013
[26] Kyung-Hoon Yoon “National Survey Report of PV Power Application in Korea 2010”, World Wide Web, International Energy Agency (IEA), http://www.iea-pvps.org/index.php?id=146.
[27] International Energy Agency, Trends in Photovoltaic Applications", Report of IEA-PVPS) T1-21, 2012
[28] Agency of Natural Resources and Energy, Committee report of Feed-in Tariff (Japanese) "Detail design of Feed-in Tariff for renewable energy", February 18th, 2011., World Wide Web, http://www.meti.go.jp/committee/summary/0004601/houkokusho_110218_01.pdf
[29] Agency of Natural Resources and Energy, "FiT of renewable energy", August, 2011, World Wide Web, http://www.enecho.meti.go.jp/saiene/kaitori/2011kai
[30] Agency of Natural Resources and Energy, "Status of Accredited Renewable Energy Systemy", End of February, 2013, World Wide Web, http://www.enecho.meti.go.jp/saiene/kaitori/index.html#setsubi
[31] Japan Photovoltaic Energy Association(JPEA), “Shipment of solar cell in Japan”, http://www.jpea.gr.jp/document/figure/index.html
[32] Sangyo Times Inc., “Comprehensive book od PV industry 2013 Jjapanese)”, February, 2013.
[33] Agency of Natural Resources and Energy, "FiT price and period in 2013", March, 2013, World Wide Web, http://www.enecho.meti.go.jp/saiene/kaitori/kakaku.htm.

Sustainability of Bioenergy

M. Z. Haq

Dept. of Mechanical Engineering, Bangladesh University of Engineering & Technology, Dhaka, Bangladesh
e-mail: zahurul@me.buet.ac.bd

Abstract

Biomass is a renewable source of energy to produce heat, electricity, fuels and bio-products. When produced and used on a sustainable basis, it is a carbon-neutral carrier and can reduce greenhouse gas (GHG) emissions. It has a good potential for income generation along its life cycle, from cultivation to harvest, processing and conversion to energy. Status of bioenergy and the research activities in BUET to use biofuel in engines are reported in the present paper.

INTRODUCTION

Bioenergy is the energy derived from biomass. Biomass is produced by green plants by converting sunlight into plant material through photosynthesis and includes all land- and water-based vegetation, as well as all organic wastes [1]. As plants grow, they absorb greenhouse gas (GHG), carbon dioxide and when these plants or the derived biomass are burned, the same amount of GHG is returned to the atmosphere. The use of biomass began hundreds of thousands of years ago, when human ancestors used wood fire to warm themselves and to cook food. Demand for biomass, especially wood, as energy source in developing countries is high as it is often the only readily available, accessible. The development of a large-scale technology to use biomass to produce electricity and biofuel was stimulated only in the late 20th century.

In view of prevailing energy crisis and emission problems, bioenergy can be used to significantly substitute petroleum based fuels [2]. At present, some forms of bioenergy are not economically competitive and therefore warrant special attention for its sustainability.

BIOENERGY SOURCES AND STATUS

Biomass can be derived from the cultivation of dedicated energy crops, perennial grasses, etc. and from biomass wastes such as sludge from organic waste or the wastes themselves. These can be classified into two groups [3]:

1. Energy Crops
   a. Woody crops
   b. Agricultural crops
2. Wastes
   a. Wood residues
   b. Temperate crop wastes
   c. Tropical crop wastes e.g. bagasse and rice husk
   d. Animal wastes e.g. animal manure, sewage sludge and poultry litter
   e. Municipal solid waste
   f. Landfill gas
   g. Commercial and industrial wastes

Biomass contains varying amounts of cellulose, hemicellulose, lignin and a small amount of other extractives (Table 1). Key biomass properties are [1]:

- Moisture content
- Lower heating value (LHV)
- Fixed carbon (FC) and volatiles (VM) ratio
- Ash/residue content
- Alkali metal content
- Cellulose/lignin ratio

Table 1. Properties of some biomass feedstock [1].

Biomass	Moisture (%)	VM (%)	FC (%)	Ash (%)	CV (MJ/kg)
Wood	20	82	17	1	18.6
Wheat straw	16	59	21	4	17.3
Barley straw	30	46	18	6	16.1
Lignite	34	29	31	6	26.8
Bituminous	11	35	45	9	34.0

The quantity of dry matter produced by a biomass species per unit area of production and its LHV are combined to estimate the energy yield of the cultivated crop (Table 2). Energy contents of biomass are found similar, laying in the range 17-21 MJ/kg. So, principal selection criteria for biomass species are growth rate, ease of management, harvesting and material properties e.g. moisture/ash/alkali content.

Table 2. Energy yields from selected biomass [1].

Biomass	Crop yield (dmt/ha/a)	CV (MJ/kg, dry)	Energy yield (GJ/ha)
Wheat	7 grain/7 straw	12.3 (straw)	123
Poplar	10-15	17.3	173-259
SRC willow	10-15	18.7	187-280
Switchgrass	8	17.4	139
Miscanthus	12-30	18.5	222-555

Biomass has always been a major source of energy for mankind and is presently estimated to contribute around 10% of the world's primary energy supply (Fig. 1). Share of biomass sources in primary bioenergy mix are shown in Fig. 2.

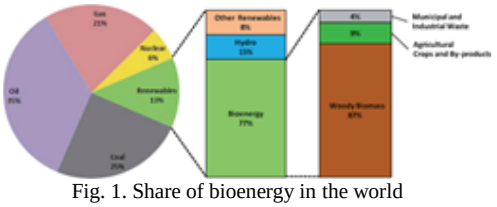

Fig. 1. Share of bioenergy in the world primary energy mix [4].

The predominant use of biomass today consists of fuel wood used in non-commercial applications, in simple stoves for domestic heating and cooking in developing countries, where biomass contributes some 22% to the total primary energy mix. In industrialized countries, the total contribution of modern biomass is on average only about 3% of total primary energy, and consists mostly of heat-only and heat and power applications [4].

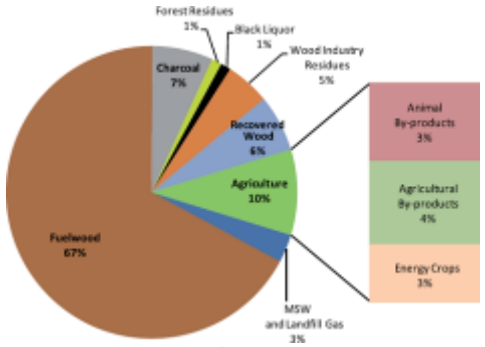

Fig. 2. Share of biomass sources in primary bioenergy mix [4].

ENERGY CONVERSION & SUSTAINABILITY

Conversion routes for producing bioenergy from biomass are plentiful and Fig. 4 illustrates the key conversion routes. Overview of biomass conversion technologies to heat and power [5] and to biofuel [6] are reported in Figs. 4 and 5, respectively.

To assess biomass sustainability, it is necessary to consider the complex linkages between the large-scale production and the use of biomass for energy and materials, food production, energy use, water use, biodiversity and climate change. In Fig. 6 this complexity is highlighted by showing some key relationships and assumptions.

Physical and combustion characteristics of biomass significantly differ from those of fossil fuels posing some technical and economic challenges:

- Bulk density and calorific value are lower, so transportation can be more difficult and costly.
- Some biomass resources are seasonal, so storage is needed to provide energy all year round.
- Untreated biomass may have higher moisture.
- Systems have to be designed specifically for clean and efficient combustion and to avoid fouling, and corrosion problems.

Expansion of bioenergy poses some more challenges: the productivity of food and biomass feedstock, the potential competition for land and raw materials, negative effects on food security and water availability, logistics and infrastructure issues [7].

A general scheme for comparing bioenergy and fossil fuel systems is shown in Fig. 7. Key environmental, social and economic aspects of biofuel and bioenergy production for sustainability are reported in Fig. 8.

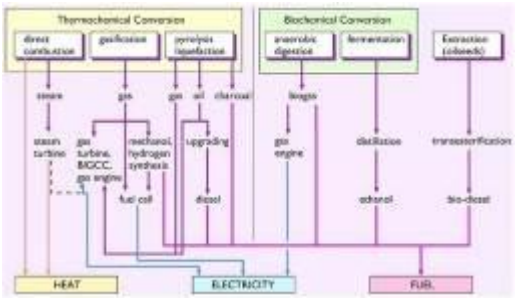

Fig. 3. Main bioenergy conversion routes [3].

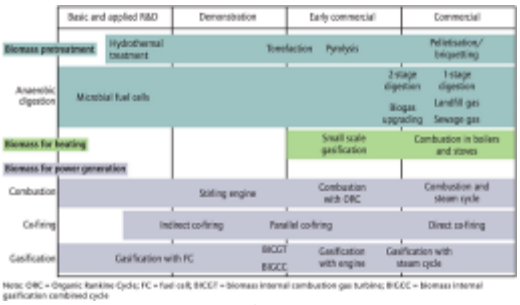

Fig. 4. Development status of main technologies to upgrade biomass and/or to convert it into heat and/or power [5].

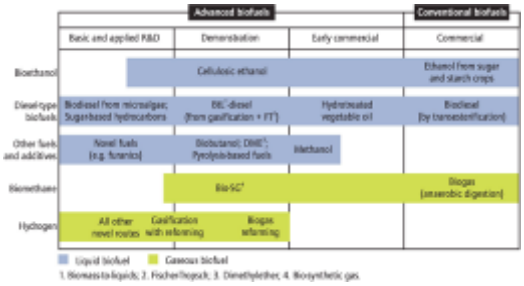

Fig. 5. Development status of the main technologies to produce biofuel for transport from biomass [6].

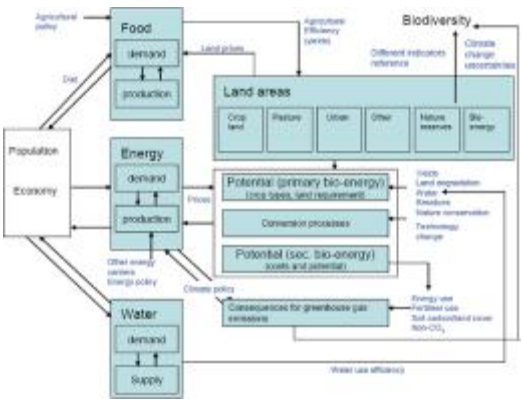

Fig. 6. Key relationships to assess bioenergy potentials [4].

Further technological development is needed to improve the efficiency, reliability and sustainability of bioenergy. In heat sector, improvement would lead to clean and reliable supply of high quality fuel, and

in electricity sector, the development of smaller and more cost-effective electricity or CHP. In transport sector, improvements could lead to sustainable biofuels for efficient and safe operations [4].

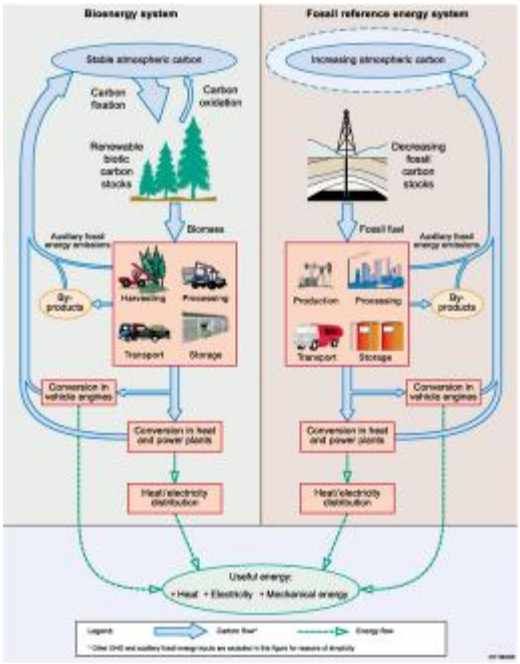

Fig. 7. Standard methodology to compare bioenergy and fossil fuel energy systems [4].

Fig. 8. Environmental, social and economic aspects of biofuel and bioenergy production [4].

BIOFUELS IN HEAT ENGINES

Biomass can be used to produce liquid biofuel, such as ethanol, methanol, biodiesel, Fischer-Tropsch diesel, and gaseous fuels, such as hydrogen and methane. Liquid biofuels are primarily used to fuel vehicles, but can also be used in engines or fuel cells to produce electricity [8]. Due to its environmental merits, the share of biofuel in the automotive fuel market is expected to grow fast. Present status of the biofuel technologies are reported in Fig. 5. Research activities of the present author and his graduate students are reported in the following subsections.

A. Vegetable oils as diesel engine fuel

High viscosity and low volatility of vegetable oils are identified as the main reasons for their unsuitability as straight diesel fuel substitute as these two parameters affect the fuel's spray pattern, atomization, vaporization and mixing with air inside engine cylinder [2]. High viscosities of such fuels are reduced to acceptable levels for diesel engines if blended with kerosene [2] or preheated to 100^{o}C [9]. Experimentally, it is seen that these fuels result in slightly reduced engine performance without any noticeable change in engine operating condition [2,9]. Vegetable oil methyl esters (biodiesel) are prominent candidates as alternative diesel fuel. However, vegetable oils blended with kerosene or preheated using exhaust gases provide a low technology solution for the rural people.

B. Biogas as diesel engine fuel

The organic fraction of almost any form of biomass can be broken down through anaerobic digestion into methane and carbon dioxide mixture called as 'biogas'. Biogas is an environment friendly, clean and cheap fuel. Existing stationary diesel engines can be retrofitted fairly easily for operation with biogas where biogas is supplied to the intake manifold of the engine by fumigation method [10] and small amount of diesel is injected to initiate ignition. Engine fuelled by diesel and biogas of two different compositions are investigated and results indicate very comparable engine indicator diagrams (Fig. 9) and subsequent similar engine performances.

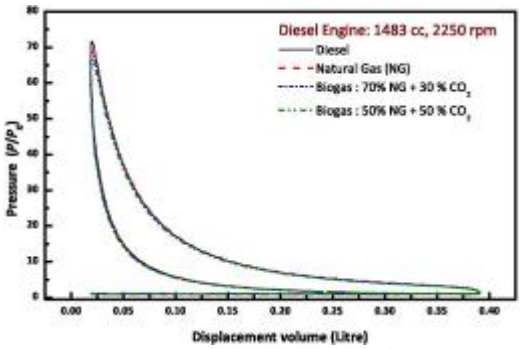

Fig. 9. Indicator diagrams for different fuels [10].

C. Alcohols as spark ignition engine fuel

Alcohols have simple molecular structure and therefore burn efficiently. These fuels reduce harmful emissions, such as carbon monoxide (CO) and unburned hydrocarbon (UHC) because of oxygen content in their molecule. High octane numbers of alcohols allow for the use of high compression ratios to lead to higher thermal efficiency. These fuels have also higher latent heat of vaporization and therefore pre-cool the intake charge to result in high volumetric efficiency and output power. Methanol, ethanol and butanol are commonly used alcohols in SI engines because of their suitable properties [11].

Because SI engines are air breathing, chemical energy entering into the cylinder depends on the fuel, and its chemical energy, stoichiometric fuel-air mass ratio, y_s and the charge density. For identical conditions of pressure and temperature, as same volume of charge is drawn into cylinder and energy density, *ED* (available energy content per unit volume) is directly related to the engine output.

Reported in Table 3 are some of heat release parameters estimated for four fuels. Lower heating values (LHVs) of the fuels are found to vary significantly. However, the values of SE (available energy content per unit mass) and ED's converge to a narrow band. Hence, in-cylinder gas pressure obtained with these fuels exhibit similar results (Fig.10) and indicated efficiencies of a SI are reported in Table 4.

Table 3. Estimated properties of some fuels [11].

Fuel	y_s	LHV	SE	ED
	(-)	(MJ/kg-fuel)	(kJ/kg-mix)	(kJ/m3-mix)
Iso-Octane	0.062	44.7	2873	3507
Methanol	0.135	21.1	2903	3424
Ethanol	0.101	27.7	2866	3466
Butanol	0.083	33.8	2878	3528

Table 4. Indicated efficiencies of a SI engine [11].

	Iso-Octane	Methanol	Ethanol	Butanol
1000 rpm	33.9%	33.9%	33.9%	33.7%
4000 rpm	35.5%	35.6%	35.5%	35.4%

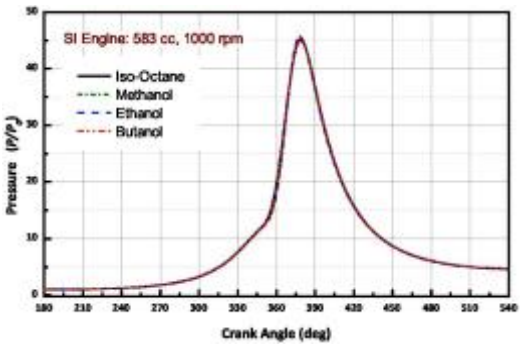

Fig. 10. Indicator diagrams of SI engine [12].

CONCLUSION

Biomass is renewable and green source of energy and it can significantly substitute the conventional fuels in a sustainable manner. It can drastically reduce GHG emissions. Most countries have biomass resources available, or could develop such a resource, making it a more evenly spread energy supply option across the globe. It is a versatile energy source, which can be used to produce power, heat, biofuels, and also serves as a feedstock for biochemicals. Biofuels can be used in spark-ignition and diesel engines without compromising engine performance.

ACKNOWLEDGMENT

Properties of the biofuels were estimated in the 'Fuel Testing Laboratory', and engine performance studies were carried out in the 'Heat Engine Laboratory' of Department of Mechanical Engineering, BUET. The author acknowledges the support extended by the staff of these laboratories.

REFERENCES

[1] P. McKendry, "Energy Production from Biomass (part 1): Overview of Biomass," *Bioresource Technology*, vol. 83, no. 1, pp. 37 – 46, 2002.

[2] M. Z. Haq, "Study of the Properties of Vegetable Oil as an Alternative to Diesel Fuel," Master's thesis, Bangladesh University of Engineering & Technology, 1995.

[3] G. Boyle, *Renewable Energy: Power for a Sustainable Future*. OUP, Oxford, 2012.

[4] "Bioenergy - a Sustainable and Reliable Energy Source", IEA Bioenergy: ExCo: 2009:06, 2009.

[5] "Technology Roadmap: Bioenergy for Heat and Power", IEA Bioenergy: ExCo: 2009:06, 2012.

[6] "Technology Roadmap: Biofuels for Transport," IEA Bioenergy: ExCo: 2009:06, 2011.

[7] S. McPhail, V. Cigolotti, and A. Moreno, Fuel Cells in the Waste-to-Energy Chain: Distributed Generation Through Non-Conventional Fuels and Fuel Cells, ser. Green Energy and Technology. Springer, 2012.

[8] A. Demirbas, "Biofuels Sources, Biofuel Policy, Biofuel Economy and Global Biofuel Projections," *Energy Conversion and Management*, vol. 49, no. 8, pp. 2106 – 2116, 2008.

[9] A. M. Morshed, "Sesame Oil as an Alternative Fuel for Diesel Engines in Bangladesh," Master's thesis, Bangladesh University of Engineering and Technology, 2008.

[10] M. Z. Haq, MH Rahman and ZA Bhutto, 2003. Performance Studies of a Biogas Fueled Diesel Engine Operating in a Dual Fuel Mode. *Proc. of Int. Conf. on Power Engineering: ICOPE*, "3-57"-"3-62", JSME.

[11] M. Z. Haq and A. Morshed, 2013. Energy and Exergy Based Analyses of a Multi-fuelled SI Engine. *Proc. of ASME 2013 Power Conference Power2013*, MA,USA.

[12] A. Morshed, "Energy and Exergy Based Analysis of a Multi-Fuelled SI Engine," Master's thesis, Bangladesh University of Engineering and Technology, 2013, in progress.

Hydrothermal Treatment of Coconut Shell and Recovery of Furfural

H Tsuji[1], S Kumagai[2], P Limsuwan[1], T Hirajima[1]*, K Sasaki[1] and H Miki[1]

[1]Faculty of Engineering, Kyushu University, Japan

[2]Organization for Cooperation with Industry and Regional, Saga University, Japan

*e-mail: hirajima@mine.kyushu-u.ac.jp

Abstract

In this study, the hydrothermal treatment of coconut shell using a batch-type reactor at 200-300 ºC was investigated. Under hydrothermal treatment at 200 ºC, 30 min, hemicellulose decomposed to xylose, acetic acid, furfural, etc. Cellulose was almost decomposed to various organic acids and 5-HMF at 250 ºC. Highest furfural concentration was obtained at 200 ºC treatment. Solid products of hydrothermal treatment were carbonized in order to be used for adsorption of furfural and compared with carbonized product without hydrothermal treatment. Carbonization products of the hydrothermally treated coconut shell adsorb furfural efficiently. Important parameter for furfural adsorption on carbon is not only specific surface area but also micro pores in carbon which are needed to be larger than furfural size.

INTRODUCTION

Authors have been studying about effective utilization of organic carbon resources such as biomass by hydrothermal treatment [1-5]. Authors also have clarified that hemicellulose was degraded to water soluble products which were mainly sugars, organic acids and furan compounds by the treatment at around 200ºC. In the water soluble products, furfural, which is very valuable chemical because it can use for feed stock, for resin, plastic and solvent [3-5]. However, the concentration of the furfural in the water soluble solution was very low, and then it existed together with sugars and organic acids. Consequently, effective separation process of them is needed. In this study, 6-type charcoals were prepared from coconut shell by various carbonization processes. Then, investigations have been conducted about the adsorption ability of furfural in solution obtained by hydrothermal treatment of coconut shell at 200ºC using prepared charcoals.

EXPERIMENTAL

A. Raw materials

Coconut shell was used in this study. It was pulverized under 2 mm before using. Chemical analysis of the coconut shell was 21.6 wt% cellulose, 23.0 wt% hemicellulose, 40.3 wt% klason lignin, 0.6 wt% ash, and 1.7 wt% ethanol extracts.

B. Hydrothermal treatment

Hydrothermal treatment was conducted in an autoclave (500 mL in volume). 60 g of pulverized coconut shell and 240g of pure water were charged into the autoclave. The air was replaced to nitrogen gas, and the pressurized at 0.5 MPa then sealed. After that, the reactor was heated by electric furnace to the desired temperature (200 to 300ºC) and kept the temperature for 30 min. After cooling to the room temperature inside the reactor using an electric fan, the reaction products were recovered and separated to water soluble residue and water insoluble by vacuum filtration with a membrane filter (ϕ 47 mm, average pore size 1.0 mm). The water insoluble residue was dried at 105ºC and weighted, while, water soluble product was analyzed by high-performance liquid chromatography (HPLC, JASCO) and total organic carbon (TOC analyzer, SHIMADZU). In this study, the solution recovered by the hydrothermal treatment at 200ºC was used for recovery of furfural and the residue (charcoal) obtained by the treatment at 200 to 300ºC (adsorbent) were used for furfural adsorption tests.

C. Carbonization (under nitrogen stream)

4 g of the raw coconut shell or hydrothermally treated coconut shell at different temperature were weighted in a ceramic boat and carbonized in the ceramic tube furnace. The carbonization reaction was conducted at 300 or 700ºC for 30 min under nitrogen stream (100 mL/min). After cooling the weight of the charcoal was measured, and then the properties were measured by ultimate analysis, surface area and pore size (BELSORP-Max instrument, BEL Inc.) and Fourier transform infrared spectroscopy (FTIR-670 Plus, JASCO).

D. Adsorption of furfural by charcoal

10 mL of water soluble products obtained by hydrothermal treatment of coconut shell at 200ºC was added in a 50 mL vial bottle with 0.5 g of charcoal. Adsorption reaction was conducted in a mechanical shaker with 120 stroke/min at 25ºC for 1 hour. After quenching reaction, reaction products were separated into two fractions, solid and supernatant. Furfural concentration in the supernatant was measured by HPLC.

RESULTS AND DISCUSSION

A. Product of hydrothermal treatment of coconut shell

The yield and properties of the solid products at different treatment conditions are presented in Table 1.

Table 1. WI yield, ultimate analysis and calorific value

Carbonization temp. (°C)	WI Yield (wt%)	Ultimate analysis (wt%, daf)				HHV (MJ/kg-dry)
		C	H	O	N	
Unprocessed	100	51.7	5.7	42.5	0.1	18.0
200 HT	63.6	56.7	5.6	37.6	0.1	20.7
250 HT	58.1	68.0	4.8	27.0	0.2	25.0
300 HT	51.0	72.2	4.7	22.9	0.2	27.1

HHV: Higher Heating Value = 0.3383C + 1.442(H-O/8)

Due to the degradation reactions, the solid product (water insoluble, WI) yield decreases at elevated temperature, indicating the degradation reactions accomplish more completely. With increasing temperature, C contents increased whereas O contents decreased. As a result, caloric value (HHV) increases with increasing temperature.

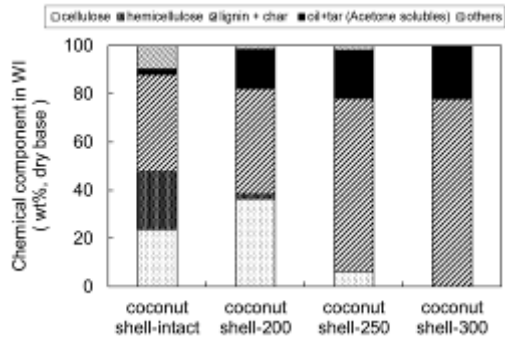

Fig. 1. Chemical composition of water insoluble at various temperature

Fig. 1 indicates the chemical composition of water insoluble at various temperatures. As shown in this figure, large part of hemicellulose was decomposed at 200°C and completed at 250°C. Cellulose was decomposed partially at 250°C and completed at 300°C. Insoluble oil and tar were increased with decomposition of hemicellulose and cellulose.

FTIR spectra for raw coconut shell and solid products obtained at various temperatures are shown in Fig.2. As shown in this figure, peak of -OH group and -O- sugar ring decreased with temperature, whereas that of -C=O group increased. As explained in Fig. 1, decomposition of hemicellulose and cellulose increased with temperature and relative amount of lignin proportion increases.

Fig. 3 shows HPLC chromatogram of solution obtained by hydrothermal treatment of coconut shell at 200, 250 and 300°C. It is known that hemicellulose is decomposed into xylose and arabinose whereas cellulose is decomposed into glucose. Furfural is one of the decomposition products from the hydrolysis of arabinose and xylose [2-5]. As shown in Fig. 3, the highest yield of furfural was detected at 200 °C (30min), however the yield of furfural in elevated temperature gradually decreased. At the same time, glucose was further decomposed to secondary products such as 5-HMF which was detected at 250°C. At 200°C, their chemical composition was mainly xylose, acetic acid and furfural. Concentrations were 7.8g/L xylose, 13.6g/L acetic acid and 8.1 g/L furfural.

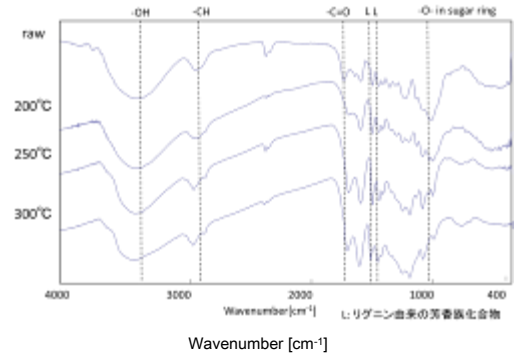

Fig. 2. FTIR spectra for raw coconut shell and solid products obtained at various temperatures.

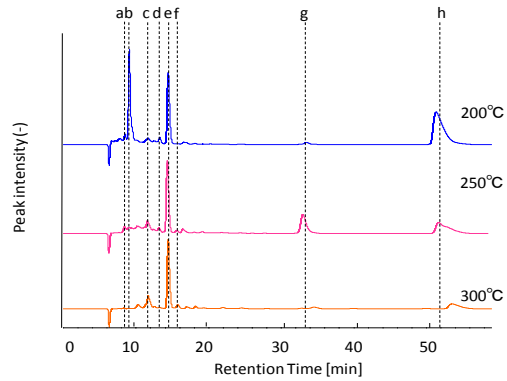

Fig. 3. HPLC chromatogram of solution obtained by hydrothermal treatment of coconut shell at 200, 250 and 300°C.
Peak No.: a)glucose, b) xylose, c)glycolic acid, d) formic acid, e) acetic acid, f) levulinic acid, g) 5-HMF, h) furfural.

B. Carbonization with/without hydrothermal treatment and its adsorption property

The properties of charcoal used in this experiment are shown in Table 2. As shown in this table, chemical composition at 300°C is quite similar at all carbonization conditions. However, charcoal yield of hydrothermal treatment at 300°C (300HT) is around 10 wt% higher than that of carbonization at 300°C under N_2 flow (300 under N_2). This phenomenon might be attributed to the following reason: during carbonization under nitrogen flow, the generated tar could be separated as gas. On the other hand, during hydrothermal treatment, tar remains in the reactor. It might be the reason why carbon contents were higher with hydrothermal treatment. When hydrothermal products at 300°C were mixed with acetone to remove tar product, 20 % of weight of hydrothermal product was dissolved as tar product. This weight

loss was almost same as the difference of these yields. Carbonization at around 300 °C condition, surface area was small because of micro pore cannot be developed under low temperature. At the higher carbonization temperature, surface area increased. Product surface area of hydrothermal treatment at 300°C and then carbonized at 300°C under N_2 flow (300HT+700 under N_2) (357.9 m^2/g) shows 3 times higher than that of 700 under N_2 (121.2 m^2/g).

Table 2. Properties of charcoal

Carbonization temp. (°C)	Yield (wt%)	Ultimate analysis (wt%, daf)				Surface area (m^2/g)
		C	H	O	N	
Unprocessed	100	51.7	5.7	42.5	0.1	-
300 HT	51.0	72.2	4.7	22.9	0.2	17.0
300 under N_2	43.0	73.9	4.3	21.6	0.2	10>
700 under N_2	28.1	93.4	1.1	4.9	0.6	121.2
300 HT + 700 under N_2	29.2	94.3	1.2	4.3	0.2	357.9

HT: Hydrothermal Treatment

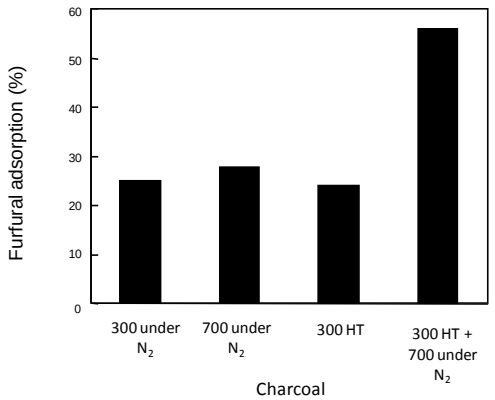

Fig. 4. Furfural adsorption ratio treated by 4-types charcoal.

With these carbonization products, valuable furfural adsorption experiments were carried out. Results are shown in Fig. 4. As shown in this figure, Charcoal obtained at 300HT+700 under N_2 indicated higher adsorption capacity than another carbonization products and it might be due to its high specific surface area. Specific surface area of 700 under N_2 was also quite higher than others, but this adsorption rate was quite low. It might be due to micro pore distribution as mentioned below.

C. Recovery of furfural by charcoal

The effect of hydrothermal treatment temperature on carbonized product at 700 °C under N_2 flow was investigated. Solid product characteristics are shown in Table 3. As shown in this table, after carbonization, carbon contents were very high at all conditions, whereas surface areas of these samples were quite different for each hydrothermal treatment condition. With increasing hydrothermal treatment temperature, specific surface area increased up to 250°C and a little bit decreased at 300°C. This result can be explained as follows. As shown in Fig. 1, hemicellulose and cellulose were decomposed gradually with increasing temperature and complete decomposition was noticed at 250°C. Because of this decomposition, products of hydrothermal treatment became porous and following carbonization, surface area of the product became large. Polymerization of water soluble product caused by decomposition of hemicellulose and cellulose was enhanced at 300 °C and the pore was filled with this polymerization product. This makes lower surface area of product 300HT+700 under N_2.

Fig. 5 shows a furfural adsorption ratio treated by 4-types charcoal. In case of treatment using a charcoal prepared under nitrogen stream at 700°C by hydrothermal treatment at 250°C, surface area of this charcoal was the highest and it was expected that the adsorption ratio could be at its maximum. However, charcoal prepared under higher temperature (300 °C) indicated almost same adsorption rate as 250 °C though the surface area was low.

Table 3. Properties of charcoal

Carbonization temp. (°C)	Yield (wt%)	Ultimate analysis (wt%, daf)				Surface area (m^2/g)
		C	H	O	N	
Unprocessed	100	51.7	5.7	42.5	0.1	-
700 under N_2	28.1	93.4	1.1	4.9	0.6	121.2
200 HT + 700 under N_2	19.2	94.3	1.3	4.2	0.2	189.0
250 HT + 700 under N_2	28.7	94.1	1.2	4.6	0.2	479.5
300 HT + 700 under N_2	29.2	94.3	1.2	4.3	0.2	357.9

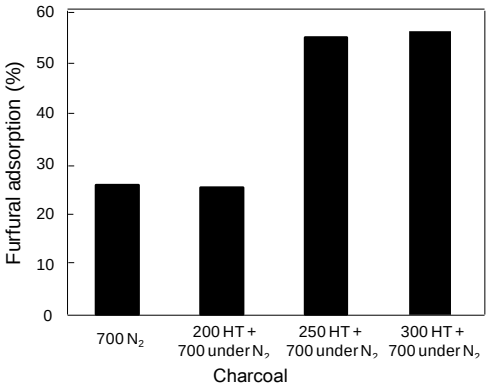

Fig. 5. Furfural adsorption ratio treated by 4-types charcoal (including lower temperature compared with Fig. 4)

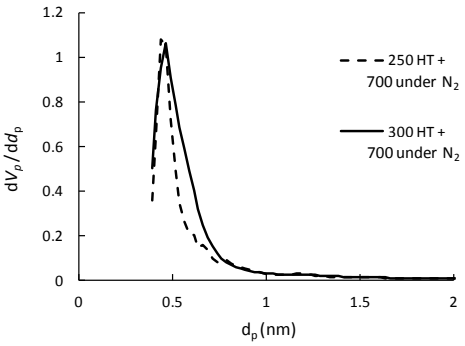

Fig. 6. Micro pore distribution of charcoal treated at various temperature followed by carbonization at 700°C

To confirm this behavior, micro pore distribution for charcoal samples was measured. Figure 6 shows the results. As shown in this figure, pore size under 250HT+700 under N_2 was smaller than that of 300HT+700 under N_2. For pore size under 250HT+700 under N_2, most of pore size is smaller than the diameter of furfural (0.57nm) and this may be the reason of low furfural adsorption rate of 250HT+700 under N_2. These results explain why only specific surface area cannot determine the furfural adsorption rate.

CONCLUSION

Hydrothermal treatment of coconut shell and following carbonization was investigated to produce effective furfural adsorbent. The following points were concluded from this study:

1. Hydrothermal treatments at 200ºC start decomposing hemicellulose, 250ºC decompose cellulose, 300ºC both are decomposed completely.
2. Hydrothermal treatments at 200ºC produce valuable furfural. Furfural concentration decreased with increasing temperature since furfural decomposition started at higher temperature.
3. Carbonization at 700ºC after hydrothermal treatment of coconut shell at 250 and 300ºC shows higher furfural adsorption ratio compared with 700ºC carbonization with or without 200ºC hydrothermal treatment. Parameter for furfural adsorption on carbon is not only specific surface area. Micro pore in carbon need to be larger than furfural size.

ACKNOWLEDGMENT

The authors are grateful for support of this research by a Grant-in-Aid for Scientific Research No. 21246135 and 24246149 from the Japan Society for the Promotion of Science (JSPS), the Global COE Program (Novel Carbon Resources Sciences, Kyushu University) and the Japan Science and Technology Agency (JST).

REFERENCES

[1] M Nonaka, T Hirajima, A Hirose and K Sasaki. 2007. Extraction Behavior during Hydrothermal treatment of Biomass and Low Rank Coal Mixture. Journal of MMIJ, 123: 532-536.

[2] Y Nagashima, S Kumagai, AT Yuliansyah, K Sasaki and T Hirajima. 2010. Hydrothermal Decomposition of Oil Palm Residue Using a Hot-Compressed Water Flow Type Equipment. *Proceedings of the 5th Biomass Science Conference*, pp. 74-75.

[3] AT Yuliansyah, T Hirajima, S Kumagai and K Sasaki. 2010. Solid fuel production from oil palm shell by hydrothermal carbonization. Wood Carbonization Research, 7 (1), 19-26.

[4] AT Yuliansyah, T Hirajima, S Kumagai and K Sasaki. 2010. Production of solid biofuel from agricultural wastes of the palm oil industry by hydrothermal treatment. Waste Biomass Valor., 1, 395-405.

[5] S Kumagai, T Hirajima, M Nonaka and N Hayashi. 2012. Hydrothermal carbonization behavior of Moso-Bamboo (*phyllostachys heterocycla*) in hot-compressed water. Wood Carbonization Research, 8 (2), 53-60.

Effects of surface modification of granular activated carbon using plasma on phenol adsorption

P Limsuwan[1], S Kumagai[2], M Nonaka[1], K Sasaki[1], and T Hirajima[1]*

[1]Department of Earth Resources Engineering, Kyushu University, Japan

[2]Organization for Cooperation with Industry and Regional, Saga University, Japan

*e-mail: hirajima@mine.kyushu-u.ac.jp

Abstract

The primary objective of this paper is plasma modification of activated carbons for enhancing phenol adsorption. Activated carbons (ACs) were surface modified with oxygen plasma at low pressure. The effects of the plasma treatment on the microstructural properties of the ACs were characterized by N_2 gas (77 K) adsorption-desorption isotherms, using a surface area and pore size analyzer and Field Emission Scanning Electron Microscope (FE-SEM). Micropores were promoted in the ACs. Moreover, the specific surface area and micropore volume increased by 22% at certain plasma treatment time and power. Changes in the structural properties of the ACs are discussed in detail with respect to plasma etching. Fourier transform infrared spectroscopy (FTIR) results revealed that new oxygen-containing groups, such as C=O stretching, and C-OH stretching, had formed on the surface of the ACs after plasma treatment. Plasma surface oxidative reactions such as the generation of radicals, the combination of the radicals and active oxygen species in the plasma chamber, and th4e generation of the various oxygen-containing groups are believed to have occurred. The effect of the plasma treatment parameters such as plasma treatment time was examined from the perspective of both surface structure and chemistry. Micropores, surface area, and phenol adsorption of the ACs were observed to increase under moderate treatment conditions.

INTRODUCTION

Activated carbons (ACs) are efficiently used in several pollution control processes due to their high adsorption capacity. A large number of contaminants may be removed from a liquid or a gas stream during their passage through an activated carbon. The activated carbon adsorption properties are attributed to its physical and chemical structure. High surface area and pore volumes as well as large micropores are typical characteristics of activated carbons. It is recognized that the pore structure and surface functional groups are the most important properties of ACs for their applications in adsorption processes [1, 2]. Therefore, to improve AC properties, it is attractive to obtain a well-developed pore structure, and make higher adsorption capacity toward novel applications of ACs either as adsorbents for pollutants removal or as catalyst supports. In the last decades, the researches on AC have focused on surface modification and characterization in order to meet the growing demand for cleaner air and water [3-6]. Plasma technique is an efficient method in the field of surface modification. The surfaces of various materials can be readily modified with plasma [7, 8]. Recently, researchers have applied plasma techniques to the surface modification of carbon-based materials. It is convenient in operation and environment-friend to put into practice, because no toxic wastewater is generated. The plasma processes cause dramatic physical and chemical effects [9]. The physical effects can change surface structure of carbon-based materials, while the chemical effects introduce functional groups onto carbon-based materials surface [10, 11]. The physical effects including ultraviolet light emission, shock waves are expected to extend the porous structure of adsorption materials, which might be more favorable for adsorption. Therefore, it is meaningful to modify adsorption materials using non-thermal plasma to improve adsorbent's adsorbability. Kodama et al. [12] examined the surface and textural properties of granular activated carbon with an oxygen non-thermal plasma treatment. They reported that the plasma treatment was an efficient method for generating new oxygen containing functional groups on the surface of the activated carbon. Shen et al. [13] found that the plasma treatment offers several potential advantages over more conventional carbon activation methods. The plasma treatment produced chemically active species affecting the adsorbability. During the plasma treatment, the slower chemical reaction by chemically active species took place only on the surface of activated carbon without changing its bulk properties at low pressure. It is possible to tailor-specific properties by changing the nature of the gas constituting the plasma. Plasma could introduce basic and acid functional groups that were determined by the gaseous resource. The semi-quantitative analysis of the surface acidic functional groups showed that a difference in treatment conditions affected the quality and quantity of the functional groups.

The main objective of this work is the examination of the modification of granular activated carbon (GAC) by using oxygen plasma treatment and the investigation of the effects of different plasma on activated carbon surface modification. The texture, surface chemistry and adsorption characteristics of GAC were investigated by N2 adsorption-desorption isotherms, FE-SEM, FT-IR and adsorption of phenol.

MATERIALS AND METHODS

A. Materials and plasma treatment

Phenol, 99.9% purity, was purchased from Wako. Granulated AC made from coal by Calgon Company was used. AC samples were treated with oxygen plasma at 100-200 Pa using a frequency of 13.56 MHz (KYOTO DENSHI-KEISOKU Co., Ltd., Model PA 1504). The effects of the plasma treatment parameters, namely, treatment time (15, 50, 80, 120 s and 900 s) and input power (50, 80, and 150 W), were examined.

B. Characterization of activated carbons

Activated carbon samples that have undergone various plasma treatment times were characterized by N_2 gas (77 K) adsorption-desorption isotherms, using a surface area and pore size analyzer (BELSORP-Max instrument, BEL Inc., Japan). The specific surface area and mean pore diameter (Dp) were calculated by applying the BET equation to the corresponding isotherms. Micropore volume (Vmi) and external surface area were determined by t-plot method, whereas total pore volume (Vt) was calculated from the volume of adsorbed N_2 held at the relative pressure (p/po = 0.99). The morphology of AC samples was analyzed using a scanning electron microscope (SEM) VE-9800, KEYENCE, Japan). The surface functional groups were studied by Fourier transform infrared spectroscopy (FTIR-670 Plus, Jasco, Japan).

C. Adsorption Experiments

Batch sorption experiments were performed at 298 K in a shaker. The reaction mixture was consisted of a total volume of 100 ml containing 0.25 g of sorbent. An initial phenol concentration of 10 ppm was used. The Flasks were removed from the shaker after the desired contact time and the solution was analyzed for phenol concentration by high-performance liquid chromatography (HPLC, JASCO and Shodex C18M) using 30% acetonitrile: 70% water as the mobile phase and UV-Vis detector at wavelength 254 nm.

The adsorption ratios were determined according to the following formula: adsorption ratio = $((C_i - C_t)/C_i)$ x100 %, wherein Ci is the initial concentration, $mg \cdot L^{-1}$; C_t is the residual concentration, $mg \cdot L^{-1}$.

RESULTS AND DISCUSSIONS

A. Structural and chemical properties of ACs

Fig. 1 shows the obtained relationship between the power of plasma treatment and the specific surface area when the treatment time was 50s, 80s, 120, and 900s, respectively. When the plasma power was adjusted to 80 W, the resultant specific surface area of every treatment time showed a peak value with a global maximum at treatment time 50s. Fig. 2 shows the nitrogen adsorption and desorption isotherms measured at 77 K for the untreated and plasma-treated AC at treatment time 15s, 50s, 80s, 120s, 900s. Table 1 shows the changes in the microstructural properties of the ACs such as specific surface area and micropore volume Vmi as a function of the plasma treatment time.

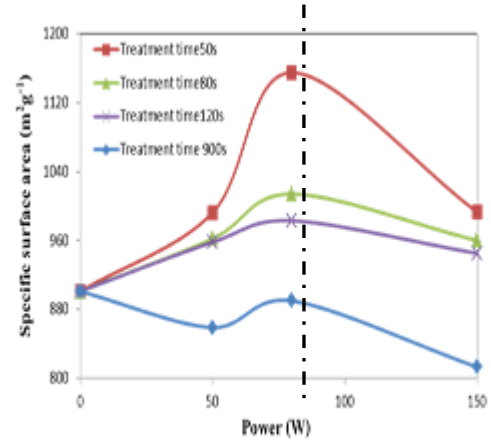

Fig. 1. Relationship between specific surface area and output power of plasma treatment.

It was found that, compared with the untreated AC, the specific surface area of the ACs increased with the plasma treatment time in the order of 900, 15, 120, 80, and 50s. Interestingly, all other microstructural properties also showed a similar trend as that observed with the specific surface area.

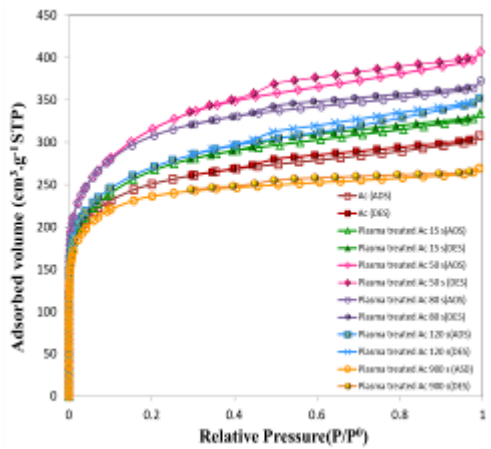

Fig. 2. Isotherms for adsorption (ADS) and desorption (DES) of untreated and plasma-treated ACs, treatment power being 80W.

Therefore it may be considered that the parallel increases in the total and micropore volumes contributed to the favorable changes in microstructure shown in Table 1. These changes may be attributed to the bombardment of the plasma particles consisting of active ions, electrons, photons, and molecules which can cause etching and burning-up effects [14]. It is considered that the active plasma species might not only affect the surface roughness of the ACs but also expose some originally isolated or blocked micropores, thereby

resulting in the observed microstructural changes. However, the cumulative bombardment effect is closely related to the treatment time. When the time was too short, the etching & burning-up effect as well as the unblocking of micropores was weak. On the contrary, if the time was too long, the etching and burning-up effect became excessive, thereby leading to the disappearance of some surface area and micropores [15].

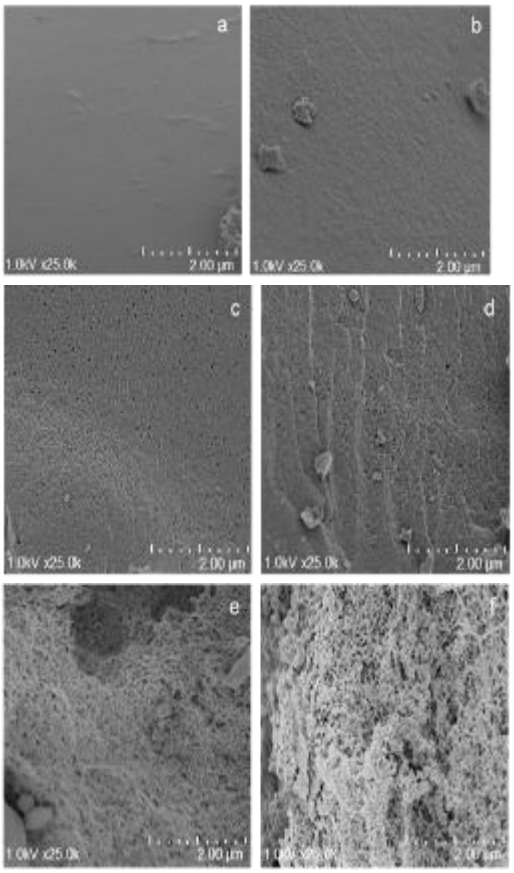

Fig. 3. FE-SEM images of untreated and plasma-treated activated carbon at different plasma treatment times: (a) untreated; (b) 15 s; (c) 50 s; (d) 80 s; (e) 120 s; (f) 900 s. (Plasma treatment power, 80 W).

To compare the changes in surface morphologies between untreated and plasma-treated ACs, FE-SEM images were taken at the same magnification, as shown in Fig. 3. The external surface of the untreated AC shown in Fig. 3(a) was rather smooth, whereas the surface became pitted after oxygen plasma treatment (Fig. 3(b-f)) due to the plasma etching effect, and this can lead to an increase in the specific surface area and total pore volume. However, if the treatment period is too long, the microstructure will be destroyed, thereby reducing the porosity, which corresponded to the structural properties shown in Table 1.

FTIR spectra of the untreated and plasma-treated AC samples are shown in Fig. 4. Both of the FTIR spectra of ACs exhibited a small peak at 2329 cm^{-1} which is due to atmospheric CO_2.

Table 1. Effect of the plasma treatment time on the structural properties of ACs

Treatment time (s)	Specific surface area (m^2/g)	Vt (cm^3/g)	Vmi (cm^3/g)	Dp (nm)	External surface area (m^2/g)
0	901	0.48	0.38	2.01	68.02
15	960	0.51	0.41	2.11	74.25
50	1156	0.63	0.49	2.21	101.01
80	1014	0.57	0.47	2.14	95.67
120	983	0.54	0.42	2.17	79.78
900	890	0.41	0.37	1.87	33.21

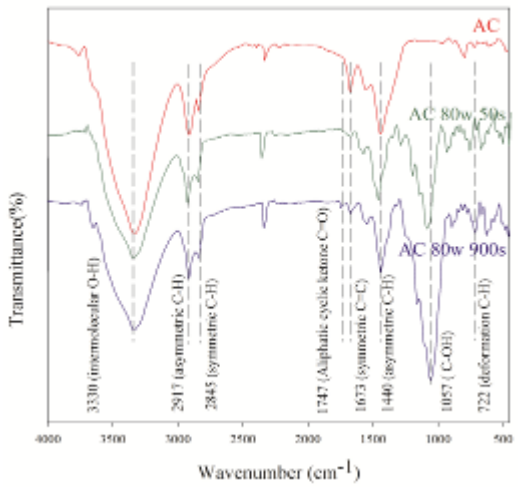

Fig. 4. FTIR spectra of untreated and plasma-treated activated carbons

It could be seen that, in case of the untreated AC, the absorption peak between 3600 and 3200 cm^{-1} indicated the existence of free hydroxyl groups; the 2917 and 2845 cm^{-1} bands might be ascribed to asymmetrical and symmetrical C-H stretching vibrations of aliphatic CH_3 and CH_2 groups; the band at 1673 cm^{-1} might be ascribed to C=C stretching of tetra-substituted alkenes; the bands at 1440 and 722 cm^{-1} might be ascribed to asymmetric bending and in-plane deformations by C-H vibrations of branched alkanes CH_3 and CH_2 groups. After plasma treatment, the oxygen-containing groups significantly increased. For examples, C=O stretching at 1747 cm^{-1} and C-OH stretching at 1057 cm^{-1} were seen [16]. It may be considered that many functional groups were generated during plasma treatment.

B. Adsorption of phenol and contact time

The adsorption of phenol in aqueous solution on plasma treated activated carbon (treatment power 80w, treatment time 15, 50, 900s), and plasma

untreated activated carbon were examined. The Fig. 5 shows the experimental results obtained for the solute adsorbed in function of time. The adsorption experiments were carried out to evaluate the change of the adsorption capacity of the modified by plasma treatment on AC with untreated AC. The working solutions (100 ml in each flask) at 10 ppm concentration of phenol were prepared. The results show that adsorption of phenol increases with time and attain equilibrium in 6 h for each adsorbent. After addition of pre-weighed quantities of the AC, these flasks were kept in an incubator shaker at 298 K for 6 h as the system attained equilibrium within this time period.

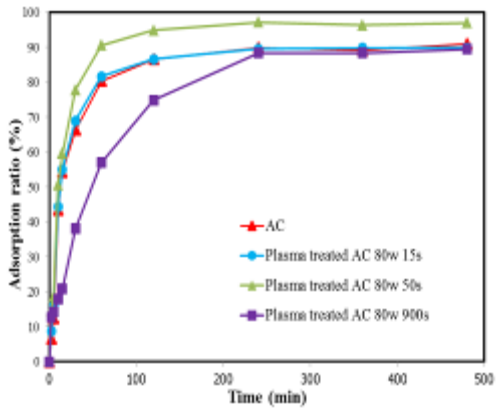

Fig. 5. Effect of treatment time on adsorption amount of phenol (initial phenol 10 ppm).

The extent of phenol adsorption in the case of plasma treated AC at 80w 50s was obtained as 97% in 120 min, whereas for untreated AC and plasma treated AC at 80w 15s the phenol adsorption were 96.5% and 96.6%, respectively. Before 120 min the rate of adsorption was higher. These results indicated that the sorption process could be considered very fast because of the largest amount of phenol attached to the sorbent within the first 120 min of adsorption. For plasma treated AC at 80w 900s under similar conditions, only 74.9% adsorption was obtained. The increase in the phenol adsorption by the plasma treatment is slightly observed, and the amount of the adsorbed phenol was increased with treating time 50s and decreased with treating time 900s. The amount of adsorbed phenol did not change significantly with treating time at 15s. Considering these results, the change in surface area of activated carbon was closely related with the enhancement of its adsorbability. It was clear that the adsorption capacity of AC after O_2 plasma modification was more than that of virgin activated carbon.

CONCLUSION

Surface modification on the ACs was performed using oxygen plasma, and the results were obtained in the microstructural properties of the ACs based on N_2 adsorption-desorption isotherms and FE-SEM results. The specific surface area, micropore volume and total pore volume were increased at certain plasma treatment times and powers. The bombardment of the plasma particles was able to etch the surface and generate tiny voids on the surface of some of the micropores, which correspondingly brought the development in the microstructural properties on the ACs. It was also found that the surface of the ACs could be over-etched and some of the micropores might be blocked at the long plasma treatment time or high plasma treatment power. New functional groups, i.e., C=O, and C-OH were generated on the surface of the ACs. An oxidative reaction mechanism was proposed, in which the formation of oxygen containing functional groups was deduced. The reactions between the plasma generated radicals and active species in the plasma atmosphere were found to be the essential for the changes in the surface functionalities. Moderate plasma treatment parameters such as 50 s and 80 W were found, at which the microstructural properties and surface functionalities could be both improved. The effects of the plasma treatment on the structural properties of the ACs were attributed to the low-pressure plasma used in this experiment. It is believed that the high kinetic energy and low-pressure plasma developed some of the micropores and weakened the burn-up effects than those in atmospheric pressure plasmas. The development of the micropores, i.e., the increased roughness and generated tiny voids might offer the space to accommodate the new functional groups, and the newly generated oxygen containing groups might not block the micropores. With regard to phenol adsorption capacity of different plasma modified ACs, the adsorption of phenol in time function revealed that O2 plasma could enhance the adsorption amount of phenol on ACs at moderate plasma treatment parameters. All these results are helpful to further explore the process of adsorption materials with O2 plasma modification and the effect of the textural characteristics on the adsorption of phenol.

ACKNOWLEDGMENT

The authors are grateful for the financial support of the Japanese government (monbukagakusho:mext) scholarship, The Global COE Program (Novel Carbon Resources Sciences, Kyushu University), the Japan Science and Technology Agency(JST), and Grant-in-Aid for Scientific Research No. 21246135 and 24246149 from the Japan Society for the Promotion of Science (JSPS).

REFERENCES

[1] JB Donnet, R Bansal, F Stoeckli, and M Dekker. 1998. Active carbon. New York.

[2] A Bouzaza, A Laplanche, and S Marsteau. 2004. Adsorption-oxidation of hydrogen sulfide on activated carbon fibers: effect of the composition and the relative humidity of the gas phase. Chemosphere, 54(4): 481-488.

[3] JP Chen, SN Wu, and KH Chong. 2003. Surface modification of a granular activated carbon by citric acid for enhancement of copper adsorption. Carbon, 41: 1979–1986.

[4] BS Girgis, AA Attia, and NA Fathy. 2007. Modification in adsorption characteristics of activated carbon produced by H_3PO_4 under flowing gases. Colloid Surf. A: Physicochem. Eng, 299: 79-87.

[5] JA Menéndez, B Xia, J Phillips, and LR Radovic. 1997. On the modification and characterization of chemical surface properties of activated carbon: microcalorimetric, electrochemical, and thermal desorption probes. Langmuir, 13: 3414-3421.

[6] JL Figueiredo, MFR Pereira, MMA Freitas, and JJ.M Órfão. 1998. Modification of the surface chemistry of activated carbons. Carbon, 37: 1379-1389.

[7] MAM Silva, AE Martinelli, C Alves Jr, RM Nascimento, MP Távora, and CD Vila. 2006. Surface modification of Ti implants by plasma oxidation in hollow cathode discharge. Surf. Coat. Technol., 200: 2618-2626.

[8] F Leroux, C Campagne, A Perwuelz, and L Gengembre. 2008. Polypropylene film chemical and physical modifications by dielectric barrier discharge plasma treatment at atmospheric pressure. J. Colloid Interface Sci., 328: 412-420.

[9] DR Grymonpre, WC Finney, and BR Locke. 1999. Aqueous-phase pulsed streamer corona reactor using suspended activated carbon particles for phenol oxidation: model-data comparison. Chem. Eng. Sci., 54: 3095-3105.

[10] EI Tochitsky, NM Chekan, VT Svirin, and IV Gasencova. 2000. Use of low-energy ion assistance for the modification of diamond-like carbon films conductivity. Vacuum, 58: 79-86.

[11] L Gu, XW Zhang, LC Lei, and Y Zhang. 2009. Enhanced degradation of nitrophenol in ozonation integrated plasma modified activated carbons. Micropor. Mesopor Mat., 119: 237-244.

[12] S Kodama, H Habaki, H Sekiguchi, and J Kawasaki. 2002. Surface modification of adsorbents by dielectric barrier discharge. Thin Solid Films, 407: 151-155.

[13] W Shen, Z Li, and Y Liu. 2008. Surface Chemical Functional Groups Modification of Porous Carbon, Recent Patents on Chemical Engineering, 1:27-40.

[14] JR Utrilla, I B Toledo, MAF Garcia, and CM Castilla. 2001. Activated carbon surface modifications by adsorption of bacteria and their effect on aqueous lead adsorption. Journal of Chemical Technology and Biotechnology, 76: 1209-1215.

[15] AB Garcia, AM Alonso, CAL Leon and JMD Tascon. 1998. Modification of the surface properties of an activated carbon by oxygen plasma treatment. Fuel, 77: 613-624.

[16] The Saddler Handbook of Infrared Spectra. Bio-Rad Laboratories, Inc., (http://www.scribd.com/doc/39589123/Sadtler-Handbook-of-Infrared-Spectra)

A Novel Low-cost Pyroelectric Device for Enhancing the Solar Cell Efficiency

S Kumar*, NC Sharma, BR Mehta**, and SK Saha

Ultrasolar Technology, Santa Clara, USA; **Indian Institute of Technology Delhi, New Delhi, India
*e-mail: santosh@ultrasolartech.com

Abstract

This paper describes a novel technology to improve the efficiency of solar cells by applying high frequency pulses from pyroelectric devices. It is shown that the application of high frequency pulses from pyroelectric devices to solar panels enhances the output of the panels by about 25%. The relevant experimental results are presented to illustrate the important aspects of pyroelectric technology to improve the efficiency of solar cells.

INTRODUCTION

Photovoltaic (PV) devices are capable of generating at least as much power as they are generating today, if the excess losses in photon energy and transmission can be eliminated [1-2]. The research impetus for achieving increased efficiency with lower cost of materials and production has resulted in the emergence of different generation of solar cells [1]. The stability and high efficiency have been the main characteristics of PV cells based on single crystalline and polycrystalline silicon. Thin film solar cells comprising of CdS-CdTe and CdS-$CuInSe_2$ junctions have the potential advantage of lower material costs. Tandem solar cells fabricated using sophisticated fabrication technologies have shown high efficiency due to optimized optical absorption. Recently, a number of new generation methodologies have been proposed to further increase the solar cell output [1]. For harvesting the energy of hot carriers, energy selective resonant tunneling contacts having near ideal tunneling probability have been employed to extract energetic carriers [1-3]. The up- and down-conversion concepts for effective absorption of photons having energy lower or higher than the band gap by using the nanoparticle and nanorod structures have also been tried out. The plasmonic nanostructures have recently been used to reduce the reflection losses and coupling the incident energy to the semiconductor layer. It needs to be mentioned that the new type of solar cells will require large modifications in the existing solar cell technology. The development of reliable methods for incorporating these concepts in large area devices and large scale applications is a serious nagging issue. Therefore, novel technologies to improve the efficiency of existing solar cells are critical for the widespread adoption of solar energy in the commercial as well as residential buildings [4]. For the first time, this paper reports the Ultrasolar Technology, Inc. developed technology, called the "UST," to increase the solar cell output by pyroelectric device-generated input pulses to the solar cells. Also, the experimental data showing the improvement in the PV cell efficiency by UST is described in this paper.

EXPERIMENTAL PROCEDURE

The central theme of UST is the generation of high voltage pulses using low-cost pyroelectric thin film structures. The pyroelectric device comprises of a multilayer structure of pyroelectric materials having an optimized number of layers, material composition, and thickness. A specially designed electronic circuitry supplies a train of pulses to the pyroelectric devices, which absorb ambient thermal energy, produce infrared standing waves and finally results in the formation of high-voltage high-frequency pulses. The pyroelectric device along with the associated circuitry is built in a system called "Quantum Boost' or 'QB.' The application of high voltage and high frequency pulses from the QB to solar panels modifies the p-n junction behavior of the cells resulting in an enhanced solar cell output. The detailed methodology is described elsewhere [4].

Figure 1 shows the test configuration used in the present study for investigating the effect of QB on solar cell output. In Fig. 1, the QB is connected in between the solar cell module and the inverter. The QB sends high frequency voltage pulses to the solar cell module and the increased power from the solar cell is fed to the inverter and grid simulator. Grid simulator provides power to a load (a set of incandescent electric bulbs in this case).

RESULTS

The procedure described in the previous section is used to improve the efficiency of existing solar panels. A typical set of test data obtained from the test configuration in Fig. 1 is reported in Table 1. Under any particular condition of illumination with or without the QB, the output (AC power) from the PV panel is the difference in grid power when the PV panel is connected (y) and not connected in the circuit (x). It is observed from the data that the PV output from the panel is 126.7 W without the QB. When QB is connected in between the PV panel and inteverter, the power output increases to 161.7 W confirming an increase of 27.6%. As already mentioned, pulse generation is the key component of the present technology. Thin film Pyroelectric module along with the electronic circuit generates

high voltage and high frequency pulses of short duration. Fig. 2 shows a typical pulse recorded on the oscilloscope indicating **a voltage, pulse frequency, and pulse width**. The collected data during the technology development cycle indicate that the increase in the output power (ΔW) depends on the voltage (V), frequency (f), and the intensity (I) of the incident solar radiation. It is observed that the value of ΔW is directly proportional to V and f and inversely proportional to I. The detailed experiment is in progress to establish a quantitative relation between ΔW and the set of parameters $\{\alpha, \beta, \gamma\}$ and extract the values of $\alpha, \beta,$ and γ.

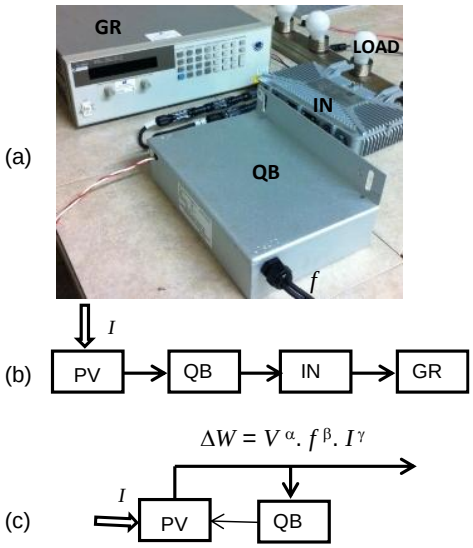

Fig. 1. Measurement system: (a) photograph; b) Schematic diagram of the test configuration showing photovoltaic panel (PV), Quantum Boost (QB), Inverter (IN), and Grid Simulator (GR); where I is the intensity of incident solar radiation; c) increase in the power output of the PV by high voltage (V) and high frequency (f) pulses.

Fig. 3 shows current-voltage characteristic of a silicon solar cell with and without the QB. It is observed from Fig. 3 that there is a large change in the value of the short circuit current density from 20 mA/cm^2 (without QB) to about 40 mA/cm^2 (with QB) due to the application of high frequency pulses. The data shown in Fig. 3 are an unambiguous demonstration of the increase in the solar output power, ΔW, using the present methodology. The overall improvement, ΔW recorded in a typical day for a 1.5 KW panel string is in the range of 30-40% when lower solar intensity is incident in the early and evening hours of the day, in comparison to that of 15-20% during the high intensity period. This is consistent with the results described earlier that the excess power, ΔW, generated by the QB is inversely proportional to light intensity. Fig. 3 shows current-voltage characteristic of a silicon solar cell with and without the QB. It is observed from Fig. 3 that there is a large change in the value of the short circuit current density from 20 mA/cm^2 (without QB) to about 40 mA/cm^2 (with QB) due to the application of high frequency pulses. The data shown in Fig. 3 are an unambiguous demonstration of the increase in the solar output power, ΔW, using the present methodology. The overall improvement, ΔW recorded in a typical day for a 1.5 KW panel string is in the range of 30-40% when lower solar intensity is incident in the early and evening hours of the day, in comparison to that of 15-20% during the high intensity period. This is consistent with the results described earlier that the excess power, ΔW, generated by the QB is inversely proportional to light intensity.

Table 1. PV output generated by the PV panel is the difference $(x - y)$ between the power supplied by the grid simulator with and without the PV panel.

Power (W)	PV Panel	Without QB	With QB
Grid (x)	No Panel	269.7	269.7
Grid (y)	With Panel	143.0	108.0
PV output $(x - y)$	With Panel	126.7	161.7

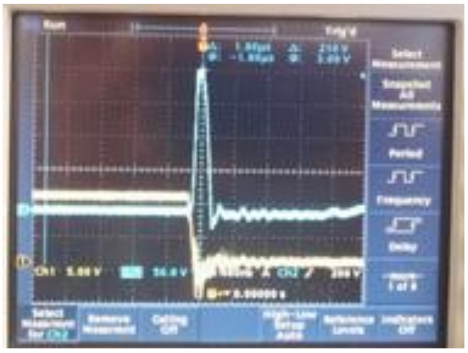

Fig. 2. The oscilloscope image showing the pulse generated by the pyroelectric device in the QB; Here, pulse height = 210 V, pulse width = 100 nsec, and frequency = 10 MHz.

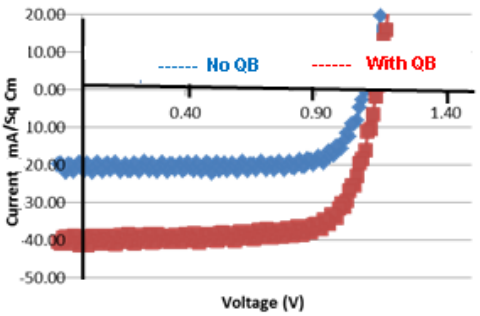

Fig. 3. $I - V$ curve of a silicon solar cell under 0.44 sun intensity with and without the QB.

DISCUSSION

Now, let us discuss the principle of operations of solar output enhancement by describing the effect of high frequency pulses on the various optoelectronic processes important for solar cell operation.

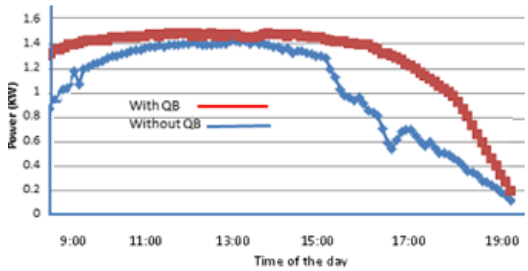

Fig. 4. Power output from a solar cell panel string with and without the QB measured on two different days having similar light conditions.

It is well known that the effectiveness of photon absorption and, carrier generation and collection are important for an efficient solar cell operation. Photon-electron interaction in a solid state material is an instantaneous process and is determined by the value of absorption coefficient. Photon-electron interaction in an indirect band-gap semiconductor is determined by the absorption or emission of a phonon to satisfy the momentum conservation. Thus, the phonon density-of-states (DOS) plays an important role in photon absorption in an indirect band-gap semiconductor. As already mentioned, a significant fraction of the incident solar energy is lost as heat during the thermalization process in which hot carriers interact with crystal lattice vibrations. Thus, the phonon DOS, also, plays an important part during the thermalization process. As per the Kleman's criterion, the presence of a gap between the acoustic and optical phonon states is a favorable condition for arresting the hot carrier thermalization process in a semiconductor [5]. The defect and surface states act as sinks for minority carriers due to infinite recombination velocity which can affect the photo-generated carriers in a semiconductor. The structural defects, surface irregularities, impurities, lattice defects, bond angle, and bond length disorders are the main sources of defect states. In bulk and thin film semiconductors, the presence of defect states is detrimental towards carrier mobility as the defect states may act as recombination or trap centers by capturing electron or holes [6]. The presence of energy states in the forbidden gap of a semiconductor can, also, modify photon absorption. For example, the defect states in ZnTe are known to increase the absorption of photons having lower energy than the band gap resulting in the formation of double energy gap [7]. It can be concluded from the above discussions that the factors which affect electronic or phononic DOS can have a strong influence on the photon absorption and carrier transport which can influence the p-n junction and solar cell properties. The application of high frequency and high voltage pulses of short duration is the key component of Ultrasolar Technology.

There is a limited published work describing the effect of high frequency pulses to a p-n junction or a photovoltaic device. It has been reported that the application of high electric field can produce metastable states in indirect band gap semiconductors. The application of external pulsed electric field (1 MV/cm) has been observed to stabilize the electron-hole excitons and decreased recombination in a number of material systems [8]. The effect of external electrical field on the dipole moment of Si-O bonds has been observed to produce changes in the phonon DOS spectra due to the electric field-dipole moment coupling [9]. The electro-acoustic effect indicating an interaction between the externally applied electric field and the phonon spectra has been observed experimentally and explained theoretically [10]. It has been shown that the carrier transport based on Boltzmann equation breaks down and quantum effects influence the electron-phonon interaction in semiconductors in the presence of high values of electric field (10 kV/cm) [12]. It can be inferred from the above results that the application of high frequency pulses can influence the optoelectronic processes in a semiconductor via formation of short life time metastable states and modify the phonon spectra. Now, at low frequency and low electric field, the changes in the depletion region can cause carrier collection process. However, at high electric field, photon absorption process can be influenced due to the presence of additional states. Thus, the changes in the phonon spectra can influence the photon absorption process in an indirect band gap semiconductor like silicon, thus, arresting the thermalization of hot carriers. The above description is schematically shown in Fig. 5.

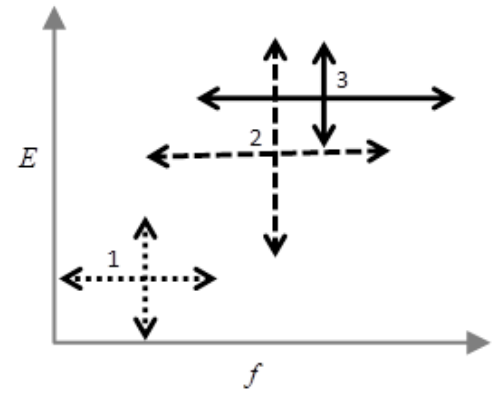

Fig. 5. A qualitative illustration of model mechanisms describing the effect of high frequency pulses to a semiconductor junction. 1: Modifications in junction field, 2: Change in the density of phonon states and 3: Creating of metastable states at different values.

Finally, to analyze the performance of PV cells, subjected to high frequency and high voltage pulses from the QB, we have developed a simplified analytical model for circuit simulation. The model considers the generation of excess electrons by the application of pulses in the PV cells from the QB and subsequent collection of theses electrons in the cells. Using this model, the circuit simulation is performed to generate $I - V$ characteristics of the solar cells as a function of the collected QB-generated excess electron density (n). From the simulated $I - V$ data, we have computed the corresponding power (P) for each n. The results are shown in Fig. 6. It is seen from Fig. 6 that the QB-generated input pulses to solar cells facilitate the generation of excess electrons and collection of these electrons in the cells to improve the solar cell efficiency [11]. The simulation data in Fig. 6, also, shows that the improvement in the solar cell performance increases with the increase in the collection of QB-generated electrons in the solar cells. It is obvious from Fig. 6 that both short-circuit current and open circuit voltage (V_{oc}) improves with the increase in the collection of QB-generated electrons in the cells. The larger increase in the value of V_{oc} in Fig. 6 compared to that in Fig. 3 is due to the consideration of ideal diode behavior of the solar cells in our circuit analysis.

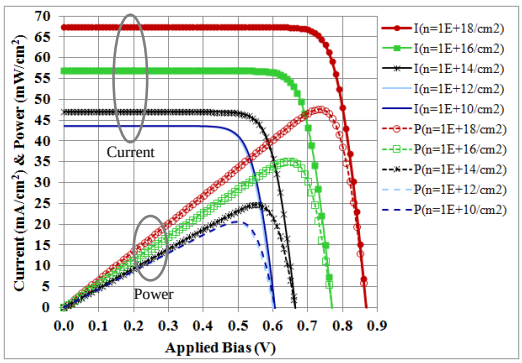

Fig. 6. The simulated $I - V$ and $P - V$ characteristics of solar cells as a function of QB-generated electron collection in a typical solar cell by high frequency and high voltage pulses.

CONCLUSION

Direct experimental results described in this paper confirm the two important components of the Ultrasolar Technology. First of all, Quantum Boost comprising of a pyroelectric thin film module and electronic circuit has been shown to generate high voltage (200-210 V) and high frequency (upto 10 MHz) pulses. Secondly, the application of high frequency pulses to solar cells has been shown to results in an increase in the solar cell output over 25% in individual solar cell and strings of solar cells. The modification in the junction field, creation of metastable states, and phononic density of states due to the application of the high frequency pulses result in the improvement in the photon absorption and carrier collection processes. The experimental data agrees very well with the circuit simulation data obtained by analytical PV cell model.

ACKNOWLEDGMENT

We greatly appreciate and acknowledge very fruitful technical discussions during this work with Dr. Joel Ager from Lawrence Berkeley National Laboratory, Berkeley, CA, USA.

REFERENCES

[1] M.A. Green, "Third generation photovoltaics: Advanced solar energy conversion," Springer, 2003.

[2] Honsberg and S. Bowden, http://pveducation.org /pvcdrom/solar-cell-operation/light-generated-current .

[3] A.L. Bris, J. Rodiere, C. Colin, J.-L. Pelouard, R. Esteban, M. Laroche, J.-J. Greffet, and J.-F. Guillemoles, "Hot carrier cells: Controlling thermalization in ultrathin devices," IEEE Journal of Photovoltaics, vol. 2, no. 4, pp. 506-511, October 2012.

[4] S. Kumar, "Non-decaying electric power generation from pyroelectric materials," US Patent 8,324,783, 2912, December 4, 2012.

[5] P.G. Klemens, "Anharmonic decay of optical phonons," Phys Rev., vol. 148, no. 2, pp.845-848, August 1966.

[6] K.L. Chopra and S.R. Das, "Thin Film Solar Cells," Plenum Press, 1983.

[7] Next Generation photovoltaics, edited by A.B.C. López, A.M. Vega, and A. L. López, Springer 2012.

[8] N.C. Giebink and S.R Forrest, "Accumulation of electric-field-stabilized geminate polaron pairs in an organic semiconductor to attain high excitation density under low intensity pumping,"Appl. Phys. Lett., vol. 89, no. 19, pp. 193502-193503, November 2006.

[9] D.E. Milovzorov, "Acoustoelectric effect in microcrystalline and nanocrystalline silicon films prepared by CVD at low and high deposition temperatures," Journal of Physics, vol. 1, no. 2,pp. 38-49, January 2012.

[10] Rotter, A. Wixforth, W. Ruile, D. Bernklau, and H. Riechert, "Giant acoustoelectric effect in GaAs/$LiNbO_3$ hybrids," Appl. Phys. Lett., vol. 73, no. 15, pp. 2128-2130, August 1998.

[11] H. Hirori, K. Shinokita, M. Shirai, S. Tani, Y. Kadoya, and K. Tanaks, "Extraordinary carrier multiplication gated by a picosecond electric field pulses," Narure Communications| DOI: 10.1038/ncomms1598, pp.1-6, December 2011.

[12] Sano and A. Yoshii, "Quantum effects on electron-phonon interaction under high electric field in semiconductors," Semicond. Sci. Technol., vol. 7, no. 3B, pp.36-38, March 1992.

Consideration of Solid Desiccant Dehumidification and Air Conditioning System for Greenhouses of Pakistan: A Feasibility Study

Muhammad Sultan[1*], Takahiko Miyazaki[2,3], Shigeru Koyama[2,3] and Bidyut Baran Saha[1,3]

[1]Interdisciplinary Graduate School of Engineering Sciences, Kyushu University, Fukuoka 816-8580, Japan
[2]Faculty of Engineering Sciences, Kyushu University, 6-1Kasuga-koen, Kasuga-shi, Fukuoka, Japan
[3]International Institute for Carbon-Neutral Energy Research, Kyushu University, Fukuoka 819-039, Japan
*e-mail: sultan@phase.cm.kyushu-u.ac.jp

Abstract

Farmers in Pakistan are used to grow the off-seasonal vegetables and fruits in greenhouses/tunnels mostly in winter (October to April). Plants are seriously encountered with high humidity and temperature problems. This result in terms of diseases, pests & fungus attack and in this way farmers have to bear yield loss. In this study, the system demands are concluded by keen research on greenhouse requirements and ambient conditions. Certainly the desiccant system has a potential to deal with such kind of situations. Various options are reviewed to establish a desiccant system which can generate desired conditions. Solid desiccant system has not only shown the promising results to control humidity but also shown the potential to deal temperature stresses by addition of temperature controlling devices. It can deal the humidity and temperature distinctly and can be operated in more flexible way by possessing vapor pressure deficit (VPD). This is a novel research in this territory and promising vigorous outcomes. In present work it is projected that the regeneration of desiccant wheel can be done by harnessing the solar energy. The paper demonstrates that desiccant system is a feasible solution for cooling/heating and dehumidification of greenhouse environment and highly substantial for Pakistan's conditions.

INTRODUCTION

Pakistan's soil is enriched in fertility and its versatile climate supports several agricultural products grown on it. But still Pakistan is not producing the variety especially in vegetables and fruits rather than hardly meeting its food demand because of improper management in this sector. The imports of vegetables are increasing every year because of production and demand gap. Growing off-seasonal products in greenhouses can justify this inefficient production as well as production & demand gap. Farmers are scared to grow in greenhouses due to inappropriate control of temperature and humidity so this bounds them to conventional cropping. Farmers are not employing the modern agricultural techniques and even they are not in position to use expensive technologies. In this paper it is tried to broadcast that how the desiccant system can make it possible to grow more profitable off-seasonal vegetables and fruits in greenhouse economically rather than the conventional crops.

Most of the existing greenhouse growers are cultivating the summer vegetables and fruits in winter by their conventional fashion and still getting the profit. Many of the times they failed to maintain the humidity and temperature level within the greenhouse / tunnels so they have to bear a big yield loss. Due to this complex regulatory of temperature & humidity, the rest of the growers especially the small land holders could not get courage to establish their greenhouse. A low cost dehumidification and temperature controlling system is compulsory to increase the number of greenhouses and the yield of existing greenhouses to overcome the production and demand gap in Pakistan.

In this paper it is presented that the desiccants based systems are not only the handy choice for controlling the humidity in greenhouses but also has a potential to deal with temperature stresses. The desiccant based air conditioning and dehumidification system can serve as an economical solution for the greenhouse problems in Pakistan.

GREENHOUSE INSIGHT

Normally in Pakistan the off-seasonal vegetables and fruits are grown in greenhouses in winter from October to April. These off-seasonal vegetables and fruits are Cucumber, Tomato, Capsicum, Green Chilli, Bitter Gourd, Brinjal (Egg Plant), Bottle Gourd, Summer Squash (Cucurbita Pepo), Sponge Gourd, Pumpkin, Musk Melon, Water Melon, Strawberry and some more. As per the guideline provided by the Department of Agriculture, Government of Punjab-Pakistan, these products require 15-30 ^{0}C temperature for their proper cultivation in winter depending upon the type of the products [1]. It is true that the level of humidity is more important as compared to temperature while growing off-seasonal products in Pakistan. The optimum relative humidity range for every vegetable and fruit grown in greenhouse varies tremendously, mostly 50-80% [1] but it may require less for a particular period when there is a threat of pests or funguses. So it is very difficult to have the ideal humidity level in greenhouse all the time.

The greenhouse growers are facing serious problems of high humidity and cold weather from

November to February especially at night time. As fog also forms during November to February in Pakistan [2] and this harm the plant severely. Some greenhouse products are considerably sensitive to fog and in some cases the permanent wilting take place if the plants are encountered with fog for long time. Fog is considered to occur when relative humidity goes 90-100% and wind condition is calm [2]. Normally fog is formed after sundown because the air and ground surface begin to cool at this time and condensation replaces the evaporation [3].The visibility is highly affected by the fog and it does not allow the sunshine to reach the plants hence reducing photosynthesis.

These conditions result either in terms of pests & fungus attack or wilting of plant and ultimately farmers have to give-up the high proportion of the yield. The productivity of some sensitive vegetables and fruits is even affected by high temperature in October, March and April especially at day time.

AMBIENT CIRCUMSTANCES

Most of the agriculture in Pakistan is performed at Punjab and Sindh provinces (Fig. 1) due to the availability of fertile soil, irrigation water and suitable environment. The present study is more focused towards these areas. The average dry bulb temperature and relative humidity at morning time for fifteen (15) agricultural cities of Punjab & Sindh from 2000-2010 during November to February varies from 9-15°C and 70-90% respectively [2]. Due to these conditions shallow frequency of fog (general visibility ranges from 500~999 meters) is developed as shown in Fig. 2.

Fig. 1 Map of Pakistan showing its territory

In case of December & January the avg. temperature falls between 5-11°C and avg. humidity ranges from 80-92%. December and January are the coolest months and there will be more fog produced in these months, especially in the eastern Punjab [4]. In the month of October, March and April the ambient temperature especially at daytime becomes slight warmer and need to be cool for ideal growth of plants. The humidity level for these months doesn't differ extremely with the plant requirements.

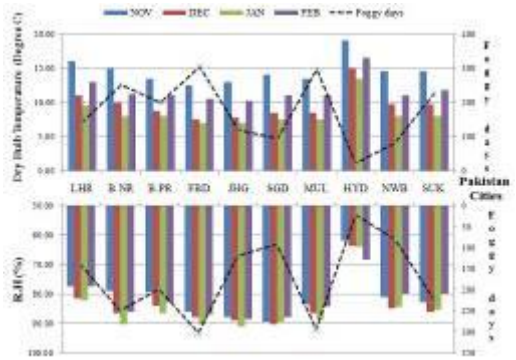

Fig. 2 Avg. dry bulb temperature, Avg. Relative Humidity and No. of Foggy days for selected agricultural areas of Punjab & Sindh (0000 UTC; from 2000-2010; November to February) Reproduced from [2]

SYSTEM DEMANDS

By critically break downing the requirement of off-seasonal product and keenly discovering the ambient conditions, the followings can be set as the demands of the system as listed in Table 1.

Table 1. System demand for off-seasonal cultivation in greenhouses of Pakistan

Months	Time	Demands˜	
		Moisture	Temp.
Nov. to Feb.	Day Time	×	×
	Night Time$^{\propto}$	Dehumidification	Heating
Oct, Mar & April	Day Time	Dehumidification	Cooling
	Night Time	×	×

˜The intensity of the demand varies according to type of the greenhouse product.
$^{\propto}$Utmost demand

Technically the humidity (moisture) and temperature level for any agricultural product is designed by its ideal vapor pressure deficit (VPD) value. VPD is the gradient measured as difference between water vapor pressure in plant leaves and ambient air. This means each temperature values (within the designed temperature range) will hold a different level of humidity to keep the vapor pressure deficit (VPD) as constant. The ideal VPD value depends upon the crop species, its maturity level and ambient environment. Table 2 shows the ideal VPD for the five growth stages of tomato for Malaysia [5]. It can be noticed here that the plant requires fluctuating VPD (i.e. temperature and humidity). This means the designed system should be proficient in dealing the humidity and temperature distinctly.

Table 2. Ideal VPD for five growth stages of tomato for Malaysia.

Growth Stage	Ideal VPD (kPa)		
	Sunny Day	Cloudy Day	Night
Germination	0.84	0.84	0.84
Seeding	0.840-0.891	0.746	0.884
Vegetable	0.855-0.963	0.843-0.955	0.841-0.935
Early fruiting	0.855-0.963	0.843-0.955	0.841-0.935
Mature fruiting	0.855-0.963	0.843-0.955	0.841-0.935

Before regulating the humidity and temperature levels in greenhouse it is important to understand some facts. Photosynthesis is most important process in plants. In this process the plants make carbohydrate using the carbon dioxide and light energy.

Carbon dioxide + water + light (energy) → carbohydrate + oxygen + water

$2n\ CO_2 + 4n\ H2O + photons \rightarrow 2(CH_2O)\ n + 2n\ O_2 + 2n\ H_2O$

Photosynthesis can only occur when the light is available. At day time plants use the light (normally from sun) and CO_2 from the ambient air to produce carbohydrates. At least in sunshine hours the system should capable to supply the ambient air enriched in CO_2 after regulating to the desired level of humidity and temperature. There is also a need to dehumidify the air at night time because the plants release the moisture by transpiration all the time.

DESICCANTS AND DEHUMIDIFICATION

Desiccants are the hygroscopic substance (solid or liquid) which can adsorb and desorb the moisture e.g. silica gel, titanium silicate, activated alumina etc. According to the type & properties of desiccant, many systems may be established for air conditioning to meet the latent / dehumidification load as well as cooling demand. Normally the desiccant rotor comprises a matrix and contained parallel channels which ensure that the laminar flow of air can occur in it. These channels increase its surface area hence providing more space for heat and mass transfer. The matrix is coated with the desiccant material and the desiccant wheel is then allows to rotate with slow speed. Fig. 3 shows that the dehumidified air is produced by the desiccant rotor. A hot regeneration air is always needed to release the moisture adsorbed by the desiccant rotor and make it ready for next adsorption cycle.

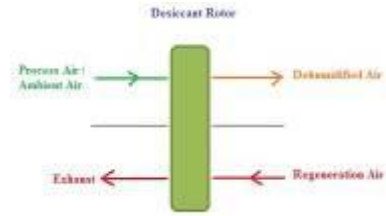

Fig. 3. Dehumidification by desiccant rotor

A. *Typical Desiccant System*

A typically solid desiccant dehumidification and air conditioning system is shown in Fig. 4. It is an open cycle system which is driven by the heat to regenerate the desiccant. The system consists of a desiccant wheel/rotor followed by the heat exchanger to recover the heat of adsorption. Many temperature controlling devices are used to incorporate with the system to obtain the desired conditions. A regeneration coil is used to produce the hot air for the regeneration of the desiccant. This heat may be carried out either using electricity/ fossil fuel heaters or renewable energy.

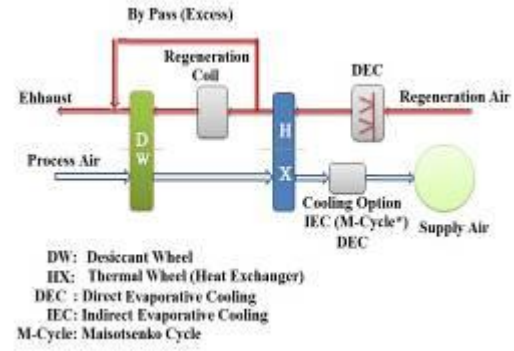

Fig. 4. Typical solid desiccant dehumidification and air conditioning system

i. *Dehumidification and Cooling*

The psychometric chart in Fig. 5 shows the simple cooling and dehumidification process by the desiccant system. During the day time of October, March and April the warm and moist air in greenhouse is required to be cooled and dehumidified. For example the warm moist ambient air having 27 ^{0}C and 13.8 g/kg humidity ratio is passed through the desiccant rotor and then it comes off at say, 45 ^{0}C and 6.2 g/kg moisture contents (process 1~2). This supply air is then passed through the thermal wheel/heat exchanger where it is sensibly cooled at say 25 ^{0}C (process 2~3). This air can further cooled up to the desire level by indirect (3~4) or direct (3~5) evaporative cooling keeping in view the demand conditions as described in Table 1. It is important that if the humidity control is not required in the greenhouse then cooling coil (3~4) can be replaced by direct evaporative cooler (3~5).

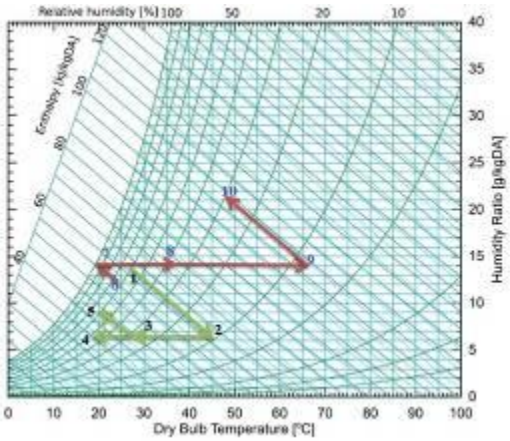

Fig. 5. Dehumidification and cooling by desiccant system for Oct, March & April (daytime)

For the cyclic use of desiccant wheel it needs to regenerate it by passing the hot air. Ambient air or return air can be used for the regeneration air. It is required to feed the fresh air into greenhouse to meet the carbon dioxide demands for photosynthesis at sunshine hours. Using the return air for regeneration and ambient air for process air will be more suitable option in order to maintain the carbon dioxide level in greenhouse without using any external source of CO_2. To reduce the system operating cost almost 20% of the return air flow by-passed the regeneration coil and desiccant [6].

The return air from the greenhouse having bit high humidity due to transpiration at say 24 ^{0}C & 12.5 g/kg moisture contents is further humidified by evaporative cooling (6~7) at say 19 ^{0}C with 14.1 g/kg moisture content. Thermal wheel heat exchanger (7~8) exchanges / recover the heat of adsorption (1~2) from the process air. As the return air leaves the thermal wheel it has been sensibly heated approximately 37 ^{0}C keeping the same humidity level. The regeneration air is then heated by some means at say 66 ^{0}C so that it can regenerate the desiccant efficiently (9~10). This regeneration heat may be supplied via renewable or waste energy option (e.g. solar etc.).

ii. Dehumidification and Heating

The psychometric chart in Fig. 6 shows the simple dehumidification and heating process by desiccant system. As Table 1 shows that the greenhouses need dehumidification and heating during the night time from November to February. It is important to notice here that how desiccant system satisfies the heating demand by using heat of adsorption. Let the cold and humid ambient air (or return air) of 12 ^{0}C and 8 g/kg moisture content is passed through the desiccant wheel to be dehumidified and it comes off at say 23.5 ^{0}C and 3.2 g/kg moisture contents (process 1*~2*). This process air is enough dry and quite warm as well. Keeping in mind the requirement of the greenhouse the dry process air can easily be achieved to required temperature and humidity level by the use of heat exchanger (process 2*~3*). Photosynthesis is not supposed to occur in plants at night due to the absence of light. Hence the plant does not require carbon dioxide rather produces it through transpiration. So the return air can be used as process air and ambient air can be used for the regeneration of the system. The regeneration air after exchanges the heat in heat exchanger is then heated up to the certain level (4*~5*) by some heating source for the regeneration of the desiccant rotor (5*~6*).

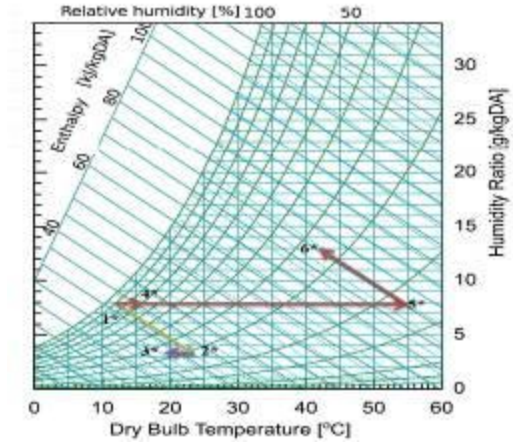

Fig. 6. Dehumidification and heating by desiccant system from November to February (night time)

Control of temperature and humidity is very significant for these four months because plants are subjected to relatively higher moist and cold stresses in this period. As discussed earlier, the fog also takes place in this period so it needs more systematic attention. The heating source is only the subject that needs more consideration. In our study we focused to use the renewable or waste energy for this heating (4*~5*). Later it is showed how this regeneration process is carried out at day time by the sun energy available abundantly in the subjected sites.

B. Solar Grounded Desiccant System

The major operating cost of the desiccant system is caused by the regeneration of the rotor. By using the solar energy the cost of the system will be minimized. The greenhouse growing areas of Pakistan has the high potential of solar energy. On average solar global insolation 5–7 kWh/m2/day exists in the Pakistan over more than 95% of its area with persistence factor of over 85% [7-8]. This renewable energy can be utilized in the desiccant system for the desiccant regeneration. As there are several researches about the solar desiccant system and it shows the promising result if enough solar radiation are available.

A simple desiccant dehumidification and air conditioning system assisted by solar thermal energy is shown in Fig. 7. There are many desiccant

dehumidification and air conditioning system in many countries which are operated efficiently on the solar energy [9]. The COP of the solar desiccant system depends upon the availability of solar radiation. Since the required temperature for an efficient regeneration of desiccant wheel is low, within the range of 45–90 ^{0}C [10], solar desiccant system, which can deal the dehumidification and air conditioning demand nicely, is expected to provide particular heat for regeneration of the rotor. Researchers concluded that the utilization of solar energy in the desiccant system increases the coefficient of performance (COP) between 50% and 120% [11].

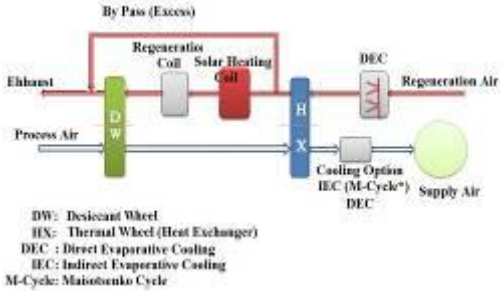

Fig. 7. Solar desiccant model for dehumidification and air conditioning

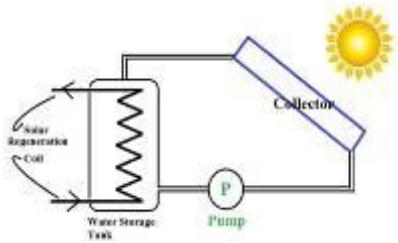

Fig. 8 Solar thermal energy assortment

The regeneration of the desiccant by the solar energy may performed by adding the solar regeneration coil with the desiccant system as shown in Fig. 8. Produce the hot water by solar thermal energy and use it for the regeneration of the rotor by the solar regeneration coil. The regeneration coil works as an additional source of heating if the solar thermal energy is not enough for regeneration process. To operate the desiccant system at night time, the regeneration of the rotor has to be made at day times. As the pest and fungus attack in citied greenhouses is more associated with humidity so the moisture control needs more attention as compared to temperature. The addition of solar thermal energy in the presented system looks more sophisticated as the greenhouse air can dehumidified directly by the renewable-solar energy.

FEASIBILITY OF **D**ESICCANT **M**ODEL

Agriculture always plays a vibrant role in the economy of Pakistan and it is the 2nd largest sector of the country that contributes 21% toward the Gross Domestic Product (GDP) and involves 45% of labor altogether [12]. Farmers are facing humidity, temperature and fog complications while growing in greenhouses to produce off-seasonal products. A low cost dehumidification and air conditioning system is the basic need for the vigorous agriculture in Pakistan to minimize the food supply & demand gap. The conventional vapor compression air conditioning system does not deal the humidity in a worthy way. Normally these systems control the humidity by extra cooling the process air to the temperature lower than its dew point hence more energy is consumed so does not ensure the certain level of humidity and temperature at the same time. The humidity & temperature demand in greenhouse changes time to time due to complex processes take place in the plants e.g. photosynthesis, transpiration, ideal VPD etc. Desiccant systems are the efficient choice to deal these constraints because it has an ability to dehumidify the air directly by the desiccant material. This is an environment friendly system which doesn't have any global warming (GWP) and ozone depletion potential (ODP). These systems have shown the promising results for dehumidifying and air conditioning [9]. The desiccant rotor produces the dehumidified air in addition with certain heat of adsorption but this dry and bit warm air has a great cooling potential because of its low humidity. In our study it is exposed that this heat of adsorption can effectively be used to meet the heating demand in our cited greenhouses at night time from November to February. The processed dehumidified air can be cooled by evaporative cooling and this allows the connective dealing of latent and sensible load even for daytime in October, March and April. Maisotsenko cycle, an indirect evaporative cooling technique can be used here efficiently to produce cool air near to the dew point without increasing the humidity. The only challenging anxiety of this system is to regenerate the desiccant rotor economically; this can be done by the solar energy as shown in Fig. 7 & 8. To run the system at night time, the desiccant will be regenerated at day time when enough sun light will be available. An additional heating source is also provided to make the system more reliable especially in foggy days when enough solar radiation will not be available and plants became more sensitive. Pakistan is facing electricity shortage these days which results in terms of long hours of load shedding. As this system can works on renewable or waste energy so will be adopted straightforwardly by the greenhouse growers.

DISCUSSION AND **C**ONCLUSION

There isn't any emblematic dehumidification and air conditioning system considered for the greenhouse condition of Pakistan. Each and every time plants require flexible humidity and temperature in greenhouse and the conventional vapor

compression air conditioners fail to generate these demand conditions as noted in Table 1. Finally the farmer doesn't have any choice to maintain the greenhouse environment which results in heavy yield loss.

Truly the desiccants have the systematic way to control the humidity and the additions of temperature controlling devices make them an ample system for air conditioning as well. Desiccant's affinity towards moisture makes the system more flexible to possess the ideal vapor pressure deficit (VPD) in greenhouse by unsettling the humidity rather than temperature. The system is capable to maintain the level of carbon dioxide in greenhouse by switching the ambient and return air as a process air. The ability to operate the desiccant system through thermal energy (solar or waste energy) makes it the epitome choice even for remote areas of Pakistan. The system is showing a feasible solution for subjected greenhouse problem and its low cost operation makes it an emerging option for small land holders to establish their own greenhouse. By this trajectory production and productivity of the greenhouses can be increased which results in secure food, more revenue, increasing exports and prosperity in the country. Even the number of greenhouses will be increased and variety of agricultural species can be grown.

The desiccant based systems activated from solar thermal energy / waste energy are not only the economical solution for the problems of Pakistan's greenhouses but also the fascinating alternative to minimize the use of electricity consumed for conventional vapor compression air conditioning.

REFERENCES

[1] Crop production technologies; Handbook for Non-seasonal vegetables; Urdu Language (Production Plan: 2011-12). Agriculture Department, Government of Punjab-Pakistan. http://www.agripunjab.gov.pk/

[2] Muslehuddin, M., Mir H., Faisal, N., (2004) Recent occurrence of fog over Pakistan (1997 to 2000), Pakistan Journal of Meteorology, 1(2), 3-18.

[3] Sand JR, Fischer JC. (2005) Active desiccant integration with packaged rooftop HVAC equipment. Applied Thermal Engineering 2005; 25:3138–48.

[4] Arun K. S., Z. K., Bora, J., Das, V., Rawat, K., Sharma, S. K. Jain, (2010) Winter fog over the Indo-Gangetic Plains mapping and modeling using remote sensing and GIS, Springer science (Natural Hazards), DOI 10.1007/sl 1069-010-9660-0.

[5] Ramin S., Wan I.W.I., (2012) Performance evaluation of ventilation and pad-and-fan systems for greenhouse production of tomato in lowland Malaysia, World Research Journal of Agricultural & Biosystems Engineering, Volume 1, Issue 1, 2012, pp.01-05.

[6] Munters Ltd. MCC-Series Cooling Cassette (Company brochure).

[7] M.A. Sheikh, (2009) Renewable energy resource potential in Pakistan, Renewable and Sustainable Energy Reviews., Vol. 13, pp. 2696-2702, 2009.

[8] Shamshad KM., (1998) Solar insolation over Pakistan. J SES (Taiyo Enerugi) 1998; 24(6):30.

[9] D. La, Y.J. Dai, Y. Li, R.Z. Wang, T.S. Ge (2009) Technical development of rotary desiccant dehumidification and air conditioning: A review. Renewable and Sustainable Energy Reviews 14 (2010) 130–47.

[10] Sabatelli V, Fiorenza G, Marano D. WP5.D1: Technical status report on solar desalination and solar cooling. New Generation of Solar Thermal Systems; November 2005. http://www.swt-technologie.de/NEGST5_D1.PDF

[11] Ertac, H., Orhan, B., Tuncay, Y., Arif, H., Irfan, U., (2012) Investigation of solar energy utilization in a novel desiccant based air conditioning system. Energy and Buildings 55 (2012) 757–764.

[12] Syed S. Amjid, Muhammad Q. Bilal, Muhammad S. Nazir, Altaf Hussain (2011) Biogas, renewable energy resource for Pakistan, Renewable and Sustainable Energy Reviews 15 (2011) 2833– 2837.

Solar Electricity at a Cost Lower Than Kerosene

Asifur Rahman[1], Hassan M. Aziz[2], Koji Ishida[3], Tanjina Y. Chowdhury[4], Tsuneo Nakanishi[5], Akira Fukuda[5]

[1]Graduate School of Information Sc. and Electrical Engg., Kyushu University, Fukuoka, Japan
[2]Department of Electrical & Electronics Engineering, AIUB, Dhaka, Bangladesh
[3]System LSI Research Center, Kyushu University, Fukuoka, Japan
[4]Smart Service Technology Co. Ltd., Fukuoka, Japan
[5]Faculty of Information Science and Electrical Engineering, Kyushu University, Fukuoka, Japan

Abstract

Kerosene lamps are the traditional source of lighting in the villages of Bangladesh. In the backdrop of availability of low cost solar home systems (SHSs) villagers blessed with remittance money and the affluent class are using solar energy primarily for lighting their houses at night. But common villagers cannot afford to procure SHS by themselves. In 2012 we conducted a survey in the Barishabo union of Kapasia upazila of Gazipur district about the overall status of utilization of SHSs (Solar Home System) by the villagers. Despite being very close to the capital city the village is out of grid electricity network. The survey demonstrate that the investment on SHSs are not being paid off to the villagers because of the following reasons: i) SHSs need regular maintenance which becomes significantly high after three years warranty period; ii) The recurring investment for battery seems higher to the villager; iii) Considering the span of a village homestead SHSs cannot eliminate the use of kerosene lamp completely. The survey also collected the requirement of domestic lightings from the villagers. We designed a solar energy based rural powerhouse using the information collected from the survey and distributed the generated power according to the need of the villagers. We designed specialized LED lamps to be used for different purpose and consume most optimum power. In some cases we also supplied the electricity to use through nano-grid system. The system is in operation for the last 18 months. We found the new approach of power usage management can supply electricity to the villagers at a cost slightly less than the cost of kerosene consumption for lighting their house. Commercializing this approach would change the usage of solar power significantly and contribute to i) improve the living of the rural people by reducing diseases related to vision, lungs etc.; ii) improving the environment by reducing the waste from the scrapped solar system.

INTRODUCTION

Rural electrification is the availability of electricity for any purposes in rural areas. In this case any technology, source, and form can be considered to achieve the goal [1]. Importance of rural electrification is documented in various literatures [2-5]. Rural electrification offers direct financial benefit to rural households. For example, the total financial benefit received by a typical non-electrified Filipino household from electrification was estimated to US$81~US$150 [6]. The expansion rate of rural electrification is improving regularly since late 70s. But the overall condition is not improved due to the gap between demand and supply. Considering the investment needed in producing electricity, expanding grid network, and developing necessary human resource, it needs quite a long time to fulfill the goal by the governments of the developing countries.

Accepting the fact that expansion of the grid network to every village will take mentionable period of time. Researchers are trying to explore options to generate and provide electricity in the off grid areas. Mini-micro-nano grids both with AC and DC current options are being considered in many countries. Different sources have been used to generate electricity for these grids. Recently the use of SHSs in Bangladesh, Sri Lanka, and India showcases innovations in system design as well as financial and institutional mechanisms. Poor people purchase the system in installment do not repay for a system not performing well. These caused severe blow to the financial aspect of many projects in South Asia. In Bangladesh the IDCOL along with its partners successfully created channels to deliver both financial and maintenance service to its clients [7]. Considering the capacities of SHSs this measure can be considered as pre-electrification option not as an alternative solution.

In this circumstance we conducted a survey in an off-grid village in the district of Gazipur, Bangladesh. The objective of the survey was to find out i) the usage of SHSs in the village; ii) categorized demand for electricity by the villagers; iii) affordability of lighting by the poor villagers. The survey data indicate: i) SHSs are out of affordable capacity of the poor villagers; ii) lighting is the primary reason for electricity for the common villagers, charging mobiles are the second in the list; iii) in many cases poor villagers control their usage of light to adjust their budget.

Based on the above findings we decided to find a solution for rural lighting rather than rural electrification that will be affordable to the common villagers. The rest of the paper is arranged as follows: in section II we discussed the existing experiments, projects, researches going on or previously happened in different part of the world.

Section III list the gap exist between the present knowledge from the mentioned researches or experiments and our goal. We also documented our analysis in details. Section IV details our research project with the financial viability analysis. Section V concludes the research with a list of future works.

EXISTING SOLUTIONS DEVELOPED GLOBALLY

Electrification is the focus for the off-grid people in the global arena. All sorts of available technologies for electricity generation are being tried in this regard. Among them the fossil fuel based generation system is capital intensive and needs to be subsidized for the common villagers. Considering expansion of national grid system fossil fuel based mini-micro grid systems are to be connected to the national grid at some point. Hence it is needed to be synchronized with the national network expansion plan to secure the return on investment. Among the renewable energy based solutions solar PV based power generation system is the most suitable for providing electricity in the off-grid localities in a country like Bangladesh. Despite different attempts for solar base micro grid projects, SHSs are the most popular option in Bangladesh. There are effective use of hydropower based micro grid systems in Sri Lanka and Nepal [7].

Regarding usage of the electricity both AC and DC grids are being used. As the mainstream of the grid system uses AC current, appliances of reliable quality for AC are available in affordable price. Solar PV system generates DC current. To operate AC based appliance a DC-AC conversion has to be performed. Most of the electronic devices internally operate in DC. So in AC grids loss in power because of conversion between AC and DC may incur 15%~40% of total energy. In case of DC grid, less number of appliances are available in the market also those suffers from quality. DC grids also have limitation on its span due to resistive loss in ware. Since in most of the cases common villagers require lighting at night, absence of suitable appliances does not affect much.

SHSs (Solar Home System) have been accepted in Bangladesh quite well. The technology, maintenance infrastructure, as well as the financial model through the microfinance institutions all are supporting each other to deliver the service successfully. Till January 2013, 1,938,957 SHSs has been installed throughout Bangladesh by IDCOL through its partners [9]. The purpose of SHSs are mostly lighting the village homestead.

Usually a DC-nano grid is created within the homestead to connect 2/3 lights, fan, and television depending on the capacity of the system. DC-AC converters are used at the connection point to change the DC voltage to operate AC devices if required. These conversions result into loss of power. According to the business model of IDCOL and its partners the system is delivered to the users in a 3 years long monthly payment scheme with an EMI of 175 taka lowest. According to the survey the systems have an average life of 4 years.

GAP ANALYSIS

Rural electrification is an ongoing process and progressing consistently. Considering the prevailing situation it will take significant time to reach the goal. There are various proven benefits of rural electrification, which we have discussed earlier. Till the time the total electrification is not being achieved, we can consider quality lighting from electricity as an interim measure. By introducing quality lighting in affordable cost we can improve the living of the poor villagers by preventing some chronic disease and cleaner environment.

Insufficient lighting for reading creates chronic vision problem for the children who are studying using kerosene lamps throughout their childhood. Kerosene lamps dissipate carbon mono oxide and carbon dust in the air which is inhaled by the residents consistently cause having lungs diseases. Kerosene lamps need to be lit throughout the night so that the residents can use it in case of necessity if they wakeup during night. Because it is not possible to lit a lamp in the dark. This burns money and cause health problem. The above facts motivated us to design a research project, which will introduce quality lighting in affordable cost in the rural areas.

A. Requirement Analysis

According to the survey, villagers use 50% energy for lighting for study and 50% energy for other domestic purpose. We observed that the requirements of lamps are different for the mentioned purposes. There are households, which need electricity for commercial purpose like sewing or some other work in the night. The common villagers usually having limited affordability purchase kerosene for short interval depending on availability of fund. There are cases where they control the duration of lighting the lamp depending on the availability of kerosene. Usual spending on kerosene by a family is around 150 Taka. We can categorize different aspects of our findings as follows:

1. *Financial*: For domestic use, the cost of usage must be low. Although it is possible to charge a higher price from the commercial users. There should be option for no use no pay and also to pay according to their use.

2. *Equipment*: To reduce the cost of usage all the equipment must be energy efficient. High illumination LED lamp with rechargeable batteries could be a suitable option. We did a detailed research on efficient LED lamp specification to be detailed later. Direct supply of electricity to the users to light LED bulbs to use for multipurpose. Here the point to note that

the higher cost of LED lamps and bulbs need to be handled in the business model to keep the monthly expense near the cost of monthly use of kerosene.

3. *Technology*: to avoid the conversion loss we need to consider using DC currents throughout the system. The user requirements can best be fulfilled using all DC components. In such consideration we can save 40% energy from conversion loss [8]. Although the use of DC current restricts the wire connection with up to 100 meters.

B. LED Lamp Design specification

According to the ophthalmology during reading the object should be lit at 100~150 LUX and a room should be lit at minimum 75 LUX to ensure visibility [10]. Based on this fact we designed one lamp for Reading purpose and one lamp for domestic use. We used high quality LEDs in perfect series register to create clear light in low power and having longer life of LEDs. To reduce the cost we made the lamp having compact plastic body with adjustable neck or reflector. The reading lamp is made 9 inch high so that the light get distributed throughout a table with 1.5 square meter top. We used Li-ion battery and low Voltage cutoff circuit inside the lamp to maintain the battery in its preferable depth of discharge level as 80% to 95%. The fast charging circuit should designed to charge at constant voltage and constant current phase for Li-ion battery with stable over charge protection. The light surface azimuth graph for both the lamps can be like Fig. 1.

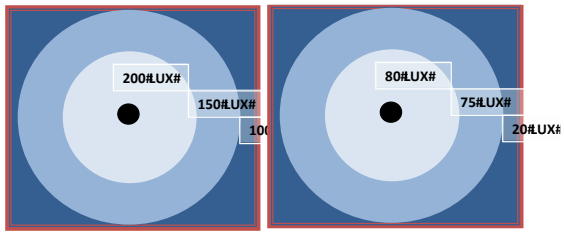

Fig.1. Left: Approximate Illumines at tabletop (1.5 Sq. meters); Right: Room of 10 square meter

SMART CENTER

To deliver the service with the goal of lighting the rural areas, we established a rural powerhouse within our smart center project that will generate electricity from solar PV panel. The electricity generated is stored in an array of lead-acid batteries. We developed specialized lamps based on the specification mentioned above. We recharge the lamps when it gets empty and take money from the users. Users pay us for the amount of electricity charged. We have implemented all the findings from our survey. Users do not pay any fixed mandatory installment. They are allowed to control their expenditure through reducing their usage. We also connected 3 households as a part of DC Nano grid to see the performance. The services that smart center is offering is displayed in fig. 2 also can be listed as:

1. Distributing energy efficient LED lamps to the users against a refundable deposit of 200 Taka.
2. Recharging the lamps as on demand.
3. Supply DC current to household.

C. Components of the Smart Center

The smart center is composed of i) LED lamp; ii) Battery; iii) Control Panel; iv) Solar PV panel; v) MPPT charge controller.

LED Lamps: LED lamps are designed to achieve the certain illumination and consume certain energy. According to the survey it is seen that average operating hours is 6 hours at night. LED lamps are used for both reading and household works. Our rechargeable LED lamps are designed for both the mentioned purpose and desired illumination is achieved by the parallel connection of four 10mm Lumileds with proper resistor that they consume 280 mA in total at supply voltage 3.7V. Thus the wattage of the device at output is 1.036 Watt. Considering the 70% DOD at 2400mAh battery the backup time is approximately 6 hours.

Fig. 2. Different services offered from Smart Center

Battery: If we consider 300 above-mentioned LED lamps of 3.7V, 2400mA Li-ion batteries are to be charged in everyday. Then the capacity of the batteries used to store electricity from solar PV panel is 1200 Ah [11] considering 70% depth of discharge (DOD), 12V system voltage, 3 autonomy days [11]. We used industrial lead-acid batteries for storing electricity.

Control Panel: In our current system FPGA controlled control panel consist of one 24 volt DC input with ten 5V USB outlet, eleven 12V LED bulb outlet and five general purpose 12V outlet. LAN connection is available with PC interface and management software. The management software deals with metering, billing and wire connections controlling. These extra interfaces are only for experiment purpose at the initial phase. The final

device will consist of 12V DC input, FPGA controller, display unit and 5 V DC outlets for lamp charging.

Solar PV Panel: To charge 300 LED lamps according to the specification mentioned above we need 1,200Wp PV panel connected to the system [11]. During this calculation we used the standard parameters applied for Bangladesh and approved by IDCOL: average peak sun hour of 4.5 hours per day; attrition factor = 1.6; efficiency of MPPT = 95%.

MPPT Charge Controller: For harnessing maximum solar energy we are using MPPT (Maximum power point Tracer) charge controller operated by PWM (Pulse Width Modulation) technique. The arrangement of the system setup is shown in Fig. 3.

D. Financial aspect of the experiment

Initial investment required for the setup to charge 300 lamps everyday is:

Item	No. x Price	Taka
Solar Panel :	1,200 × Tk.80	98,000
Battery	6 × Tk.17000	102,000
MPPT charge Controller	2 × Tk.6700	13,400
Total system price		211,400

Fig. 3. System arrangement in Smart Center

During the above calculation we used standard market price in Bangladesh. Considering 300 batteries as a load for 5 hours per day for 3 years the generation cost per Watt-hr:

211,400/ (3,175 × 365 × 3) = 0.061 taka

Cost for charging a 2400 mAh Li-ion battery:

(2.4 Ah × 4.2 V) × 0.061 = 0.61 taka

Other costs involved in the projects are:

Control panel cost is ≈ 30,000 taka

Lamp Unit price = 400 taka

Cos t of 300 lamp = 400 × 300 = 120,000 taka

So, all together initial business setup cost ≈ 350,000 taka

According to the survey the conventional small kerosene lamp needed 1litre of kerosene per month which costs 70 taka, It's implies that the expenditure against a small lamp 2.33 taka per day.

So if an entrepreneur takes 2 taka for charging one battery then he will earn 600 taka everyday. Thus at the end of the year the amount of collected revenue will be (Taka 600 x 365) 219,000 taka and after 3 years it will be (Taka 219,000 x 3) 657,000 taka. This earning is good enough to cover the investment, interest on investment and day-to-day operations cost. At the same time the villagers are spending less than what they are spending on kerosene.

CONCLUSION AND FUTURE WORKS

The project was initiated as a proof of concept with intent of providing descent lighting to the poor villagers who cannot invest a bulk amount of money to procure SHSs. The financial terms of the services are planned to suit the daily expenditure pattern on kerosene consumption of the poor villagers. The project is running in the Chordurlovkhan village of Barishabo union of Kapasia Upazila of Gazipur district in Bangladesh for last 18 month. Presently 40 lamps are being used for piloting the service. All the users are extremely satisfied with the service. The lamps and control panel are custom made. Hand made lamps need extensive maintenance and costs higher.

As the projects has been proven to be a financially self-sustainable one. Now the researchers are working on to involve related technology companies in Japan to produce necessary devices commercially. Although this lighting initiative is an interim measures until the grid electricity reaches to every village, the demand for such business is expected to prevail for a decade in Bangladesh and globally the demand should exists much longer.

During the commercial phase alternative measures might be considered to transport only batteries instead of lamps. Because transporting lamps everyday increase the maintenance demand. Also it need good amount of space in the smart center for charging. The harsh environment influences the life of the lamps and other devices.

ACKNOWLEDGMENT

The research was funded by Smart Service Technologies Co. Ltd. Fukuoka, Japan.

REFERENCES

[1] Barnes D. F., "Electronic power for rural growth: how electricity affects rural life in developing countries", Rural studies series rural sociological society (USA) pp. 250, 1988

[2] "Energy for the Poor: Underpinning the Millennium Dev Goals", DFID, London, 2002

[3] "Reaching the Millennium Development Goals and Beyond: Access to Modern Forms of Energy as a Prerequisite". Global Network on Energy for Sustainable Development, Denmark, 2007

[4] "Designing Sustainable Off-Grid Rural Electrification Projects: Principles and Practices", The Energy and Mining Sector Board Operational Guidance for World Bank Group Staff; Washington, DC: The World Bank, 2008

[5] "Economic and Social Impact Evaluation Study of the Bangladesh Rural Electrification Program". NRECA International Ltd., Dhaka, 49pp, 2002

[6] Barnes D., "Rural Electrification and Development in the Philippines: Measuring the Social and Economic Benefits", Joint UNDP/World Bank Energy Sector Management Assistance Programme (ESMAP) Report. Washington DC: The World Bank. 169pp, 2002

[7] "Off-grid electrification experience in South Asia: Status and best practices", EPSRC/ DFID funded Research Grant EP/ G063826/1, pp34~36, 2010

[8] P. Savage, R.R. Nordhaus, S.P. Jamieson, "DC Microgrids: Benefits and Barriers", Yale School of Forestry and Environmental Studies, March 2010.

[9] http://www.idcol.org/energyProject.php accessed 2013/07/03 at 22:42

[10] http://eeref.engr.oregonstate.edu/@api/deki/files/993/ accessed 2013/07/03 at 22:43

[11] Chowdhury S.A., and Aziz S., "Solar- Disel Hybrid model for base transceiver stations (BTS) of mobile phone operators", 2nd International Conference on the Development in Renewable Energy Technology (ICDRET), 2012.

Effect of Blade Profile and Blade Setting Angle on the Performance of the Intelligent Wind Power Unit

Ahmed M. Galal[1] and Toshiaki Kanemoto[2]

[1]Production and Mechanical Design Department, Faulty of Engineering, Mansoura University, Mansoura – Egypt; *e*-mail: ahmadgalal2007@yahoo.com

[2]Faculty of Engineering, Kyushu Institute of Technology, Sensui 1-1, Tobata, Kitakyushu 804-8550, Japan
e-mail: kanemoto@mech.kyutech.ac.jp

Abstract

The authors have invented the superior wind power unit, which is composed of the tandem wind rotors and the double rotational armature type generator without the traditional stator. The large-sized front wind rotor and the small-sized rear wind rotor drive, as for the upwind type, the inner and the outer rotational armatures respectively, in keeping the rotational torque counter-balanced between both wind rotors/armatures. The unique rotational behaviors of the tandem wind rotors and the fundamental performances of the unit have been discussed previously. Continuously, this paper investigates experimentally the performance of the Intelligent Wind Power Unit while changing the blade setting angles and the blade profiles of the tandem wind rotors. The front and rear blades designed contribute to improve the output and can resultantly improve acceptably the overall performance of the Intelligent Wind Power Unit.

NTRODUCTION

Wind power is significantly promising as a sustainable and renewable energy resource that will play a very important role in the electric power generation at the 21st century. The wind turbines are developed and improved to increase the output, and positively/effectively provided for the power stations. The authors have invented a superior wind power unit as shown in Fig. 1, and called "Intelligent Wind Power Unit" [1, 2]. This unit is composed of the large-sized front wind rotor, the small-sized rear wind rotor and the peculiar generator with the double rotational armatures without the traditional stator. The front and the rear wind rotors drive, as for the upwind type, the inner and the outer armatures, respectively. The fundamental concept of the tandem wind rotors has been previously proposed [3] and the commercial Navier-Stokes code EllipSys3D predicted that the tandem wind rotors make the output increase as compared with the single wind rotor [4]. Ahead of the above prediction, Appa Technology Initiative increased the output by the tandem wind rotors where both rotors with two blades are 4 m in diameter [5]. The tandem wind rotors with the small-sized front wind rotor and the large-sized rear wind rotor also increased the output, where both rotors together drive the inner armatures of the traditional generator through the gearbox [6]. In similar technologies, the small-sized front wind rotor and large sized-rear wind rotor, driving the inner armature and the outer stator casing respectively, could make the output increase [7, 8].

In the contrary, not only the profiles but also the operations of the tandem wind rotors proposed here quite differ from the surveyed above. The rotational directions and the speeds of both wind rotors/ armatures are automatically and optimally adjusted in response to the wind velocity, as shown in Fig. 2. Both wind rotors start to rotate at low wind velocity, namely the cut-in wind velocity, but the rear wind rotor counter-rotates against the front wind rotor. The rear wind rotor reaches the maximum rotational speed at the rated wind velocity. With more increase of the wind velocity, the rear wind rotor decelerates gradually, stops and then begins to rotate at the same direction of the front wind rotor, so as to coincide with the larger rotational torque of the front wind rotor.

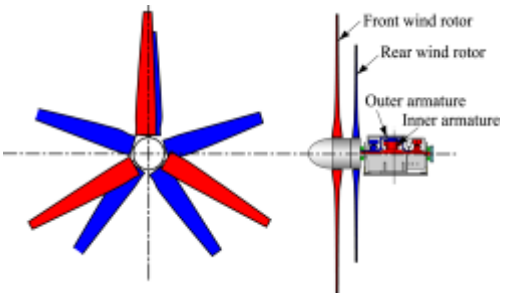

Fig. 1 Intelligent wind power unit (upwind type)

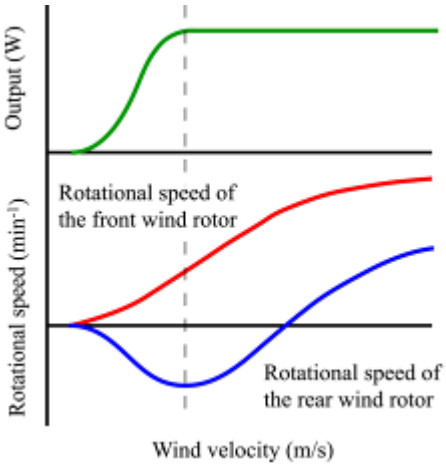

Fig 2. Predicted operations of the intelligent wind power unit

Such superior operations of the tandem wind rotors have been confirmed experimentally [1, 2] and the—profiles/specifications/dimensions taking the acceptable output have been proposed fundamentally [2, 9]. Continuously, this paper investigates and discusses experimentally the performance of the unit under changing the blade setting angles and the blade profiles.

MODEL WIND ROTORS AND EXPERIMENTS

The model wind rotors were set perpendicular to the wind direction, at the outlet of a wind tunnel with a nozzle diameter of 800 mm, as shown in Fig. 3. The front and the rear wind rotors connect directly and respectively to the isolated motors with the inverters, in place of the peculiar generator. The diameter of the front wind rotor is d_F = 500 mm and the diameter of the rear wind rotor is d_R = 420mm, so that the diameter ratio D_{RF} [= d_R / d_F] is 0.84. The dimensionless axial distance between the front and the rear wind rotors L [= l / d_F, l: axial distance as shown in Fig. 3] is 0.08. These dimensions were optimized at previous works [1]. The blade profiles of the front and the rear wind rotors are shown in Fig. 4, where the front and the rear blade setting angles β_F, β_R measured from the tangential direction at the blade tip (see Fig. 5) are adjusted as requested. Front Blade G was formed with MEL002 airfoil and has a twist to get the desirable angle of an attack α =7 degrees irrespective of the radial position. The angle is optimized as a single wind rotor, at a tip speed ratio λ_F = 6 [= (the front blade tip speed) / (the wind velocity)] with β_F = 0 degree. Front Blade H shown in Fig. 4 is also designed with a tip speed ratio λ = 6 as a single wind rotor. It has a MEL002 airfoil at a tip side and twist to get the desirable angle of attack α = 8 degrees with the tip speed ratio λ_F = 6. Rear Blade G was formed with MEL002 airfoil and has a twist to get the desirable angle of attack α = 11 degrees irrespective of the radial position [10]. The inlet flow direction against the rear blade used the outlet flow conditions of the Front Blade G measured by 5 holes pitot tube at the steady state condition, while Front Blade G rotates at maximum output condition as the single wind rotor (λ_F = 4.2with β_F = 0 degree) [11]. The angle is also optimized as a single wind rotor, at the tip speed ratio λ_R = 6 [= (the rear blade tip speed) / (the average wind velocity of inlet condition)] with β_R = 0 degree. The blade number of the front and the rear wind rotors are Z_F = 3, Z_R = 5 which are also optimized at previous work [1]. Hereafter, the tandem wind rotors are called "Tandem Wind Rotors GG, HG" which are composed of Front Blade G or H and the Rear Blade G, where "Single Wind Rotor G" is composed with Front Blade G.

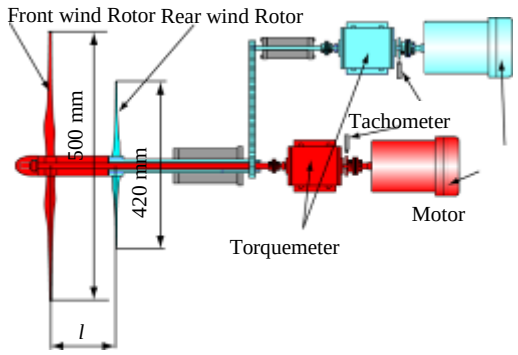

Fig. 3 Test stand for model tandem wind rotors

ROTOR WORK MEETING EXPECTATIONS

Fig. 6 shows the performances of Tandem Wind Rotor GG in the generating mode, where the rated wind speed was tentatively set at V = 10 m/s. The tandem wind rotors were driven at the maximum output point in slower wind velocity, namely the under rated wind velocity, and driven so as to keep the output constant in the rated operation. The rotational speeds N_F and N_R take the superior behaviors in response to the wind speed without the breaks and pitch control mechanisms, as predicted.

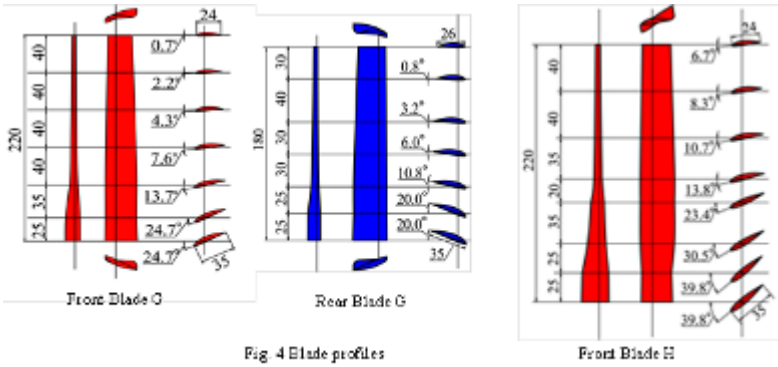

Fig. 4 Blade profiles

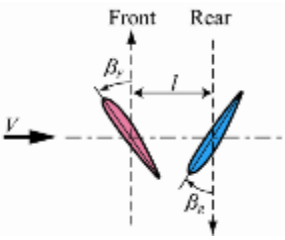

Fig. 5 Blade setting angles

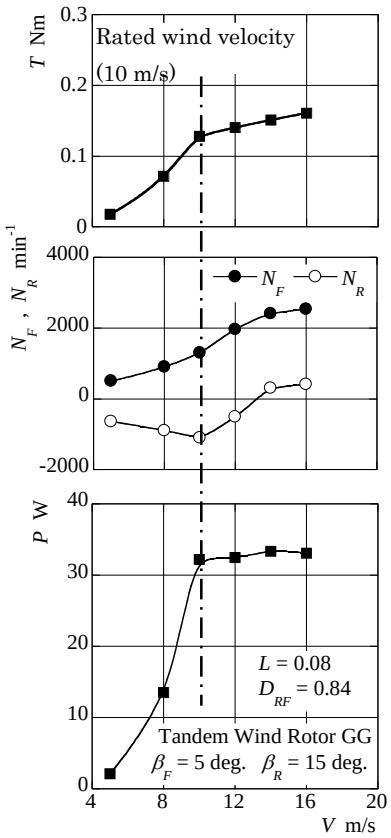

Fig. 6. Performances at the generating mode

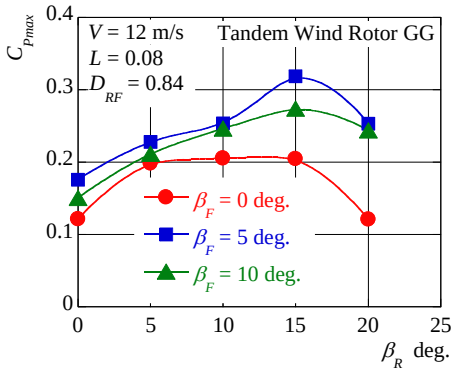

Fig. 7. The effect of the blade setting angles on the output.

AEFFECT OF THE BLADE SETTING ANGLES ON THE OUTPUT

The maximum outputs at each blade setting angles are shown in Fig. 7, where the angle β_F and β_R are referred in Fig. 5, C_{Pmax} is the maximum of the output coefficient defined by $C_P = P / (\rho A V^3/2)$, P is the output, A is the rotational area of the front wind rotor projected vertically to the flow direction, ρ is the ambient air density, and V is the wind velocity. The maximum output coefficient can be obtained at the front and the rear blade setting angles β_F = 5 degrees and β_R = 15 degrees, in presented setting angles (Fig. 5). The front blade G cannot get the desirable angle of attack because the inlet flow conditions were changed. That is, the axial velocity component of attacking wind may be decelerated by the blockage effect of the rear wind rotor.

EFFECT OF TIP SPEED RATIO ON THE OUTPUTS

The output coefficient C_P against the relative tip speed ratio λ_T, in comparison with C_P of Single Wind Rotor G and the Tandem Wind Rotors GG and HG are shown in Fig 8. The relative tip speed ratio λ giving the maximum output of Tandem Wind Rotor GG is faster than that of Single Wind Rotor G, and the output coefficient of Tandem Wind Rotor GG is higher than that of Single Wind Rotor G. The latter is caused by the rear wind rotor without the twist. The Front Blade G was modified to the Front Blade H, as shown in Fig. 3. The maximum output coefficient for Tandem Wind Rotor HG could be improved successfully at nearly the same relative tip speed ratio λ_T of Tandem Wind Rotor GG.

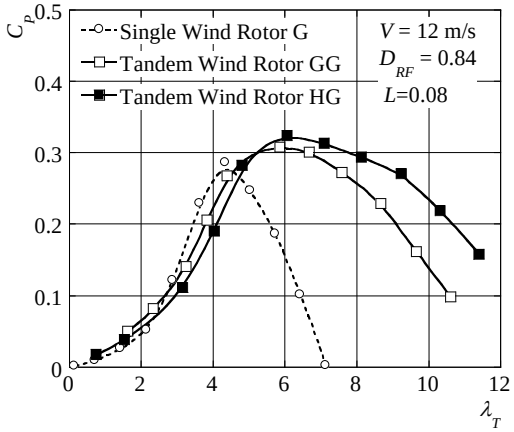

Fig. 8. Output characteristics of Tandem Wind Rotor GG, and HG.

CONCLUDING REMARKS

The effect of Blade Setting Angles and the blade profiles of the model tandem wind rotors were investigated experimentally. The results suggested that the profile of the tandem wind rotors and the blade setting angles should better be optimized so that not only to absorb more wind energy but also to give away enough wind energy to the rear wind rotor of the smaller radius. The designed blade profiles contributed in improving the output and can resultantly improve acceptably the overall performance of the Intelligent Wind Power Unit.

ACKNOWLEDGMENT

The authors wish to thank to Dr Koichi Kubo, Mr. S. Nonoue, Miss. H. Kugai and Miss. S. Inai who

graduated from Kyushu Institute of Technology, for helpful in doing experiments and discussion.

REFERENCES

[1] T. Kanemoto, A.M. Galal, Development of Intelligent Wind Turbine Generator with Tandem Wind Rotors and Double Rotational Armatures, JSME International Journal, Ser. B, Vol. 49, No.2, (2006), 450-45.

[2] Wei, Tong (Editor), Wind Power Generation and Wind Turbine Design, WIT Press, Southampton, 2010, 333-360.

[3] David A. Spera, Wind Turbine Technology, ASME Press, New York, USA, 1994, 93. K. Appa, Counter Rotating Wind Turbine System, Energy Innovations Small Grant (EISG) Program Technical Report, 2002.

[4] W.Z. Shen, V.A.K. Zakkam, J.N. Sørensen, K. Appa, Analysis of Counter-Rotating Wind Turbines, Journal of Physics, Conference Series, 75 (012003), (2007), 1-9.

[5] S.N. Jung, T.S. No, K.W. Ryu, Aerodynamic Performance Prediction of 30kW Counter-Rotating Wind Turbine System, Renewable Energy, Vol. 30, No. 5, (2005), 631-644.

[6] T.J. Jang, H.K. Heo, Study on the Development of Wind Power System Using Mutually Opposite Rotation of Dual Rotors, Proceedings of the Renewable Energy 2008, (2008), CD-ROM O-WE-015.

[7] Ushiyama, T. Shimota, Y. Miura, An Experimental Study of the Two Staged Wind Turbines, Proceedings of World Renewable Energy Conference, 1996, 909-912.

[8] Kubo, T. Kanemoto, Development of Intelligent Wind Turbine Unit with Tandem Wind Rotors and Double Rotational Armatures (2nd Report, Characteristics of tandem wind rotors), JSME International Journal, Ser. B, Vol. 3, No. 3, (2008), 370-378.

[9] Performance and geometry of airfoil supply system, online at: http://riodb.ibase.aist.go.jp/db060/index.html

[10] Toshiaki Kanemoto, Ahmed Mohamed Galal, Kota Ikeda, Hiromi Mitarai, and Koichi Kubo, Intelligent Wind Turbine Generator with Tandem Rotors Applicable to Offshore Wind Farm (Characteristics of Peculiar Generator, and Performance of Three Dimensional Blades), Proceedings of the 17th International Offshore and Polar Engineering Conference, Lisbon, Portugal, (2007), pp.363-368.

Potential Stability of Hybrid Capacitors of $Li_4Ti_5O_{12}$/Activated Carbon

Soo-Gil Park[1] and Shigeto OKADA[2]

[1] Dept. Engineering Chemistry, Chungbuk National Univeristy, Cheongju, Korea; *e*-mail: sgpark@cbnu.ac.kr
[2] Institute for Materials Chemistry and Engineering , Kyushu University, Kasuga, Japan
e-mail:s-okada@cm.kyushu-u.ac.jp

Abstract

We observed a potential change occurring at 1V - 3V charge-discharge process of the hybrid capacitor using activated carbon as the positive electrode and using LTO made by a sol-gel method as the negative electrode. As the result of observation of the change in potential at the charge-discharge process according to change in thickness of the positive electrode, in other words, the change of the mass of the activated carbon, if it exceeds the specific range, the maximum voltage value at the positive electrode is reduced and the decreased potential moves to the negative electrode. It is considered that such a result is formed by the difference in potential driving coming from the difference of the storage mechanism of the anode and cathode on the characteristics of the hybrid capacitor.

INTRODUCTION

Development of high-density ultra-compact energy storage device has been made by the sustainable development of small electronic devices which is laptop, mobile phone, atc in the market. And a need for large capacity storage device also is increasing rapidly due to market expansion of electric vehicles, medium and large electronic devices. The field of new renewable energy such as solar cells, fuel cells, and wind power generation that have been researched and developed as an energy source of high-reliability and smart grid business for the purpose of efficient energy use through the system which is micro grids, management of the power grid and power management of user for efficient energy usage are in full swing. The storage system required for power production system as described above is some lead-acid battery and a lithium secondary battery which are type of small capacity. The large capacity storage methods such as NaS battery, thermal energy storage method, the dam energy storage method, flywheel system and clean energy storage facility have been studied. Further, the need for energy storage device of ultra-high capacity type is increasing by the development of portable electronic devices, and the need for current compensation device for rapid-discharge form was increased by an increase in maximum current value used in the electronic device [1-4].

For these reasons, Energy storage device demands high power density and high energy density and requires the development of ideal energy storage device holding the long-life performance.

Lithium ion secondary battery (LIB) and Electric double layer capacitor (EDLC) that are an energy storage device typically has difference from the direction of development on the basis of their characteristics, and especially LIB having a lower power density and cycle performance than that of the high energy density tries to improve performance through nano particles, and new materials. In other hand, the development direction of the capacitor for the improvement of low energy density is to overcome the disadvantages through an asymmetric structure atc, and it has been researched. In this paper, we tried to apply the $Li_4Ti_5O_{12}$ (LTO) material to negative electrode in order to improve low energy density of the electric double layer capacitor. Hybrid capacitor applied LTO shows a improved energy density of about double as higher as the existing EDLC. But, it has a low potential stability. Therefore, in this study, we consider the electrochemical properties of hybrid capacitor applied LTO for the purpose of stable potential drive stable [5-6].

EXPERIMENTAL

A. Synthesis of LTO

LTO was prepared by the sol–gel process from LiOH (Sigma–Aldrich) and tetra titanium isopropoxide (TTIP; Sigma–Aldrich) using ultrasonication. Briefly, LiOH and TTIP solutions were first individually prepared in 2-methoxy ethanol, and then the latter was added drop-wise to the former, followed by stirring for 2 h. The Li/Ti molar ratio was adjusted to 4.5:5. The mixture was ultrasonicated for 5 h, and then the solvent was removed by drying at 110 ◦C in vacuum overnight. The obtained precursor was sintered at 850 ◦C for 5 h in an Ar atmosphere and finally cooled to room temperature to afford a white powder.

B. Preparation of electrode

The negative electrode comprised the active material, LTO (78 wt%), together with carbon black (12 wt%) for conduction and a combination of carboxymethyl cellulose (CMC), styrene butadiene rubber (SBR), and polytetrafluoroethylene (PTFE) (2, 4, and 4 wt%, respectively) as the binder on aluminum foil. The positive electrode was prepared by the same method and comprised AC (87 wt%), together with carbon black (8 wt%) for electrical conduction and CMC, SBR, and PTFE (1, 2, and 2 wt%, respectively) as a binder on aluminum foil. The coated thickness of the positive electrode (AC) was a series of 100–220μm layers per 40μm negative electrode thickness was a constant 20μm m. Each electrode was dried under vacuum at 120℃ for 24 h.

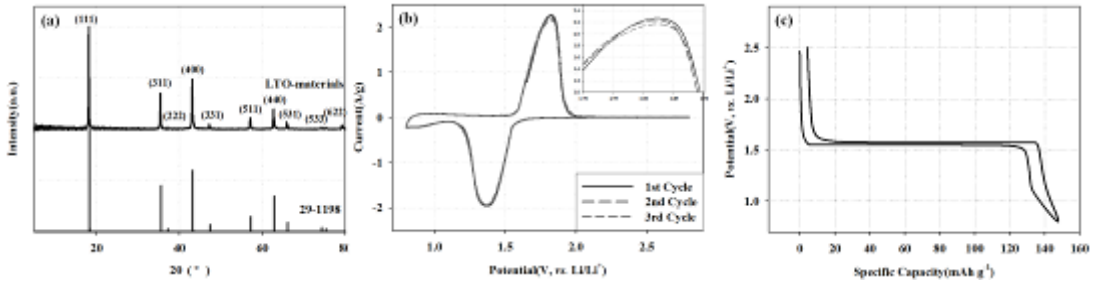

Fig. 1. Properties of LTO materials, (a) XRD patterns, (b) Cyclic voltammogram, (c) Charge-discharge curves, in $LiBF_4$ in PC electrolyte.

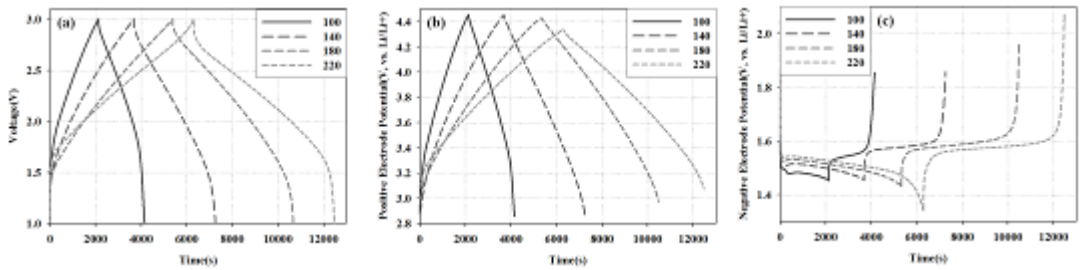

Fig. 1. Profiles of hybrid capacitors, (a) Cell charge-discharge curves, (b) Positive electrode potential profiles, (c) Negative electrode potential profiles.

C. Fabrication of cell

The HCs were assembled to form a three-electrode cell with a lithium disk as the reference electrode in 1 M $LiBF_4$/propylene carbonate electrolyte. The cells were charged and discharged from 1 V to 3 V at room temperature.

RESULTS AND DISCUSSION

The XRD patterns (Fig. 1(a)) of the prepared LTO matched all of the peaks in JCPDS file no. 26-1198, confirming that pure LTO was obtained. Furthermore, the redox characteristics and specific capacity of LTO were measured in an electrochemical test. As shown in Fig. 1(b), reversible redox peaks were observed from 1.45 to 1.75 V due to the redox reactions of Ti3+ and Ti4+. In addition, as shown in Fig. 1(c), LTO exhibited a very flat charge–discharge curve with a specific capacity of approximately 132 mAh g−1.

The Fig. 2 shows the potential profile measured by the charge-discharge process of LTO / AC hybrid capacitor which was produced by changing the thickness of the positive electrode. The Fig.2 (a) is voltage of the cell itself, and the Fig.2 (b) is the potential change of the positive electrode, and the Fig.2 (c) is potential change of the negative electrode. Charge-discharge voltage range of the cell itself in the fig.2 (a) is fixed at 1 - 3V, but it can be confirmed that as the thickness of the anode material is changed, the maximum voltage measured at the positive electrode is reduced. The Fig. 3 shows termination voltage of each section of Fig. 2. The potential driving of the positive electrode of Fig. 3 (a) shows in Fig. 2 (a) and Fig. 3 (a).

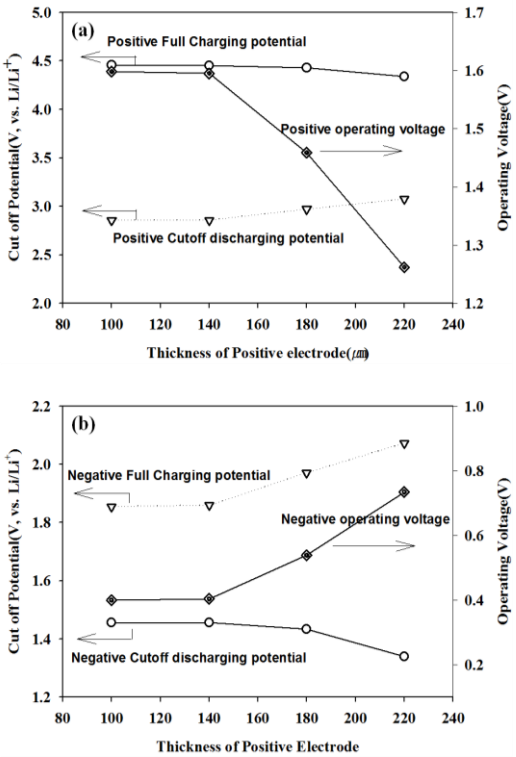

Fig. 3. Potential-driven results of the positive electrode and the negative electrode.

As thickness of the anode increases or as the mass of activated carbon that is coated on the anode increases, the maximum potential value in a fully charged state is reduced and the potential value in the maximum discharged state is increased. As a result, the driving voltage of the positive electrode will be reduced sharply as its thickness goes beyond 140 ㎛. At this time, the reduced voltage is fully reflected to the negative electrode, and its value would be determined on the basis of 1V and 3V as cut off potential.

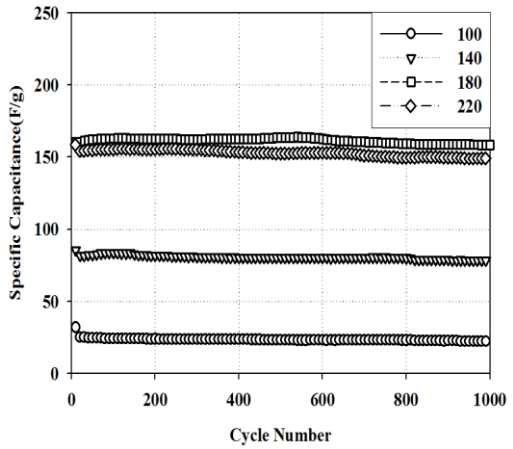

Fig. 4. Cycle ability of hybrid capacitors.

The Fig. 4 is a result of converting the capacitance of the hybrid capacitor on the basis of the weight of the negative electrode. The cycle characteristics do not show A big difference within the 1000 cycle, but if it can not support the positive electrode mass of more than a certain mass, value of the mass of the entire cell is significantly reduced on the basis the value of the result of the measurement, and it is judged that it does not exceed more than the reference mass of the negative electrode in the mass increase of the activated carbon more than a certain mass.

CONCLUSION

In conclusion, hybrid capacitor having a different storage mechanism of positive and negative electrodes is required balancing for stability of the potential, which could be confirmed by changing the mass of the electrode, and as a result , it seems to be able to ensure the stability of the potential at a specific mass ratio.

ACKNOWLEDGMENT

This research was financially supported by the Ministry of Education (MOE) and National Research Foundation of Korea (NRF) through the Human Resource Training Project for Regional Innovation (No. 2012025592).

REFERENCES

[1] B.E. Conway, “Electrochemical Supercapacitor-Scientific Fundamentals and Technological Application”, Kluwer Academic, New York, 1999, pp. 29–31.

[2] R. Kötz, M. Carlen, “Principles and applications of electrochemical capacitors”, Electrochim. Acta 45 (2000) 2483.

[3] V. Khomenko, E.R. Pi ˜nero, F. Beguin, “Optimisation of an asymmetric manganese oxide/activated carbon capacitor working at 2 V in aqueous medium”, J. Power Sources 153 (2006) 183.

[4] S.W. Hwang, S.H. Hyun, “Synthesis and characterization of tin oxide/carbon aerogel composite electrodes for electrochemical supercapacitors”, J. Power Sources 172 (2007) 451.

[5] G.G. Amatucci, F. Badway, A.D. Pasquier, T. Zheng, “An Asymmetric Hybrid Nonaqueous Energy Storage Cell”, J. Electrochem. Soc. 148 (2001) A930.

[6] J.J Yang, C.H, Choi, H.B. Seo, H.J. Kim, S.G. Park, “Voltage characteristics and capacitance balancing for $Li_4Ti_5O_{12}$/activated carbon hybrid capacitors”, Electrochim. Acta 86 (2012) 277.

Efficient FPGA Implementation of Secured and Transparent Electronic Voting Machine Using Verilog HDL

Tabia Hossain*, Syed Shihab Uddin , Iqbalur Rahman Rokon,
K. M. A. Salam, M Abdul Awal

Department of Electrical Engineering and Computer Science, North South University
Plot 15, Block B, Bashundhara Dhaka 1229, Bangladesh

*e-mail: tabi_friend@yahoo.com

Abstract

Electronic Voting Machine is an electronic voting device used for conducting the parliamentary elections electronically. It consists of two units that can be inter-linked; a ballot unit which a voter uses to exercise his vote and a control unit which used by the polling officials. As there is no available design of Electronic Voting Machine using Verilog FPGA, in this paper, we introduce an efficient, transparent and secured FPGA implementation of EVM using Verilog HDL. The design is coded in Verilog hardware description language at Register Transfer Level (RTL), simulated in ModelSim, synthesized in Quartus II and implemented in Cyclone II FPGA using the AlteraDE1 board.

INTRODUCTION

Bangladesh is a democratic country. For a democratic country, public opinion is the most important determinant to establish a government. Voting is the process through which people display their opinion and help to setup a democratic government. So the voting system should be reliable, accurate and it must be transparent. The voting system of Bangladesh is still paper ballot based, a very outdated process. The whole world is looking forward to E-voting rather than using paper ballots in voting. In recent times, using Electronic Voting Machines has become a major concern in electoral mechanisms in general elections. Considering these points, we made the design for an Electronic Voting Machine using Verilog FPGA, which absolutely is an original design of our own where with the advantages of VLSI design methodology and Verilog codes; we focused on implementing an efficient, secured, transparent, and satisfactorily error free electronic voting device.

DESIGN DESCRIPTION

Our Electronic Voting Machine (EVM) works in two major units: *Control Unit* and *Ballot Unit.* The control unit counts the individual party results as well as the total vote counts. The ballot unit makes a beep sound and gives a green signal when a cast vote is accepted. It will also give out a punched paper for the appropriate party. If any error occurs, the ballot unit will give a red signal indication an error and hence, it will display an error message. Validity of a voter for a certain vote centre will be checked at fist. Only a valid voter with a valid NID can access the machine to cast a vote. Error can occur in three ways: firstly, wrong ID encounter; secondly repetition of the same voter and thirdly, if more than one party is pressed simultaneously. When a vote is successfully accepted, along with the sound and the green signal, a punched paper will come out putting a seal on the appropriate party's logo. Individual party counts and the total counts will be monitored and recorded successfully after each successive voting process is done.We used Finite State Machine (FSM) approach in our design. The state diagram of our design is following:

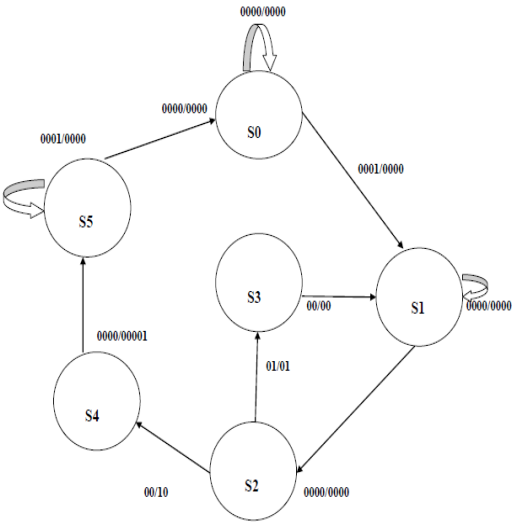

Fig. 1. State Diagram of EVM

DESIGN HIERARCHY

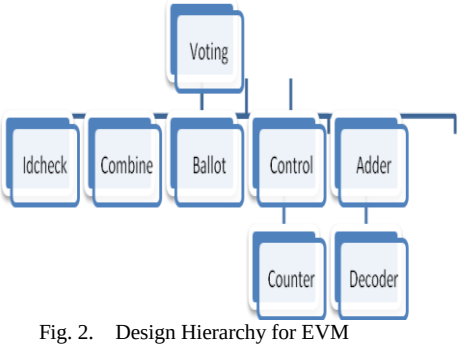

Fig. 2. Design Hierarchy for EVM

TOP **V**IEW OF EVM

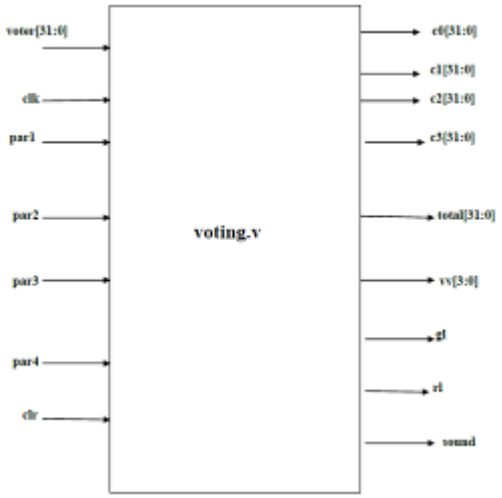

Fig. 3 Top view of EVM

BLOCK **D**ESCRIPTION

A. Idcheck

It consists of clk, sz, voter and xx. This module checks whether the voter id valid or not. Whenever voter id matches with the stored data it makes xx high and allows the voter for the next state.

B. Combine

Calcium carbonate dissolution rates increased and saturation states (Ω_{arg}) decreased with 33olution rate and saturation state (r=–0.99; p=0.0002)(Fig. 5). It consists of con and party. Whenever id check unit makes xx high this unit allows voter to access his/her vote to any of the party (par1, par2, par3, par4) specified by the machine. Whenever con becomes binary 0001, vote is accepted for the party1, binary 0010 indicates vote for party2, binary 0100 for party3 and binary 1000 for party4.

C. Ballot

It consists of clk, gl, rl, sound, and state. This module also consists of a decoder module which is instantiated inside the ballot module. Whenever a vote is properly accepted this unit gives beep sound and green signal which indicate the vote is accepted. If the vote was not accepted or any error occurs during the voting process, this module gives a red signal which indicates the process is wrong and turns the voter back to the second state.

D. Control

It consists of the result of four individual party (c0, c1, c2, c3), punch (vv), clk, clr, con and sound. It also consists of a counter module which is instantiated inside it. In this unit machine gets the beep sound from the ballot unit and the counter starts to count the particular party's vote and punches the specific party's logo on a ballot paper. This module gives individual result of the individual party and punches out the sealed hard paper which can be stored outside the machine.

E. Adder

It consists of individual results of the parties (co, c1, c2, c3) and total result. This unit adds individual results of the parties and gives the total number of vote accepted by the machine

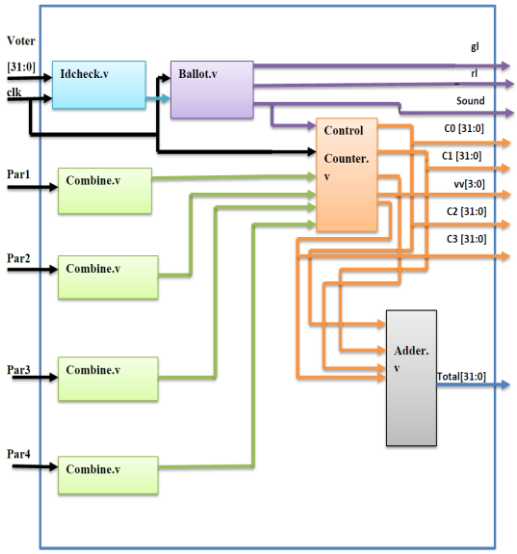

Fig. 4. Block diagram of EVM

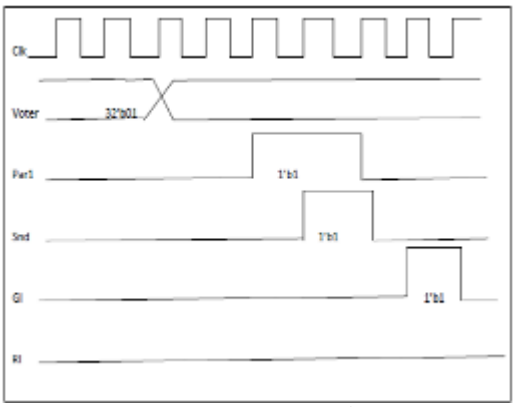

Fig. 5. Timing Diagram of Ballot

METHODOLOGY AND **H**ARDWARE **A**RCHITECTURE

In this section, the design procedure and the architecture of EVM has been described. Fig. 4 shows the different stages of the design. [2] The Verilog Codes were at first simulated with ModelSim and then synthesized with Quartus II Software targeted for Cyclone II (EP2C20F484C7) device and [1] FPGA technology was chosen because it provides some important advantages over general purpose processors and application specific integrated circuits (ASICs).

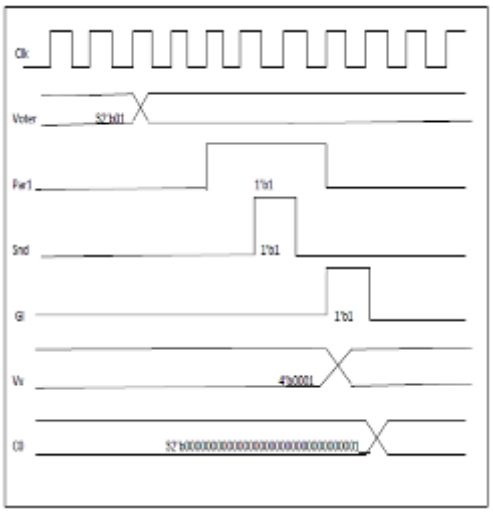

Fig. 6. Timing Diagram of Control

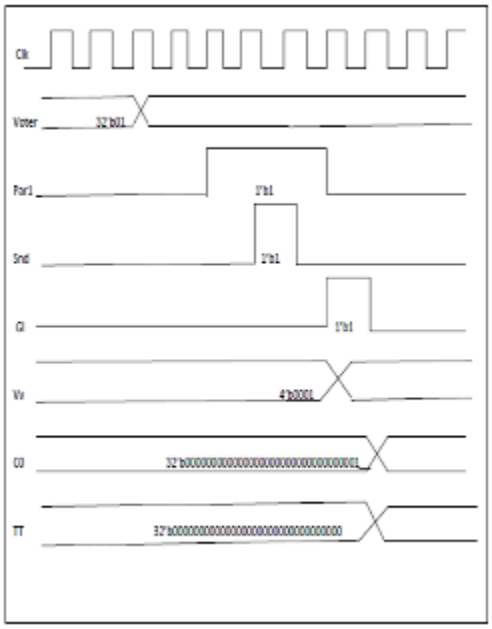

Fig. 7. Timing Diagram of Adder

Fig. 8. Implementation Flow

RESULTS

Fig. 9 and Fig. 10 shows the RTL schematic diagram of EVM and the internal block diagram of EVM, respectively, and Fig. 11 describe the simulation result of EVM.

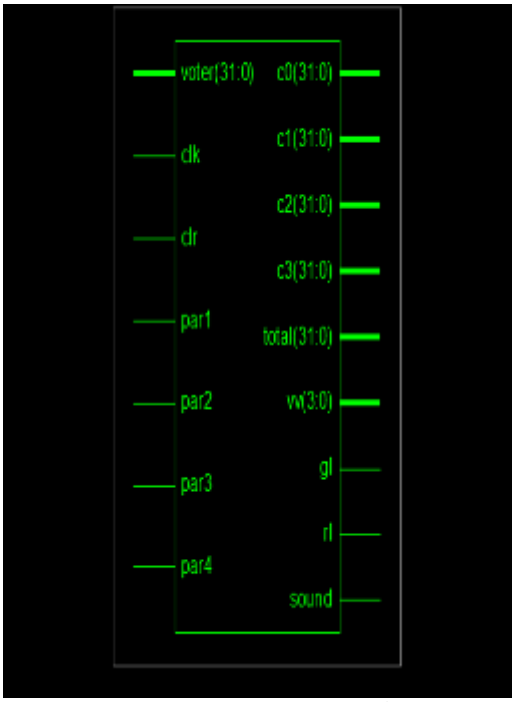

Fig. 9. RTL Schematic Diagram of EVM

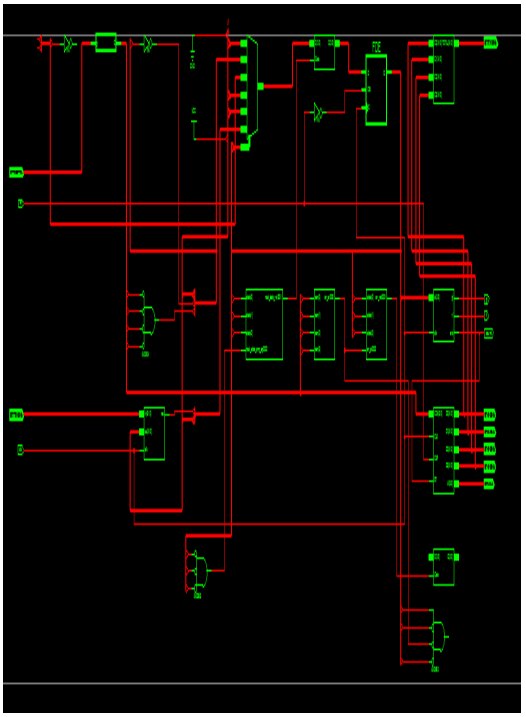

Fig. 10. Internal Block Diagram of EVM

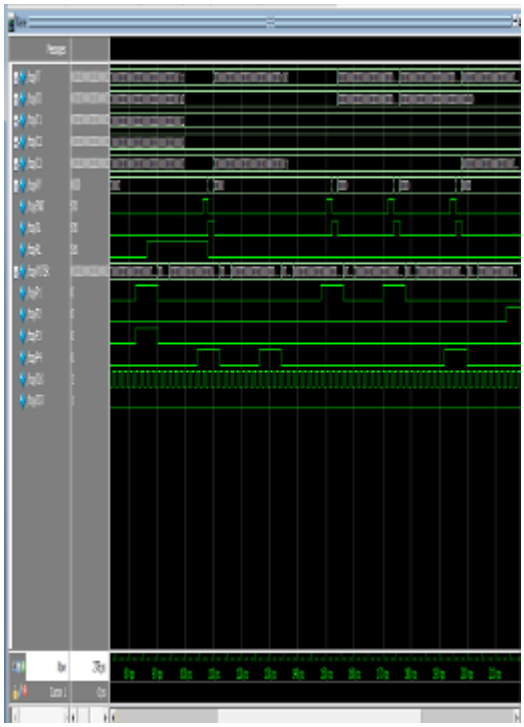

Fig. 11. Output waveform of EVM

Fig. 12 Shows the synthesis summary of EVM and Fig. 13 Shows the FPGA implementation on Altera DE1 Board.

Flow Summary	
Flow Status	Successful - Sat May 25 16:48:01 2013
Quartus II Version	11.0 Build 208 07/03/2011 SP 1 SJ Web Edition
Revision Name	voting
Top-level Entity Name	voting
Family	Cyclone II
Total logic elements	250 / 14,448 (2 %)
Total combinational functions	250 / 14,448 (2 %)
Dedicated logic registers	137 / 14,448 (< 1 %)
Total registers	137
Total pins	205 / 315 (65 %)
Total virtual pins	0
Total memory bits	0 / 239,616 (0 %)
Embedded Multiplier 9-bit elements	0 / 52 (0 %)
Total PLLs	0 / 4 (0 %)
Device	EP2C15AF484C7
Timing Models	Final

Fig. 12. Synthesis Summary

ADVANTAGES OF OUR ELECTRONIC VOTING MACHINE

A. FPGA based design advantages.

By using simple Verilog simulations, we can easily hardware implement the design in our real life environment satisfying the issues of efficiency, cost and the transparency. So by using FPGA based EVM, we can save around 1100 corers of taka in the 5 years of electro cycle.

We can also save huge amount of power by using this voting system as the battery is required only to activate the EVMs at the time of polling and counting. As soon as the polling is over, the battery can be switched off and this will be required to be switched on only at the time of counting.

For each national election alone it is estimated that about 10,000 tons of ballot paper (roughly 200,000 trees) would be saved by using Electronic Voting Machine. There is of course many more state and city/village level elections and the cost of printing those ballot papers would be also enormous.

The vote-counting is very fast and the result can be declared within 2 to 3 hours as compared to 30–40 hours, on an average, under the ballot-paper system.

Fig. 13. Altera DE1 Board

CONCLUSION

Considering the fact of the uncompromising advancement of VLSI technology, we have successfully implemented an efficient Electronic Voting Machine on FPGA by satisfactorily meeting the related issues of security and transparency for an EVM. Our EVM deals with the sensitive cases in voting processes like restriction of an invalid voter, prohibition of same voter and simultaneous vote cast for more than one candidate. Along with that, if the punched paper results matches with the software results then we can say the machine result is also transparent. We can use this efficient, secured and transparent voting machine successfully for electoral voting process in Bangladesh and worldwide.

ACKNOWLEDGEMENT

At first the authors would like to thank Allah forgiving them the opportunity to do this work. Then they would want to mention their parents who supported them with mental and financial support.

REFERENCES

[1] Field Programmable Gate Array. Wikipedia the free encyclopedia. Retrieved on February16, 2012 from http://en.wikipedia.org/wiki/Fpga.

[2] Palnitkar,S.(2008). *Verilog HdL*(2nd).Pearson Education.

[3] *K.C.C.* Wai and S. J. Yang, "*Field Programmable Gate Array Implementation of Reed- Solomon Code, RS (255, 239)*", New York (2006).

[4] *fpga4fun*. (2010, September 07). Retrieved on September 07, 2010, from fpga4fun: http://www.fpga4fun.com/PCI1.html

[5] Verilog Hardware Description Language Reference, Manual, Version 2.09, Los Gatos, CA, Open Verilog International, March 1993

[6] *Altera DE1 board*.(n.d.). Retrieved December 10, 2010, from terasic: http://www.terasic.com.tw/cgi-bin/page/archive.p1?Language=English&No=83

[7] Barlow L,(2003, November), *An Introduction to Electronic Voting*, Retrieved from http://brahms. emu.edu.tr/rza/Electronic%20Voting.pdf

[8] Indian Voting Machine, Wikipedia the free encyclopedia. Retrieved from March 28, 2010, from http://en.wikipedia.org/wiki/Indian voting machine